SOURCE DATA   TRANSPARENT PROCESS   OPEN ACCESS

Cancer-associated mutations in *VAV1* trigger variegated signaling outputs and T-cell lymphomagenesis

Javier Robles-Valero[1,2,3] [iD], Lucía Fernández-Nevado[1,2,3] [iD], L Francisco Lorenzo-Martín[1,2,3] [iD], Myriam Cuadrado[1,2,3] [iD], Isabel Fernández-Pisonero[1,2,3] [iD], Sonia Rodríguez-Fdez[1,2,3] [iD], Elsa N Astorga-Simón[1,2] [iD], Antonio Abad[1,3] [iD], Rubén Caloto[1,2,3] [iD] & Xosé R Bustelo[1,2,3,*] [iD]

Abstract

Mutations in *VAV1*, a gene that encodes a multifunctional protein important for lymphocytes, are found at different frequencies in peripheral T-cell lymphoma (PTCL), non-small cell lung cancer, and other tumors. However, their pathobiological significance remains unsettled. After cataloguing 51 cancer-associated *VAV1* mutations, we show here that they can be classified in five subtypes according to functional impact on the three main VAV1 signaling branches, GEF-dependent activation of RAC1, GEF-independent adaptor-like, and tumor suppressor functions. These mutations target new and previously established regulatory layers of the protein, leading to quantitative and qualitative changes in VAV1 signaling output. We also demonstrate that the most frequent *VAV1* mutant subtype drives PTCL formation in mice. This process requires the concurrent engagement of two downstream signaling branches that promote the chronic activation and transformation of follicular helper T cells. Collectively, these data reveal the genetic constraints associated with the lymphomagenic potential of *VAV1* mutant subsets, similarities with other PTCL driver genes, and potential therapeutic vulnerabilities.

Introduction

VAV1 is a multifunctional protein that plays signaling amplification and diversification roles downstream of the T-cell receptor (TCR) (Bustelo, 2014; Rodriguez-Fdez & Bustelo, 2019). One of the main functions of VAV1 is to catalyze the activation of the RHO GTPase RAC1 (Crespo *et al*, 1997; Bustelo, 2014; Rodriguez-Fdez & Bustelo, 2019) (Fig 1A). This enzyme reaction is mediated by a central cassette of the protein composed of the catalytic Dbl homology (DH) domain and the adjacent pleckstrin homology (PH) and C1-subtype zinc finger (ZF) regions (Fig EV1A) (Movilla & Bustelo, 1999; Zugaza *et al*, 2002; Chrencik *et al*, 2008; Rapley *et al*, 2008; Bustelo, 2014; Rodriguez-Fdez & Bustelo, 2019). The activation of RAC1 leads to the remodeling of the F-actin cytoskeleton and the stimulation of downstream elements such as the cJun N-terminal kinase (JNK) and the transcriptional factors AP1 and serum responsive factor (SRF) (Bustelo, 2014; Rodriguez-Fdez & Bustelo, 2019). VAV1 also activates other signal transduction pathways using adaptor, catalysis-independent mechanisms. One of them is the stimulation via the VAV1 calponin homology (CH) domain of a phospholipase Cγ1 (PLCγ1)-dependent pathway that leads to the stimulation of the nuclear factor of activated T cells (NFAT) (Fig 1A) (Wu *et al*, 1995; Kuhne *et al*, 2000). NFAT is involved in the regulation of proliferation and cytokine production by T cells (Muller & Rao, 2010). More recently, it has been involved in other T-cell-specific responses such as the differentiation of follicular helper T (T$_{FH}$) cells (Martinez *et al*, 2016). A target of NFAT, the thymocyte selection-associated HMG-box protein (TOX) (Scott *et al*, 2019), is also involved in this latter differentiation process (Xu *et al*, 2019). Another adaptor-like function of VAV1, which is associated with tumor suppressor roles in T-cell acute lymphoblastic leukemia of the TLX[+] subtype, is the negative regulation of the active intracellular fragment of NOTCH1 (ICN1) (Fig 1A) (Robles-Valero *et al*, 2017). This pathway is mediated by the most C-terminal VAV1 SH3 (CSH3), which promotes the ubiquitin-mediated degradation of ICN1 by forming complexes with the E3 ubiquitin ligase CBL-B (Casitas B-lineage lymphoma B) (Robles-Valero *et al*, 2017). The VAV1 CSH3 can bind to additional partners such as the heterogeneous nuclear ribonucleoprotein K (HNRNPK) and dynamin 2 (DNM2) (Bustelo *et al*, 1995; Gomez *et al*, 2005), suggesting that

VAV1 might play additional adaptor-like functions both in normal and cancer cells.

One of the main regulatory features of VAV1 is that its ability to stimulate both the RAC1 and NFAT pathways is highly dependent on its tyrosine phosphorylation state (Bustelo, 2014). Thus, in nonstimulated cells, nonphosphorylated VAV1 is in an inactive state due to inhibitory interactions established by the N-terminal (CH and acidic region) domains and the CSH3 region with the central DH-PH-ZF cassette. These interactions are eliminated upon the phosphorylation of VAV1 on tyrosine residues located on the acidic (Ac), ZF, and CSH3 regions. This activation step is mediated *in trans* by the SH2 and most N-terminal SH3 (NSH3) region that facilitate the interaction of VAV1 with upstream protein tyrosine kinases and adaptor molecules, respectively (Bustelo, 2014).

VAV1 was identified in 1989 due to its oncogenic activity in focus formation assays (Katzav *et al*, 1989). Despite this, its role in cancer has been circumscribed so far to the upregulation of the wild-type protein (Bustelo, 2014). This has changed recently, since the characterization of cancer genomes has revealed that *VAV1* is frequently mutated in a number of PTCL subtypes such as adult T-cell leukemia/lymphoma (ATLL, 17% of total cases), PTCL-not otherwise specified (PTCL-NOS, 7% of total cases), and angioimmunoblastic T-cell lymphoma (AITL, 6% of total cases) (Yoo *et al*, 2014; Crescenzo *et al*, 2015; Kataoka *et al*, 2015; Boddicker *et al*, 2016; Vallois *et al*, 2016; Abate *et al*, 2017; Park *et al*, 2017). Mutations have also been detected at much lower frequencies in anaplastic large cell lymphoma (ALCL), cutaneous T-cell lymphoma (CTCL), and non-small-cell lung cancer (NSCLC) (Crescenzo *et al*, 2015; Boddicker *et al*, 2016; Campbell *et al*, 2016; Abate *et al*, 2017; Park *et al*, 2017) (Fig EV1A and B). The actual relevance of these mutations from a functional and pathobiological perspective remains, however, ill-defined. In this context, recent studies have shown that some tumor-associated *VAV1* mutations lead indeed to gain-of-function (GOF) events (Boddicker *et al*, 2016; Abate *et al*, 2017; Fukumoto *et al*, 2020). However, these analyses have been limited to a very small (8%) and overlapping subset of mutations that target obvious regulatory layers of the protein. Moreover, those studies have not tested all the spectrum of downstream signals elicited by this protein (Boddicker *et al*, 2016; Abate *et al*, 2017; Fukumoto *et al*, 2020). As a result, we do not know yet whether most *VAV1* mutations found in tumors act as *bona fide* oncogenic drivers *in vivo* and, if so, whether they do it autonomously or in combination with ancillary inputs from other genetic lesions and/or cancer cell-extrinsic events. Likewise, we do not know the spectrum of downstream signaling pathways that have to be engaged to promote full cell transformation.

To address these relevant knowledge gaps, we have measured qualitatively and quantitatively the functional impact of 51 *VAV1* mutations found in tumors on all known VAV1-dependent signaling outputs. This strategy allowed us to generate a comprehensive signaling and functional catalogue of the tumor-associated *VAV1* mutations. Using adoptive cell transfer experiments, we have also demonstrated that the most frequent functional subclass of *VAV1* mutations identified in our study can drive AITL formation. Finally, we have identified the main signaling and pathobiological programs involved in the generation of *Vav1*-driven tumors using a combination of cellular, signaling, and genome-wide gene expression approaches. These findings suggest that *VAV1* mutations probably play clinical-relevant roles in AITL and other tumor types. They also pinpoint several VAV1 signaling-based pharmacological strategies to treat them.

Results

Variegated functional impacts of *VAV1* mutations found in tumors

To start building a functional catalogue of the *VAV1* mutations present in tumors, we decided to comprehensively analyze the impact of 51 mutations recently found in PTCL and NSCLC (Fig EV1A and B) using several experimental readouts for the main downstream signaling pathways engaged by this protein (Fig 1A and B). The mutations tested encompassed an internal deletion, four fusions, four truncations, and 42 missense changes. In the case of point mutations, we included in the analyses allelic variants found in some codons. First, we investigated the impact of the 51 mutations on the two main catalysis-dependent (RAC1–JNK and RAC1–SRF) and CH-dependent (PLCγ1–NFAT) pathways regulated by VAV1 (Fig 1B). To this end, we carried out in the former case luciferase-based reporter assays to measure the effect of the interrogated mutant proteins on the activity of both JNK and SRF in Jurkat (nonstimulated and TCR-stimulated) and exponentially growing COS1 cells, respectively (Fig 1B). In the case of the NFAT pathway, we carried out luciferase-based reporter experiments in nonstimulated and TCR-stimulated Jurkat cells to measure the impact of the mutants in the transcriptional activity of an *Il2* promoter containing three NFAT-binding sites (Fig 1B). It is worth noting that, unlike the case of RAC1-dependent pathways, the optimal stimulation of the NFAT pathway by VAV1 requires parallel signaling inputs from the antigen receptor in this assay. As a result, the activation of this transcriptional factor is enhanced upon the engagement of the TCR even in T cells that express fully deregulated, constitutively active VAV1 versions (Barreira *et al*, 2014). As positive control, we included in these analyses the lab-made Vav1^{Y174E} and Vav1^{Y174F} mutant proteins that are known to promote high levels of stimulation of both the RAC1 and NFAT pathways (Lopez-Lago *et al*, 2000; Barreira *et al*, 2014). The results obtained for all the interrogated Vav1 mutants in these assays, compared with the reference basal (Vav1^{WT}) and positive (Vav1^{Y174F}, Vav1^{Y174E}) controls, are collectively depicted using a heatmap representation in Fig 1C and D. The wet-lab data used to generate these heatmaps are shown both in the Appendix Figs S1–S8. Using this approach, we found that 25% of the interrogated mutations elicit a bivalent GOF effect on the RAC1 and NFAT pathways (Fig 1C and D; residues shown in red). These mutants can be further subdivided according to their specific impact on the signaling output of the protein as weak (e.g., E556D), intermediate (e.g., Y174C, G819S), and strong (e.g., Δ820–845) (Fig 1D). Only the latter ones, which are associated with the generation of C-terminally truncated and fusion proteins, exhibit fully constitutive, phosphorylation-independent biological activity (Fig 1D). More unexpectedly, we observed that 12% of the *VAV1* mutations display signaling branch-specific effects that cause the specific stimulation of either the RAC1 or the NFAT pathway (Fig 1C and D; residues labeled in red and blue colors at the same time). Finally, 63% of the interrogated mutations show either WT-like (47%, Fig 1C and D;
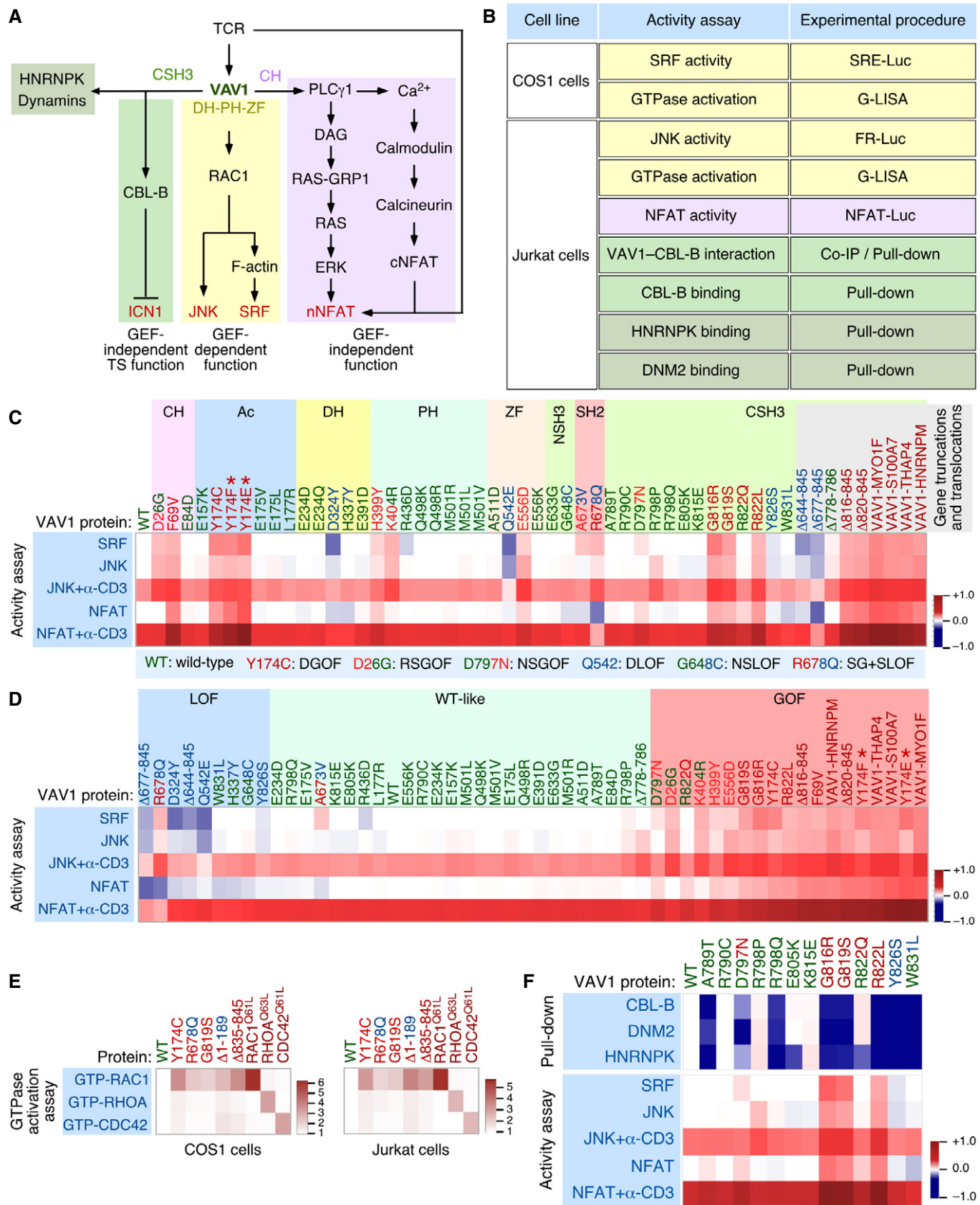
Figure 1.

Figure 1. Functional impact of *VAV1* mutations in the RAC1 and NFAT pathways.

A Depiction of the three main signaling branches of VAV1 in T cells. Additional binding partners of the CSH3 domain that will be studied in this work are also shown. Signaling crosstalk between the NFAT route and parallel TCR-triggered pathways is also depicted. DAG, diacylglycerol; RAS-GRP1, Ras GDP releasing protein 1; cNFAT, cytosolic NFAT; nNFAT, nuclear NFAT. Rest of abbreviations have been introduced in the main text.

B Vav1-dependent biological readouts and cell types used to test the biological activity of Vav1 mutant proteins. The color of each assay represents the VAV1-regulated downstream pathway shown in panel (A). Please, note that the GTPase activation and protein–protein interaction experiments were done with smaller subsets of mutants than the JNK, SRF, and NFAT experiments.

C, D Heatmap representations summarizing the activity of VAV1 mutants (top) in the indicated assays tested (left). The mutations are clustered according to their specific distribution within the primary structure of the protein (C) and type of behavior in these experiments with the rest of mutants tested (D). Activity scores are depicted on a dark blue (lowest activity) to dark red (highest activity) scale relative to the activity levels found for Vav1^{WT} under nonstimulated conditions (which was given an arbitrary value of 1) ($n = 3$ independent experiments, each performed in triplicate). The color code used for each mutant is associated with the biological activity exhibited in these assays following the color code indicated in (C) (bottom box). DGOF, double gain of function in RAC1 and NFAT pathways; RSGOF, RAC1 single gain of function; NSGOF, NFAT single gain of function; DLOF, double loss of function; NSLOF, NFAT single loss of function; SG+SLOF, RAC1 gain of function and NFAT loss of function. The laboratory-made VAV1 mutants used as positive control are indicated by asterisks.

E Heatmap representation summarizing the activity of VAV1 mutants (top) in COS (left panel) and Jurkat (right panel) cells on the indicated GTPases. Activity scores are depicted on a white (WT activity) to dark red (highest activity) scales relative to the activity levels found for Vav1^{WT} (which was given an arbitrary value of 1). $n = 3$ independent experiments, each performed in duplicate. The color code used for each mutant is as in panels (C and D). Activated RHO-GTPase proteins (Rac1^{Q61L}, RhoA^{Q63L}, and Cdc42^{Q61L}) were used as positive control in the appropriate assay.

F *Top*, heatmap summarizing the results obtained in our GST pull-down experiments with the indicated CSH3 mutant proteins. Binding partners tested are shown on the left. The mutations are represented in a sequential manner and following the color code used in panels (C and D). Activity scores are depicted on a dark blue (lowest interaction) to dark red (highest interaction) scale relative those obtained with the CSH3^{WT} (which was given an arbitrary value of 1) ($n = 3$ independent experiments). *Bottom*, heatmap showing the biological activity of the indicated CSH3 mutants obtained in the experiments described in panels (C and D). This heatmap has been included to facilitate the comparison of the activities of these mutants in all the assays used in this figure.

Source data are available online for this figure.

residues labeled in green) or reduced activity in these two assays (16%, Fig 1C and D; residues labeled in blue). It is worth noting, however, that some of these mutants will induce the elimination of the tumor suppressor pathway regulated by VAV1 and, therefore, must have an impact in Notch1 signaling (see below in this section). As a complementary avenue to the data obtained using the indirect JNK and SRF assays, we used the G-LISA method to test the direct effect of 3 VAV1 mutants belonging to the bivalent (Y174C, G819S) and signaling branch-specific (R678Q) subsets on the activation of the three main RHO family GTPases in both COS1 and Jurkat cells. As positive controls, we utilized constitutively active versions of VAV1 (Δ1-189 and Δ835-845), RAC1 (Q61L), RHOA (Q63L), and CDC42 (Q61L). When compared to VAV1^{WT}, we found that all the chosen VAV1 mutants could activate the incorporation of GTP onto RAC1 irrespectively of the functional subclass involved (Fig 1E and Appendix Fig S9). By contrast, they exhibited much lower activities on RHOA and CDC42 (Fig 1E and Appendix Fig S9). This RAC1 specificity is consistent with previous biochemical and cell-based experiments (Crespo *et al*, 1997; Aghazadeh *et al*, 2000; Couceiro *et al*, 2005; Rapley *et al*, 2008).

We next investigated the effect of specific mutations on the recently described tumor suppressor pathway regulated by VAV1 (Fig 1A). According to our previous data (Robles-Valero *et al*, 2017), this function must be lost in the case of all the truncation and translocation VAV1 mutants that have lost the CSH3 domain. In agreement with this, we found that the Vav1$^{Δ677–845}$ protein cannot coimmunoprecipitate CBL-B when expressed in Jurkat cells (Fig EV2A). The role of this mutation must be specifically associated with the elimination of this suppressor pathway, given that Vav1$^{Δ677–845}$ shows reduced activity when tested in the JNK, SRF, and NFAT assays (see above, Fig 1C). By contrast, VAV1^{WT} and versions of VAV1 with mutations outside the CSH3 that exhibit WT-like activities in the previous assays (Fig 1C) do associate with this E3 ubiquitin ligase (Fig EV2A). This suggests that these latter mutations are probably bystanders. Since missense mutations targeting

residues located in the CSH3 can also lead to the loss of the suppressor function (Robles-Valero *et al*, 2017), we next carried out GST pull-down experiments to evaluate the interaction of the 13 VAV1 CSH3 point mutants with CBL-B, HNRNPK, and DNM2. As negative control, we used the nonchimeric GST protein and, in some experiments, a GST fusion protein containing a mutant version of the VAV1 CSH3 (P833L) that cannot interact with any known protein partner (Barreira *et al*, 2014; Robles-Valero *et al*, 2017). As positive control, we used a GST-VAV1 CSH3^{WT} fusion protein as bait. A heatmap summarizing the data obtained in all these experiments is shown in Fig 1F. The raw data can be found in Fig EV2B–D. These analyses revealed that 65% of the Vav1 CSH3 mutants analyzed have impaired physical interactions with CBL-B and the other two protein partners (Fig 1F, see scheme in Fig EV2E). They also identified a smaller subset (15%) of Vav1 CSH3 mutants with a selective impairment of the interaction with either HNRNPK (E805K, R822Q) or DNM2 (D797N) (Fig 1F, see scheme in Fig EV2E).

Taken the results from all the experimental readouts together, we conclude that 49% of the interrogated VAV1 mutations are likely passengers according to the currently known functions of VAV family proteins (Bustelo, 2014; Rodriguez-Fdez & Bustelo, 2019). Many of these mutations, as expected, retain WT-like activity in all the assays used. However, we also include in this category mutations that cause the inhibition of RAC1 and/or NFAT activities without the elimination of the tumor suppressor activity of VAV1 as they must not significantly contribute to the chronic activation of the downstream signaling of the protein. The remaining *VAV1* mutants (51%) interrogated in this work do cause some type of GOF effect in the activity of the protein. Such mutants can be classified in five main functional subtypes according to the spectrum of signaling branches specifically affected by them (Fig 2A). The most prevalent subclass includes mutations that lead to a concurrent activation of the RAC1 and NFAT pathways as well as to the elimination of the tumor suppressor activity of VAV1 (35% of all cases; Fig 2A, trivalent subclass). In terms of incidence, this mutant subset is found in

ALCL, PTCL-NOS, AITL, and lung adenocarcinomas (Fig 2B). This trivalent subclass mostly includes fusion and truncated proteins, with very few cases involving missense mutants (Fig 2C). All of them target, as expected (Barreira *et al*, 2014; Robles-Valero *et al*, 2017), the CSH3 domain (Fig 2A). The second most frequent subclass (27%) corresponds to proteins that have specifically lost the tumor suppressor activity (Fig 2A, monovalent subclass). We include in this category mutants that exhibit either WT-like or different types of inhibitory effects on the RAC1 and NFAT pathways (Fig 2A). These alterations, which are found in lung tumors, CTCL, AITL, and ATLL (Fig 2B), are associated with the generation of either large truncations (lung tumors, AITL) or single amino acid changes (ATLL, CTCL) in the mutant protein (Fig 2C). These mutations target the CSH3 or the SH2-CSH3 region (Fig 2A). Mutants that promote a bivalent GOF effect on the RAC1 and NFAT pathways constitute the third most frequent functional category (15% of mutants with deregulated activity; Fig 2A, bivalent subclass). These alterations, which are found in decreasing frequencies in ATLL, AITL, lung adenocarcinoma, and PTCL-NOS (Fig 2B), are exclusively associated with missense changes (Fig 2C) in the CH, Ac, PH, or ZF domains (Fig 2A). A fourth subclass encompasses mutants showing enhanced GDP/GTP exchange activity and variegated effects on the NFAT pathway (15% of mutants with deregulated activity; Fig 2A; uncoupling subclass 1). This subclass, which is found in ATLL and lung tumors (Fig 2B), is composed of missense mutations (Fig 2C) located on the CH (subtype 4a), PH (subtype 4a), and SH2 (subtype 4b) regions (Fig 2A). Finally, the least frequent subclass (8%) includes mutants that lead to the specific activation of the NFAT pathway while maintaining WT-like RAC1 activity (Fig 2A, uncoupling subclass 2). Interestingly, these mutants are the only ones that show specific alterations in the binding to either HNRNPK (subtype 5a) or DNM2 (subtype 5b) (Fig 2A). This subclass, which is preferentially found in CTCL, AITL, and ATLL (Fig 2B), is associated with missense mutations targeting the CSH3 region (Fig 2B and C). By far, the most common hot spot region of the protein based on these analyses is the CSH3 domain (Fig 2A). These data also indicate that the tumors with the highest percentage of functionally relevant mutations are ALCL, AITL, and PTCL-NOS (Fig 2B). By contrast, the tumors with more passenger mutations include ATLL, CTCL, lung adenocarcinoma, and lung squamous cell carcinoma (Fig 2B).

New regulatory layers unveiled by the *VAV1* mutations

The reason for the high biological activity exhibited by most bivalent and trivalent GOF VAV1 mutations found in this study can be explained well according to the current regulatory model for this protein family (Fig EV3A) (Bustelo, 2014; Rodriguez-Fdez & Bustelo, 2019). Consistent with this, most of them target common regulatory hot spots of the protein such as the CH, Ac, PH, and CSH3 domains (Fig EV3A). As an example, it is likely that bivalent GOF effect created by the CH domain-located F69V mutation is generated by the disruption of the interactions that the F69 residue establishes with the PH (D^{406}), the DH α_{11} helix (F^{386}), and the first PH β strand (Y^{441}) (Fig EV3A and B). These interactions are critical for maintaining the autoinhibited structure of nonphosphorylated VAV1 (Yu *et al*, 2010). Similarly, the bivalent Y174C GOF mutation targets a phosphorylation site located in the Ac region that

contributes to the autoinhibitory structure by making interactions with a hydrophobic pocket present in the DH domain (Yu *et al*, 2010) (Fig EV3A and C). Hence, these two missense alterations must trigger an opening of the molecule similar to that induced by the laboratory-made Y174F and Y174E mutations (Lopez-Lago *et al*, 2000; Barreira *et al*, 2014, 2018) (Fig 1C). It is likely that other mutations not surveyed in our analyses could belong to this functional class (Δ151–158, Δ165–174) (Fig EV1B), given that they can either displace or eliminate the critical regulatory phosphosites Y^{160} and Y^{174} that are also present in the Ac region of the protein. The GOF effects triggered by most mutations targeting the CSH3 are also consistent with the elimination of the autoinhibitory and/or suppressor functions of this domain (Barreira *et al*, 2014; Robles-Valero *et al*, 2017). However, the present results indicate that the CSH3 autoinhibitory surface is larger than anticipated because the cancer-associated mutation target residues (G^{816}, G^{819}) located away from the two previously characterized inhibitory interfaces of that domain (Fig 3A, residues shown in raspberry color) (Barreira *et al*, 2014). Unlike the case of the lab-made mutations targeting those previously characterized inhibitory sites (Barreira *et al*, 2014), the mutations of the G^{816} and G^{819} residues also impair the interaction with CBL-B (Fig 1F). As a result, they simultaneously alter the VAV1-regulated RAC1, NFAT, and tumor suppressor pathways. Hence, the effect of these mutations is analogous to the truncations and translocations that eliminate the entire CSH3 domain. However, the effects found with other VAV1 mutations indicate that there must exist extra regulatory layers involved in the control of the signaling output of this protein. Thus, the bivalent GOF effect induced by mutations in the CH-located D^{26} residue (E^{26} in mouse) is quite unexpected since this residue does not participate in any of the known intramolecular interactions that stabilize the inactive structure of the protein (Aghazadeh *et al*, 2000). It is possible therefore that this residue could be involved in the formation of interdomain inhibitory interactions with the CSH3 (Barreira *et al*, 2014) or the SH2 (this work, see below) domains. Likewise, the GOF effects elicited by mutations located in the PH (H^{399} and K^{404}) and ZF (E^{556}) were also somewhat unexpected, given that the targeted residues do not participate in any of the known intramolecular interactions that contribute to stabilize the inactive state of nonphosphorylated VAV1 (Yu *et al*, 2010). These residues are located in an area of the catalytic DH-PH-ZF cassette (Fig EV3D–F) that harbors residues involved in the phosphorylation-dependent activation of VAV1 activity (Y^{541}, Y^{544}) (Barreira *et al*, 2014), the overall spatial organization of the catalytic cassette (Chrencik *et al*, 2008; Rapley *et al*, 2008; Yu *et al*, 2010), and the inhibitory interactions with both the CH and the CSH3 regions (Yu *et al*, 2010; Barreira *et al*, 2014). This area also undergoes a significant spatial reorientation during the transition of VAV1 from the inactive to the active state (Yu *et al*, 2010). It is likely therefore that the bivalent GOF effect induced by the N399Y and E556D mutations is mediated by the displacement of the CH from the autoinhibitory site, leading to the chronic stimulation of the RAC1 and NFAT pathways. Unlike the foregoing residues, we have found that the K404R promotes the stimulation of the RAC1 but not of the NFAT pathway (Fig 1C). Given the multiple direct and indirect interactions established by this residue in the VAV1 structure (Fig EV3F), it is likely that its mutation promotes the exposure of the catalytic site of VAV1 through the displacement of PH α helix away from ZF and DH domains that, in turn, change the spatial

orientation of the CH region. However, the lack of activation of NFAT suggests that the displacement of the CH does not involve in this case the full exposure of the effector interface that engages that

pathway. Alternatively, this mutation can induce a conformation of the whole protein not compatible with optimal NFAT signaling by that domain. The latter possibility seems more plausible, given that
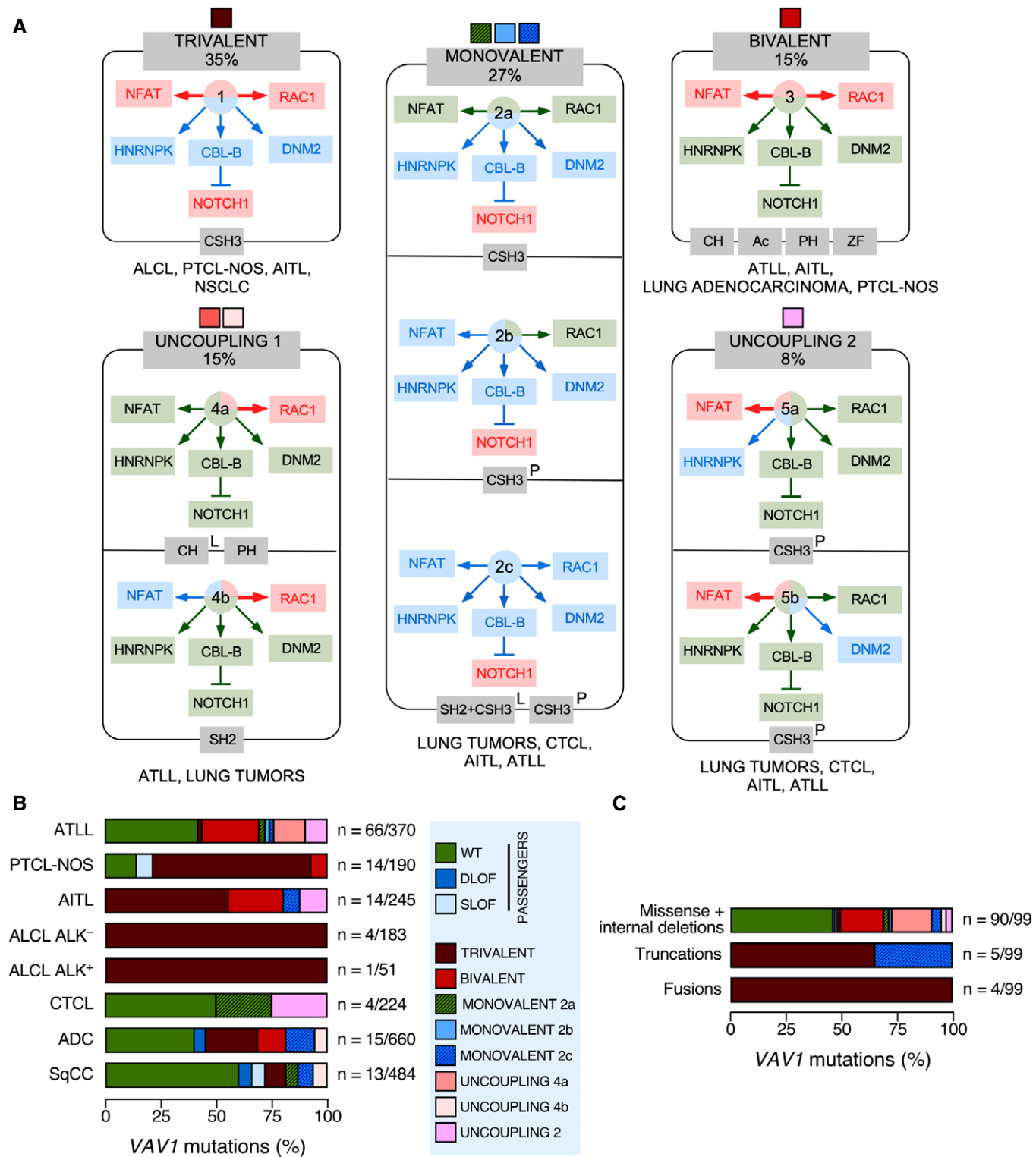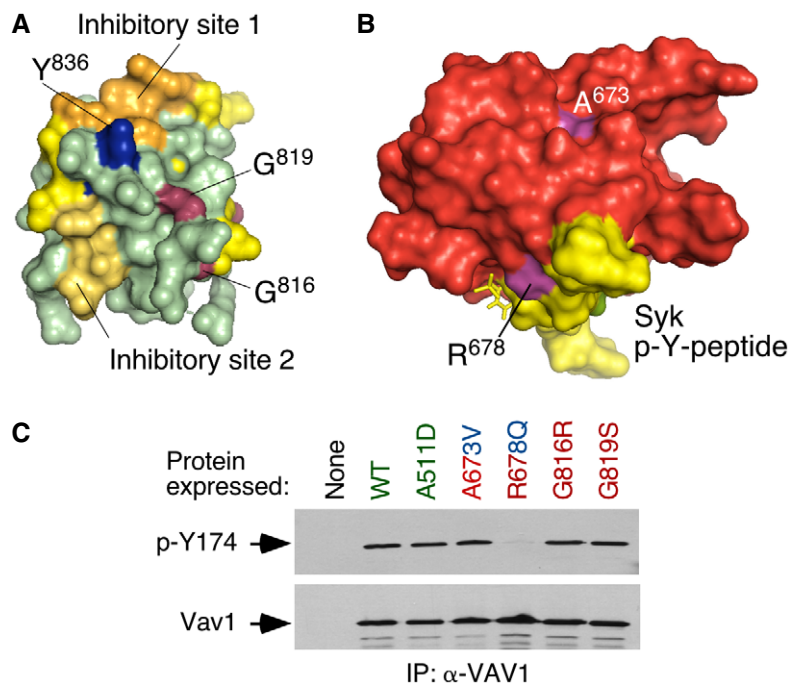

Figure 2.

mutations in the SH2 and CSH3 also promote a similar dissociation of the activation of the RAC1 and NFAT (Fig 1E). Signaling uncoupling effects have been previously observed with lab-made mutations targeting specific tyrosine phosphorylation and lysine acetylation sites of the protein (Barreira *et al*, 2014, 2018; Rodríguez-Fdez *et al*, 2020).

Our studies have also revealed a hitherto unknown regulatory role of the SH2 domain in the intramolecular inhibition of the nonphosphorylated protein. To date, the main function of this domain has been associated with the tyrosine phosphorylation-mediated activation of the RAC1 and NFAT pathways (Bustelo & Barbacid, 1992; Bustelo *et al*, 1992; Bustelo, 2014; Rodriguez-Fdez & Bustelo, 2019). Consistent with this, Vav1 proteins bearing lab-

generated mutations in this domain are always inactive when tested in RAC1 and NFAT assays (Zugaza *et al*, 2002). Against this well-established paradigm, we have found two NSCLC-associated SH2 mutations (R673V and R678Q) that unexpectedly cause the stimulation of the RAC1-dependent pathways (Fig 1C). Also, against the long-held consensus regulatory model for the Vav family, one of those mutations targets a residue in the phosphotyrosine-binding site (R^{678}) that is critical for the interaction with both the upstream protein tyrosine kinases and downstream effectors (Fig 3B). Consistent with this, we have found that Vav1^{R678Q} cannot become tyrosine phosphorylated when ectopically expressed in Jurkat cells (Fig 3C). It is unlikely that the negative regulatory role of the R^{678} residue is due to the participation of the VAV1 SH2 domain in the

Figure 3. New regulatory layers unveiled by the *VAV1* mutations.

A 3D structure of the Vav1 CSH3 domain. The previously described intramolecular inhibitory sites 1 and 2 of the Vav1 CSH3 domain are depicted in orange and yellow, respectively (Barreira *et al*, 2014). The regulatory Y^{836} phosphosite is highlighted in blue (Barreira *et al*, 2014). The residues present in the new inhibitory interface of the CSH3 are shown in raspberry color.

B 3D structure of the VAV1 SH2 (red) bound to a Syk tyrosine-phosphorylated peptide (yellow). The mutated residues are shown in purple. p-Y, tyrosine phosphorylated.

C Levels of phosphorylation of the Y^{174} phosphosite of the indicated Vav1 mutant proteins immunoprecipitated from Jurkat cells (upper panel). The total amount of Vav1 immunoprecipitated in each sample is shown in the bottom panel ($n = 3$ independent experiments).

Source data are available online for this figure.

interaction of an inhibitory phosphorylation site of the molecule, because other mutations that inactivate this domain (e.g., G691V) trigger a full LOF rather than a GOF effect in the molecule (Zugaza et al, 2002; Rodríguez-Fdez et al, 2020). In line with this, the second activating SH2 mutation found in this study that maps outside the phosphotyrosine-binding site does not impair the overall phosphorylation levels of the protein (Fig 3C, residue A673V). Interestingly, these two SH2 mutations show reduced levels of NFAT activation, thus suggesting that the targeted residues are also important for the optimal engagement of the PLCγ1–NFAT axis in lymphocytes (Fig 1C). To our knowledge, this is the first time in which activating mutations in the SH2 domain have been ever described for any VAV family member.

Vav1$^{\Delta C}$ drives PTCL formation when expressed in CD4$^+$ T cells

To investigate the relevance of *VAV1* mutations and the downstream pathways activated by them in tumorigenic processes *in vivo*, we next carried out adoptive T-cell transfer experiments to assess the impact of deregulated Vav1 signaling in T lymphomagenesis. We chose this model because, according to the results from the above sections, ALCL, AITL, and PTCL-NOS are the tumors that show the highest percentages of functionally relevant *VAV1* mutations (Fig 2B). These alterations usually involve the concurrent activation of RAC1, NFAT, and ICN1 signaling (Fig 2B). In line with this, we decided to use in these experiments a mutant version of Vav1 with a truncated CSH3 (amino acids 835-845, referred to hereafter as Vav1$^{\Delta C}$) that is functionally analogous to the trivalent *VAV1* mutant subclass frequently observed in those lymphoma subtypes. We also included in these experiments a catalytically dead version of Vav1$^{\Delta C}$ (ΔC+E201A) to assess the specific relevance of the concurrent upregulation of the NFAT and ICN1 pathways to the tumorigenic processes in the absence of RAC1 activation. To this end, we infected TCR plus CD28-stimulated mouse splenic CD4$^+$ T cells with retroviral vectors encoding bicistronically each mutant Vav1 protein and EGFP and, subsequently, introduced them into *Vav1$^{-/-}$; Vav2$^{-/-}$; Vav3$^{-/-}$* mice to test the potential development of lymphomas (Fig 4A). These recipient mice are T lymphopenic (Fujikawa et al, 2003; Bustelo & Dosil, 2016), a feature that facilitates their utilization in transplantation experiments involving even cells of human origin (Lorenzo-Martín et al, 2020). The long-term follow-up of these mice indicated that those transplanted with Vav1$^{\Delta C}$-expressing CD4$^+$ T cells progressively develop an expanded population of CD4$^+$ T cells associated with T$_{FH}$ immunosurface features (PD1$^+$, CXCR5$^+$) (Fig 4B). These animals die within a 3-month period after the initial detection of this population ($t_{1/2}$ = 8 months after the transplantation step) (Fig 4C), indicating that these Vav1$^{\Delta C}$-expressing cells have been oncogenically transformed. Unlike the case of other mutations found in PTCL cases (e.g., *RHOA^{G17V}, FYN-TRAP3IP2*) (Cortes et al, 2018; Moon et al, 2021), the Vav1$^{\Delta C}$-driven lymphomagenesis does not require the use of CD4$^+$ T cells deficient for the 5-methylcytosine oxidase Tet2, a suppressor protein that is lost in a large number of human PTCLs (Fiore et al, 2020). Necropsies performed in tumor-bearing animals showed the recurrent presence of mild splenomegaly as well as enlarged and vascularized lymph nodes (Fig 4D and E). Histological analyses also showed that these tissues display effaced boundaries between the red and the white pulps (spleen) and the cortical and

medullary regions (lymph nodes) (Fig 4E). These animals also exhibit an expanded population of PD1$^+$, CXCR5$^+$, and CD4$^+$ T cells (Fig 4F–H) that are highly decorated with ICOS (Fig 4I–K) and CD69 (Fig 4J and L), two surface markers typically associated with an activated T$_{FH}$ state. All these histological and immunophenotypical features are consistent with the development of AITL-like tumors in these mice. No alterations in CD4$^+$ T cells were observed in mice transplanted with either EGFP- or EGFP+Vav1$^{\Delta C+E201A}$-expressing cell at the same post-transplantation time (Fig 4F–L).

Further buttressing the T$_{FH}$ cell-like phenotype of these tumor cells, we found using quantitative reverse transcription-PCR (qRT–PCR) that they express high levels of transcripts encoding typical follicular helper cell markers such as PD1, CXCR6, ICOS, Bcl6, and interleukin 21 (Fig 4M, left panel). In addition, they show elevated levels of canonical Notch1 target genes such as *Hes1*, *Dtx1*, and *Ptcra* (Fig 4M, right panel). Most of these transformed cell isolates also display high levels of p-Akt (Figs 4N and EV4A) and p-Erk (Figs 4O and EV4A) when compared to EGFP$^+$ lymphocytes. These molecular and signaling features are not observed in cells expressing the catalytically deficient Vav1$^{\Delta C+E201A}$ mutant protein (Fig 4M). The Vav1$^{\Delta C}$-transformed cells show wild-type-like levels of the tumor suppressors Tp53 and Tet2 (Fig EV4A and B). These results indicate that the expression of Vav1$^{\Delta C}$ in mouse CD4$^+$ T cells can trigger AITL-like tumors in a Tp53- and Tet2-independent manner. They also demonstrate that: (i) The catalytic activity of Vav1$^{\Delta C}$ is essential to drive this lymphomagenic process. (ii) The activation of the NFAT and ICN1 is not enough *per se* to drive T lymphomagenesis in these experimental conditions.

Vav1$^{\Delta C}$ triggers a vast proliferative program in transformed T$_{FH}$ cells

Microarray analyses revealed that Vav1$^{\Delta C}$-transformed cells contain 2,277 differentially expressed genes (1,554 upregulated, 823 downregulated) when compared to normal CD4$^+$ T lymphocytes (Fig 5A and Dataset EV1). No significant differences were detected between the transcriptomes of cancer cells obtained from the spleen and lymph nodes (Fig 5A), suggesting that the Vav1$^{\Delta C}$-driven gene expression program is rather tumor niche-independent. Consistent with our previous analyses, gene set enrichment analyses (GSEAs) indicated that this transcriptome is highly similar to the T$_{FH}$ cell gene expression landscape (Fig 5B). Functional annotation analyses revealed that the Vav1$^{\Delta C}$ upregulated transcriptome is mainly composed of proliferation-related genes (Figs 5C and EV5A, and Dataset EV1). Yet, principal component analyses indicate that this transcriptome is more closely related to PTCLs than to other unrelated proliferative tumor types (Fig EV5B). The downregulated subset of the Vav1$^{\Delta C}$-induced transcriptome is mainly enriched in genes linked to TCR signaling and activation (Fig 5C and Dataset EV1). Although counterintuitive, this feature is commonly found in previously reported AITL-associated transcriptomal programs in both mice and humans (Zang et al, 2017). GSEA further revealed that Vav1$^{\Delta C}$ promotes the expression of genes linked to heme metabolism, inflammatory processes, the unfolded protein response, and the mTORC pathway (Fig EV5A). From a more molecular perspective, the Vav1$^{\Delta C}$-driven transcriptome is enriched in gene signatures typically associated with Vav1 downstream signaling elements such
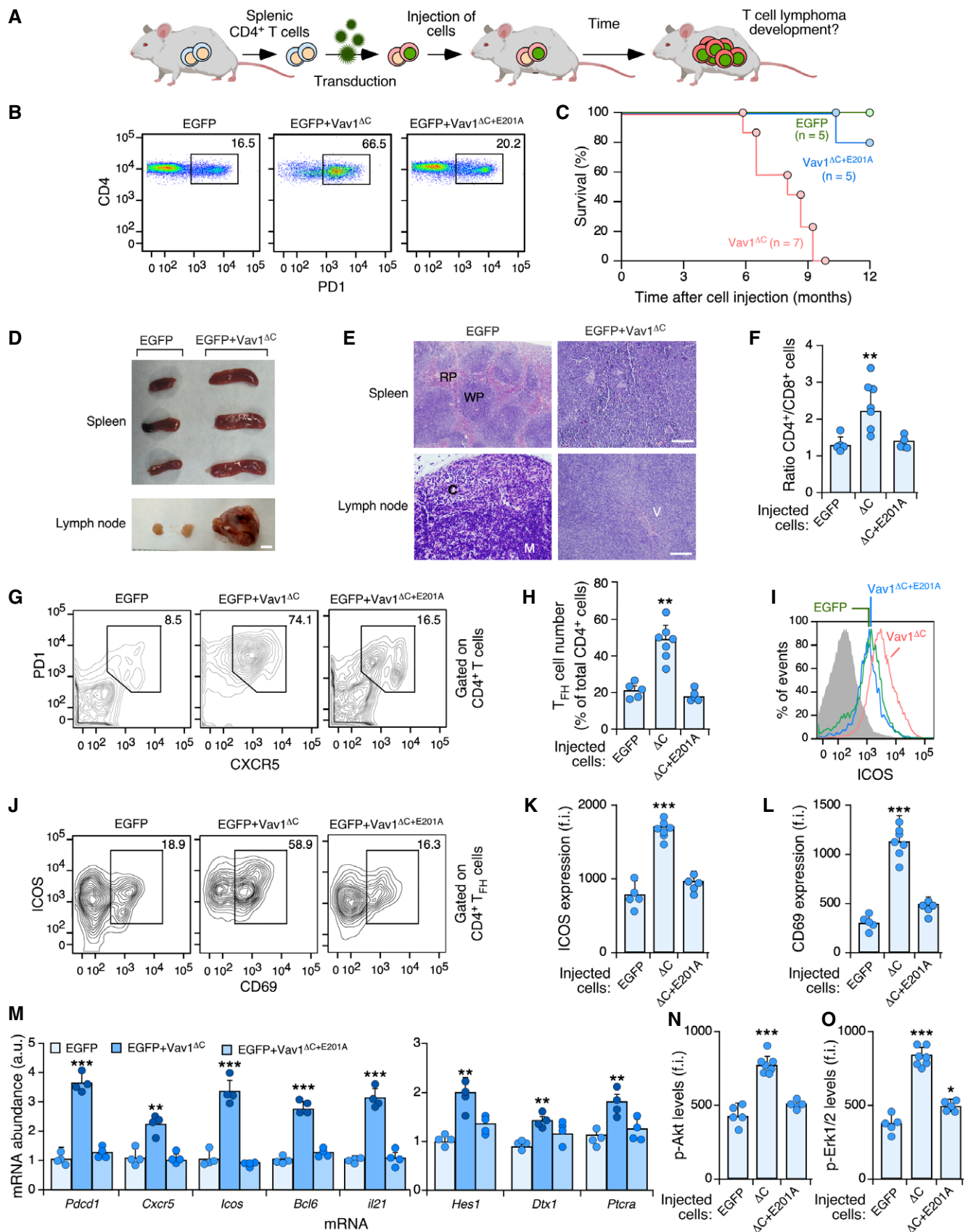
Figure 4.

Figure 4. Vav1$^{\Delta C}$ drives PTCL formation when expressed in CD4$^+$ T cells.

A   Depiction of adoptive T-cell transfer experiments used in this figure. See Materials and Methods for further details.

B   Flow cytometry detection of PD1$^+$ CD4$^+$ T cells in the peripheral blood from recipient mice 6 months after being transplanted with CD4$^+$ T cells expressing the indicated proteins (top). Numbers indicate the relative percentage (%) of the EGFP$^+$ population (boxed) found in each case. Same results were obtained in recipient mice transplanted with EGFP- ($n = 5$), Vav1$^{\Delta C}$- ($n = 7$) and Vav1$^{\Delta C+E201A}$-transduced ($n = 5$) CD4$^+$ T cells.

C   Survival curves of mice transplanted with CD4$^+$ T cells expressing the indicated proteins. The number of animals used is indicated in the graph. Note: The mouse transplanted with EGFP-transduced cells that has died in these experiments did not show any sign of tumor development according to anatomopathological analyses (data not shown).

D   Representative images of spleen and lymph nodes from recipient mice transplanted with cells expressing the indicated combination of proteins (top) at the time of euthanasia. Scale bar, 1 cm.

E   Representative examples of hematoxylin–eosin-stained sections of a spleen (top) and a lymph node (bottom) from recipient mice transplanted with the indicated cells (top). Scale bars, 100 μm. $n = 4$ animals per class analyzed. RP, red pulp; WP, white pulp; C, cortex; M, medulla; V, venules.

F   Quantification of CD4$^+$ versus CD8$^+$ T-cell ratio in peripheral blood from mice transplanted with CD4$^+$ T cells expressing the indicated proteins (bottom). Each point represents the measurement of an individual mouse. n as in (B).

G   Surface expression of PD1 and CXCR5 in CD4$^+$-gated splenocytes from recipient mice transplanted with CD4$^+$ T cells expressing the indicated combination of proteins (top). Numbers indicate the relative percentage (%) of the cell population that has been interrogated (boxed).

H   Quantification of the percentage of T$_{FH}$ cells in CD4$^+$-gated splenocytes isolated the indicated experimental conditions. Each point represents the measurement of an individual mouse. n as in (B).

I   Example of a flow cytometry determination of ICOS expression in T$_{FH}$ cells from recipient mice transplanted with cells expressing the indicated proteins. The gray shaded histogram represents the fluorescence obtained with the isotype-matched control antibody.

J–L   Representative flow cytometry analysis (J) and quantification of the surface levels of ICOS (K) and CD69 (L) in T$_{FH}$ cells from mice transplanted with CD4$^+$ T cells expressing the indicated proteins. In (J), numbers indicate the relative percentage (%) of the cell population that has been interrogated (boxed). In (K and L), each point represents the values obtained with a single experimental mouse. n as in (H).

M   Abundance of indicated transcripts (bottom) in splenic cells from control (EGFP$^+$), tumor-bearing mice (expressing EGFP and Vav1$^{\Delta C}$) and mice transplanted with cells transduced with the catalytically dead version of Vav1$^{\Delta C}$ (expressing EGFP and Vav1$^{\Delta C+E201A}$). Values are given relative to the expression of each transcript in samples obtained from EGFP controls (which was given an arbitrary value of 1). $n = 4$ animals per class analyzed. a.u., arbitrary unit.

N, O   Flow cytometry determination of p-Akt (N) and p-Erk1/2 (O) levels in CD4$^+$ T$_{FH}$-gated splenocytes from recipient mice transplanted with cells expressing the indicated proteins (bottom). In both panels, each point represents the values obtained with a single experimental mouse. n as in (H).

Data information: In panels (F, H, K, L, M, N, and O), data represent the mean ± SEM. Statistical values obtained using the Student's t are given relative to control EGFP$^+$ cells. *$P \leq 0.05$; **$P \leq 0.01$; ***$P \leq 0.001$.

Source data are available online for this figure.

as SRF (Fig 5D), AP1 (Fig 5E), the NFAT–Tox axis (Fig 5F), and ICN1 (Fig 5G). Concurring with increased levels of Akt-mTORC signaling in Vav1$^{\Delta C}$-transformed cells (Figs 4N and O, and EV4A), we also identified gene signatures linked to the downregulation of Foxo (Fig EV5C), a transcriptional factor negatively regulated by p-Akt (Manning & Toker, 2017). Unbiased GSEAs further revealed the enrichment in E2F- (Figs 5H and EV5A) and Myc-regulated (Figs 5I and EV5A) gene signatures in this transcriptome.

Vav1$^{\Delta C}$ shares pathobiological programs with PTCL driver genes and human AITL

Given the AITL-like phenotype exhibited by Vav1$^{\Delta C}$-transformed T$_{FH}$ cells, we next decided to investigate the level of similarity of the transcriptome of those cells with the gene expression changes previously seen associated with the deletion of Tet2 and/or the expression of a dominant-negative (G17V mutation) version of the GTPase RhoA in CD4$^+$ T cells (Zang *et al*, 2017). It has been shown before that the combination of these two genetic events in CD4$^+$ T cells is required for driving the transformation of CD4$^+$ T cells (Zang *et al*, 2017; Cortes *et al*, 2018). This cooperativity has been attributed to the downmodulation of Foxo levels that take place upon *Tet2* ablation (Zang *et al*, 2017). In addition, we have included in these *in silico* comparisons the transcriptome previously described in the AITL-like condition that spontaneously develops in Swiss Jim Lambert (SJL)/J mice (Jain *et al*, 2015; Mhaidly *et al*, 2020). This disease is primarily derived from the exacerbation of IL21 signaling in T$_{FH}$ cells (Jain *et al*, 2015). *In silico* analyses revealed a high degree of similarity of the Vav1$^{\Delta C}$-driven transcriptome with those

found deregulated in *Tet2*$^{-/-}$ cells (490 genes), RhoA^{G17V}-expressing WT cells (394 genes), and RhoA^{G17V}-expressing *Tet2*$^{-/-}$ cells (576 genes) (Fig 5J and K, and Dataset EV2). Interestingly, all the genes associated with proliferative processes are found specifically enriched in the transcriptomal subset shared between Vav1$^{\Delta C}$-expressing cells and RhoA^{G17V}-expressing *Tet2*$^{-/-}$ cells (Dataset EV2). By contrast, the downmodulation of Foxo is found in the overlapping transcriptomes between Vav1$^{\Delta C}$-expressing cancer cells and the preneoplastic *Tet2*$^{-/-}$ cells (Dataset EV2). This further suggests that the Tet2-independent transformation triggered by Vav1$^{\Delta C}$ could be associated with the depletion of Foxo levels in T$_{FH}$ cells. We did not find any statistically significant similarity with the transcriptome previously described in the SJL/J mouse model, indicating that the similarity found between the Vav1$^{\Delta C}$ and the RhoA^{G17V}; *Tet2*$^{-/-}$ model is specific. In fact, in the case of SJL/J mice, we found quite opposite transcriptomal patterns when using GSEAs (Fig EV5D and E).

The above results indicate that 69% of the 2,277 genes found differentially expressed in Vav1$^{\Delta C}$-transformed cells are not shared by the rest of datasets used in these *in silico* analyses (Dataset EV3). This gene subset is basically enriched in proliferation-related genes (Fig EV5F), suggesting that Vav1$^{\Delta C}$ promotes the amplification rather than the rewiring of the transcriptomal changes commonly present in AITL cells. In line with this, we observed using further *in silico* analyses that this very specific Vav1$^{\Delta C}$ transcriptomal subset is associated with a larger enrichment in SRF, AP1, E2F, Myc, the NFAT–Tox axis, mTORC, and ICN1 gene signatures (Fig 5L). By contrast, the Foxo-related signature is quite similar between Vav1$^{\Delta C}$-expressing and Tet2-deficient cells (Fig 5L). This result

further emphasizes the convergent action of Vav1 GOF and Tet2 LOF events on the repression of this transcriptional factor.

Further *in silico* analyses indicated that the Vav1$^{\Delta C}$-driven transcriptome found in the transformed T$_{FH}$ cells bears high levels of similarity with the differential expression programs present in a large percentage of AITL patients (Fig EV5G and H). Such similarity is significantly higher in the Vav1$^{\Delta C}$ upregulated (49.5% of cross-species overlap) than in the downregulated (19.2% of cross-species overlap) gene subset (Fig EV5H). The overlapping transcriptomal subsets are enriched in gene signatures linked to the function of E2F
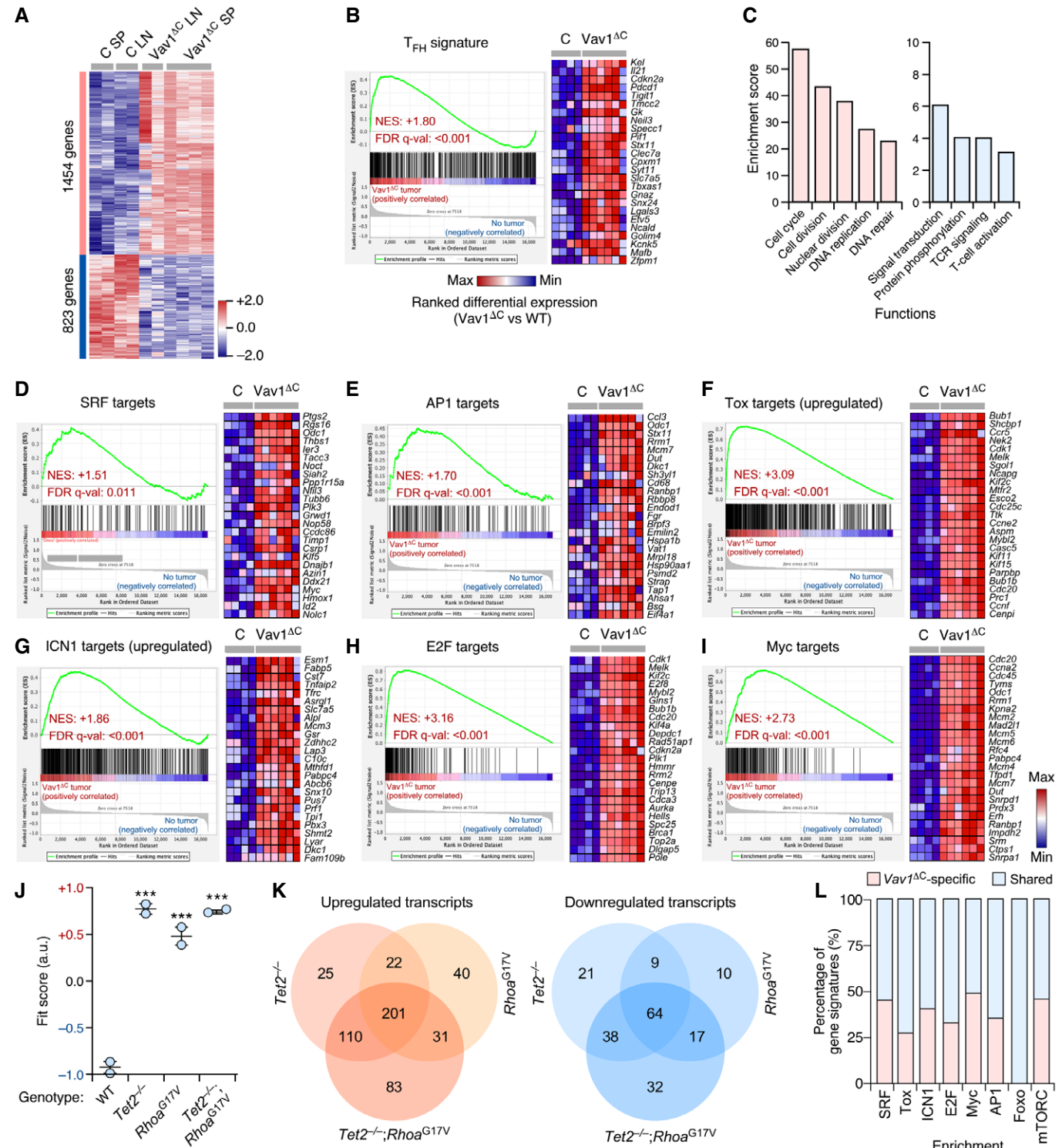

Figure 5.

Figure 5. Vav1$^{\Delta C}$ triggers a vast proliferative program in transformed T$_{FH}$ cells.

A   Genes up- (red) and downregulated (blue) in the tumor cells from lymph nodes (Vav1$^{\Delta C}$ LN) and spleen (Vav1$^{\Delta C}$ SP) of recipient mice transplanted with Vav1$^{\Delta C}$-expressing CD4$^+$ T cells. As comparative control, we used CD4$^+$ T cells from spleen (C SP) and lymph nodes (C LN) of control recipient mice. Rows represent individual genes. Columns represent experimental replicas. Total number of genes is indicated on the left. Relative changes in abundance are shown in color gradients according to the color scale shown on the right.
B   GSEA showing enrichment of T$_{FH}$-associated gene signatures in the transcriptome of Vav1$^{\Delta C}$-transformed cells. The expression profile of the top 25 leading-edge genes in the transcriptome of CD4$^+$ T cells from healthy control (C) and Vav1$^{\Delta C}$-tumor-bearing mice (Vav1$^{\Delta C}$) is shown. The normalized enrichment scores (NES) and false discovery rate values (FDR, using q values) are indicated inside the GSEA graph. Relative changes in abundance are shown in color gradients according to the color scale shown at the bottom. q-val, q value.
C   Main functional categories encoded by the Vav1$^{\Delta C}$-dependent transcriptome. For all of them, $P \leq 0.001$ (Fisher's exact test).
D–I GSEAs showing enrichment of indicated gene signatures (top) in the transcriptome of Vav1$^{\Delta C}$-transformed cells. In each case, we show the expression profile of the top 25 leading-edge genes in healthy control (C) and Vav1$^{\Delta C}$-tumor-bearing mice (Vav1$^{\Delta C}$). NES and FDR values (FDR, using q values) are indicated inside each GSEA graph. Relative changes in abundance are shown in color gradients according to the same color scale shown in panel (I).
J   Dot plot of the Vav1$^{\Delta C}$-dependent gene signature fit score in the indicated experimental groups (bottom) that were retrieved from a previous work (Zang et al, 2017). Dots represent values from an individual sample. Bars represent the mean enrichment value $\pm$ SEM for the overall sample set. ***$P \leq 0.001$ (according to Tukey's honest significance difference test).
K   Venn diagrams representing the number of up- (left) and downregulated (right) genes from the Vav1$^{\Delta C}$-dependent transcriptome shared with the indicated datasets.
L   Level of enrichment of indicated gene signatures that are either Vav1$^{\Delta C}$-specific (red) or shared with the different datasets (blue) used in panel (J).

and the NFAT–Tox axis, although SRF-, ICN1-, AP1-, Foxo-, and mTORC-related gene expression programs are also observed (Fig EV5I and J). As expected (Fig 5J and K), a similar overlap is seen between the transcriptomes of human and mouse RhoA^{G17V}; Tet2$^{-/-}$ AITL samples (Fig EV5J). However, unlike the case of the Vav1$^{\Delta C}$-driven transcriptome, we could not observe any consistent enrichment in this case in Notch1-related gene signatures (Fig EV5J, right panel). Collectively, these data indicate significant levels of similarity of the gene expression program of Vav1$^{\Delta C}$-transformed CD4$^+$ T cells and human AITL cases.

Vav1$^{\Delta C}$ drives proliferation in very early preneoplastic stages

To further dig into the signal transduction pathways and early pathobiological programs triggered by Vav1$^{\Delta C}$, we next analyzed its early effects in primary CD4$^+$ T cells (Fig 6A). To this end, CD4$^+$ lymphocytes were isolated from the spleen of WT mice, stimulated with antibodies to the TCR and CD28, and then infected with retroviral particles encoding bicistronically EGFP and the indicated versions of Vav1 (Fig 6B). Finally, the resulting EGFP$^+$ cells were analyzed three days later using a number of biological and signaling readouts (Fig 6A). In all cases, the effective transduction of cells and Vav1 expression obtained with each viral pool was assessed using both flow cytometry and immunoblotting (Fig 6C and D). These experiments demonstrated that the short-term expression of Vav1$^{\Delta C}$ promotes elevated levels of proliferation (Fig 6E and F) and expression of the NFAT target Tox (Fig 6G) in TCR plus CD28-primed cells. These two effects can be observed even though the stimulation of lymphocytes carried out before the transduction step already leads to a significant upregulation of these two readouts (Fig 6F and G). By contrast, the expression of Vav1^{WT} or Vav1$^{\Delta C+E201A}$ does not upregulate those two responses (Fig 6F and G). None of the interrogated Vav1 proteins changed the levels of ICOS (Fig 6H), CD25 (Fig 6I), or ICN1 (Fig 6J) in the primed cells. It is worth noting, however, that the effects of Vav1$^{\Delta C}$ on those three proteins could be obscured by the levels of induction that are already triggered upon the concurrent engagement of the TCR and the CD28 coreceptor in these cells (Fig 6H–J). The activation of

ICN1 under these cell stimulation conditions is consistent with previous data in CD4$^+$ T cells (Palaga et al, 2003; Steinbuck et al, 2018; Mitra et al, 2020).

Interestingly, we observed that both Vav1$^{\Delta C}$ and Vav1$^{\Delta C+E201A}$ promote higher levels of both p-Akt (Fig 6K and L; blue bars) and p-Erk (Fig 6M and N; blue bars) in primed cells when compared to the EGFP$^+$ and Vav1^{WT} controls. The restimulation of Vav1$^{\Delta C}$-expressing cells leads to a hysteresis response in the phosphorylation of those two signaling elements, a phenomenon that does not occur in the case of Vav1$^{\Delta C+E201A}$-expressing CD4$^+$ T cells (Fig 6L and N; red bars). These results indicate that the short-term expression of Vav1$^{\Delta C}$ in normal lymphocytes recapitulates many biological features that are subsequently observed in Vav1$^{\Delta C}$-transformed T$_{FH}$ cells.

Vav1$^{\Delta C}$-mediated proliferation requires engagement of several downstream pathways

The above experiments indicate that both the early signals and the long-term lymphomagenesis triggered by Vav1$^{\Delta C}$ in T$_{FH}$ cells are catalysis dependent. The lack of activity shown by the Vav1$^{\Delta C+E201A}$ mutant also suggests that the concurrent engagement of NFAT and ICN1 pathways cannot drive T-cell transformation per se. However, they do not clarify the issue of whether the catalysis-dependent pathways work fully autonomously or require the participation of other Vav1 downstream pathways to promote the abnormal proliferation of those cells. To tackle this issue, we included in these short-term experiments an additional mutant version of Vav1 that lacks both the CH and Ac domains (Vav1$^{\Delta N}$) (Fig 6B). This protein exhibits constitutive, phosphorylation-independent enzymatic activity due to the removal of the CH-Ac region (Schuebel et al, 1998; Zugaza et al, 2002). However, due to the lack of the CH domain and the presence of a functional CSH3, it cannot stimulate the PLCγ1-NFAT and ICN1 pathways (Wu et al, 1995; Robles-Valero et al, 2017) (Fig 6B). Due to this, this mutant is similar to those belonging to the uncoupling 4a subset described in Fig 2A. Despite being expressed at levels comparable to Vav1$^{\Delta C}$ in the transduced cells (Fig 6C), Vav1$^{\Delta N}$ cannot trigger the proliferation (Fig 6F) or the
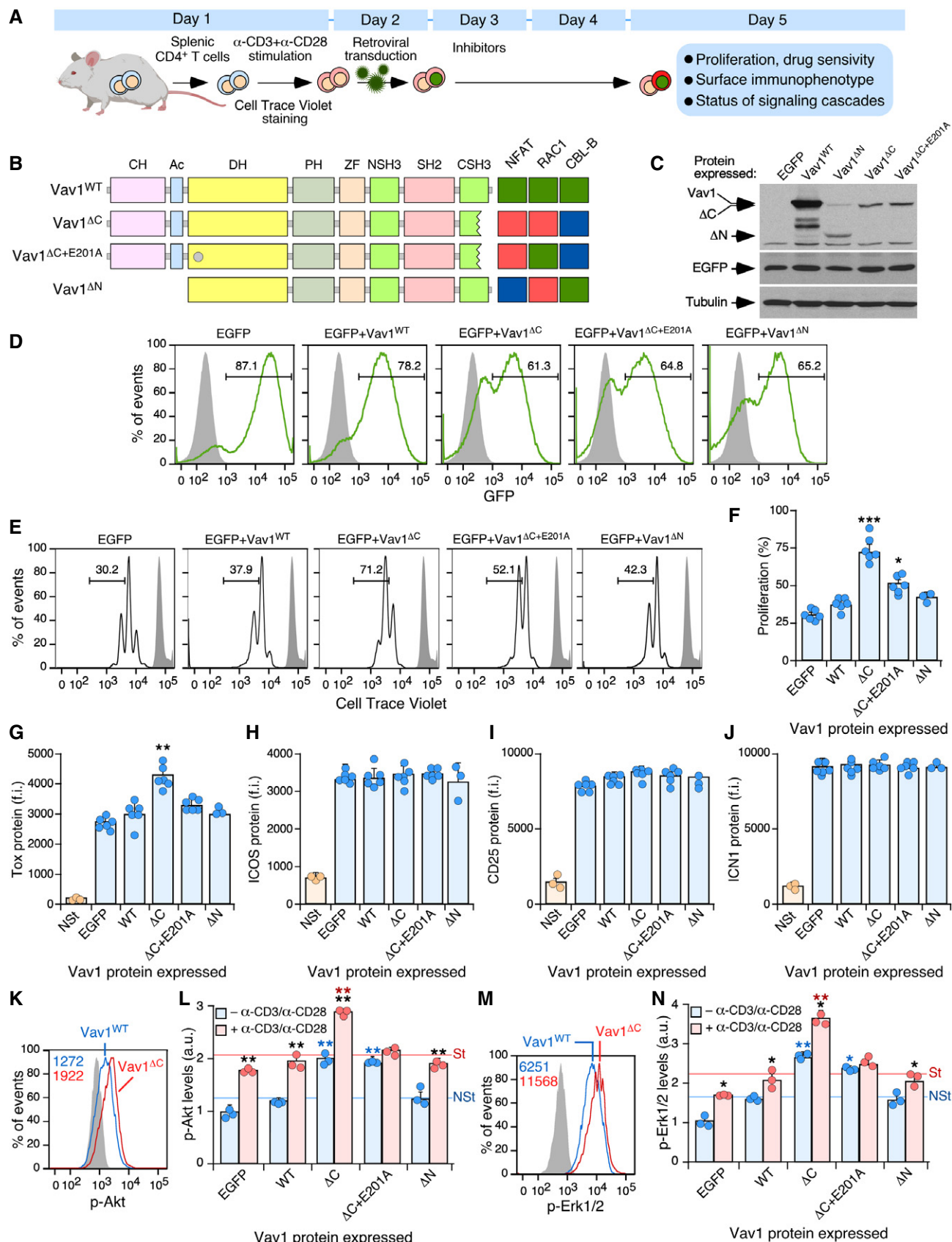
Figure 6.

Figure 6. Vav1$^{\Delta C}$-mediated proliferation requires engagement of several downstream pathways.

A   Schematic representation of the experiments used in this figure. See details in main text and Materials and Methods.
B   Depiction of the Vav1 mutants used in these experiments. The E201A mutation is shown as a gray circle. The activity of each mutant is represented on the right. Green box, WT activity; red box, gain of function; blue box, loss of function.
C   Representative immunoblot showing the abundance of the ectopic Vav1 proteins, EGFP, and the endogenous tubulin α (loading control) in CD4$^+$ T cells transduced with retrovirus particles used in these experiments (top).
D   Representative FACS plots showing EGFP epifluorescence in CD4$^+$ T cells transduced with retroviruses encoding the indicated proteins (top). Numbers indicate the relative percentage (%) of the EGFP$^+$ cell population in each case. Gray shaded histograms represent the fluorescence obtained from CD4$^+$ T cells nontransduced with retrovirus particles. Similar results were obtained in CD4$^+$ T cells transduced with virus encoding EGFP ($n = 6$), Vav1^{WT} ($n = 6$), Vav1$^{\Delta C}$ ($n = 6$), Vav1$^{\Delta C+E201A}$ ($n = 6$), and Vav1$^{\Delta N}$ ($n = 3$).
E, F   Representative FACS plots (E) and quantification (F) of the proliferation of EGFP$^+$ CD4$^+$ T cells expressing the indicated proteins using the Cell Trace Violet method. In (E), the gray shaded histograms represent the fluorescence obtained from nonstimulated CD4$^+$ T cells before stimulation and retroviral transduction. In (F), each point represents the values obtained with a single experimental mouse. $n = 6$ per each experimental condition, except in the case of Vav1$^{\Delta N}$ ($n = 3$).
G–J   Flow cytometry determination of Tox (G), ICOS (H), CD25 (I), and ICN1 (J) expression in EGFP$^+$ CD4$^+$ T cells expressing the indicated Vav1 proteins. NSt, nonstimulated cells (CD4$^+$ T cells before stimulation and retroviral transduction). In all panels, each point represents the values obtained for a single experimental condition. f.i., mean fluorescence intensity relative to the isotype-matched control antibody. $n = 6$ per each experimental condition, except for the Vav1$^{\Delta N}$ and NSt conditions ($n = 3$).
K–N   Example of a flow cytometry analysis (K and M) and final quantification of p-Akt (L) and p-Erk1/2 (N) levels in EGFP$^+$ CD4$^+$ T cells expressing the indicated Vav1 proteins in primed (blue bars) and restimulated (red bars) cells. In K and M, the gray shaded histograms represent the fluorescence obtained with the isotype-matched control antibody. In L and N, NSt, nonstimulated, St, stimulated. $n = 3$ per each experimental condition.

Data information: In panels (F, G, H, I, J, L, and N), values are shown as means ± SEM from three independent experiments. In panels L and N, *P*-values are given relative to nonstimulated (blue asterisks) and stimulated (red asterisks) cells expressing Vav1^{WT}. We also included *P*-values for the values exhibited by each Vav1 mutant protein relative to those obtained in nonstimulated condition (black asterisks). *$P \leq 0.05$; **$P \leq 0.01$; ***$P \leq 0.001$ (Student's *t*-test). Source data are available online for this figure.

elevation of Tox levels (Fig 6G) seen in Vav1$^{\Delta C}$-expressing CD4$^+$ T cells. Similarly, Vav1$^{\Delta N}$ cannot increase the levels of p-Akt (Fig 6L) and p-Erk (Fig 6N) in primed and restimulated cells. Vav1$^{\Delta N}$ shows in fact less activity than the Vav1$^{\Delta C+E201A}$ mutant in primed CD4$^+$ T cells before the restimulation step (Fig 6L and N; blue bars). These results suggest that the full perversion of these signaling responses requires, at least, the concurrent hyperstimulation of the CH- and catalysis-dependent signaling branches of Vav1. In addition, they indicate that those branches cooperate in a stepwise manner to promote (the CH-mediated pathway) and amplify (the catalysis-dependent pathway) the phosphorylation of both Akt and Erk in primed and restimulated CD4$^+$ T cells, respectively.

Given that we could not properly assess the role of Vav1$^{\Delta C}$ in the upregulation of ICN1 signaling in this experimental setting, we decided to indirectly address whether the activation of this pathway could affect the effects triggered by Vav1$^{\Delta C}$ in CD4$^+$ T lymphocytes. To this end, we used Compound E, an inhibitor that eliminates the proteolytic cleavage of NOTCH1 required to generate the active ICN1 fragment by blocking the γ-secretase endoproteinase (Kopan & Ilagan, 2009). We used as comparative control the treatment of cells with FK506, an inhibitor of the calmodulin-dependent calcineurin phosphatase (Fig 1A) (Clipstone & Crabtree, 1992). This protein catalyzes the dephosphorylation of cytoplasmic NFAT, an essential step for the nuclear translocation and activation of this transcriptional factor (Muller & Rao, 2010). The γ-secretase inhibitor abrogates the proliferative advantage (Fig 7A and B) and the elevation of Tox levels (Fig 7C) previously seen with Vav1$^{\Delta C}$ in the primed CD4$^+$ T cells. These effects are specific since Compound E does not affect these two readouts in the case of the control EGFP$^+$ cells (Fig 7A–C). As expected, this drug reduces the levels of ICN1 in both control and Vav1$^{\Delta C}$-expressing cells (Fig 7D). FK506 reduces the proliferation of both control (EGFP$^+$) and Vav1$^{\Delta C}$-expressing cells (Fig 7A and B). It also eliminates the upregulation of the NFAT-regulated Tox protein (Fig 7C) while it has no overt effects on the abundance of ICN1 (Fig 7D). We could not observe any effect

of those two compounds on ICOS levels (Fig 7E). These results indicate that Vav1$^{\Delta C}$ needs to engage at least the downstream Rac1 and NFAT pathways to effectively alter the proliferative state of primary CD4$^+$ T cells. They also indicate that NOTCH1 signals will play a relevant role in this process (Fig 7F).

Discussion

Our findings indicate that the *VAV1* mutations found in tumors can generate a complex panoply of signaling outcomes (Fig 2A). They have also provided new and, in some instances, quite unexpected information regarding the regulatory and effector layers of this protein. Thus, in addition to targeting well-established regulatory VAV1 hot spots, these mutations have unveiled: (i) An additional surface of the CSH3 domain involved in the intramolecular autoinhibition of the protein (encompassing residues G^{816} and G^{819}) (Fig 3A). (ii) New intramolecular regulatory areas associated with the DH α$_{11}$ helix-PH-ZF region (H^{399}, K^{404}, E^{556}). (iii) A quite unsuspected role the SH2 domain in the intramolecular inhibition of the protein that has been unveiled by the catalytic GOF effect found by mutations targeting the A^{673} and R^{678} residues (Fig 1C). (iv) Mutations causing signaling branch-specific effects in the RAC1 and NFAT pathways (Fig 2A, uncoupling subclasses 1 and 2). Those mutations target residues present in the CH (D26G), PH (K404R), NSH3 (G648C), SH2 (A673V, R678Q), and CSH3 (D797N, R822Q) regions. Similar uncoupling effects have been observed before with mutations targeting specific tyrosine phosphorylation and lysine acetylation sites of the protein (Barreira *et al*, 2014, 2018; Rodríguez-Fdez *et al*, 2020). In those cases, this effect has been associated with the freezing of the molecule in intermediary conformational states that precede the fully phosphorylated and activated condition (Barreira *et al*, 2014, 2018; Rodríguez-Fdez *et al*, 2020). It would be important to solve the structure of the some of these mutant proteins to figure out the exact conformational and signaling

problems associated with all these uncoupling effects. (v) Mutations that preferentially eliminate the binding of either HNRNPK or DNM2 to the VAV1 CSH3 (Figs 1F and EV2). The relevance of this change in the binding to downstream protein partners is currently unknown. However, it is intriguing that, similarly to CBL-B, HNRNPK and some DNM family members (e.g., DNM3) have been associated with tumor suppression functions (Gallardo *et al*, 2015; Zhang *et al*, 2016) (Fig 7F). Another possibility is that the main advantage created by these alterations is just the stimulation of the NFAT pathway that is commonly observed in all the mutants of this functional subtype (Fig 2A, uncoupling subclass 2). Addressing these possibilities, which are not mutually exclusive, deserves further attention in the near future.

Our adoptive T-cell transfer experiments with our collection of Vav1 mutants indicate that only the most potent mutations that lead to the concurrent hyperstimulation of the RAC1 and NFAT pathways will be able to autonomously drive T_{FH} cell lymphomagenesis in patients (see scheme in Fig 7F). Our short-term *in vivo* experiments
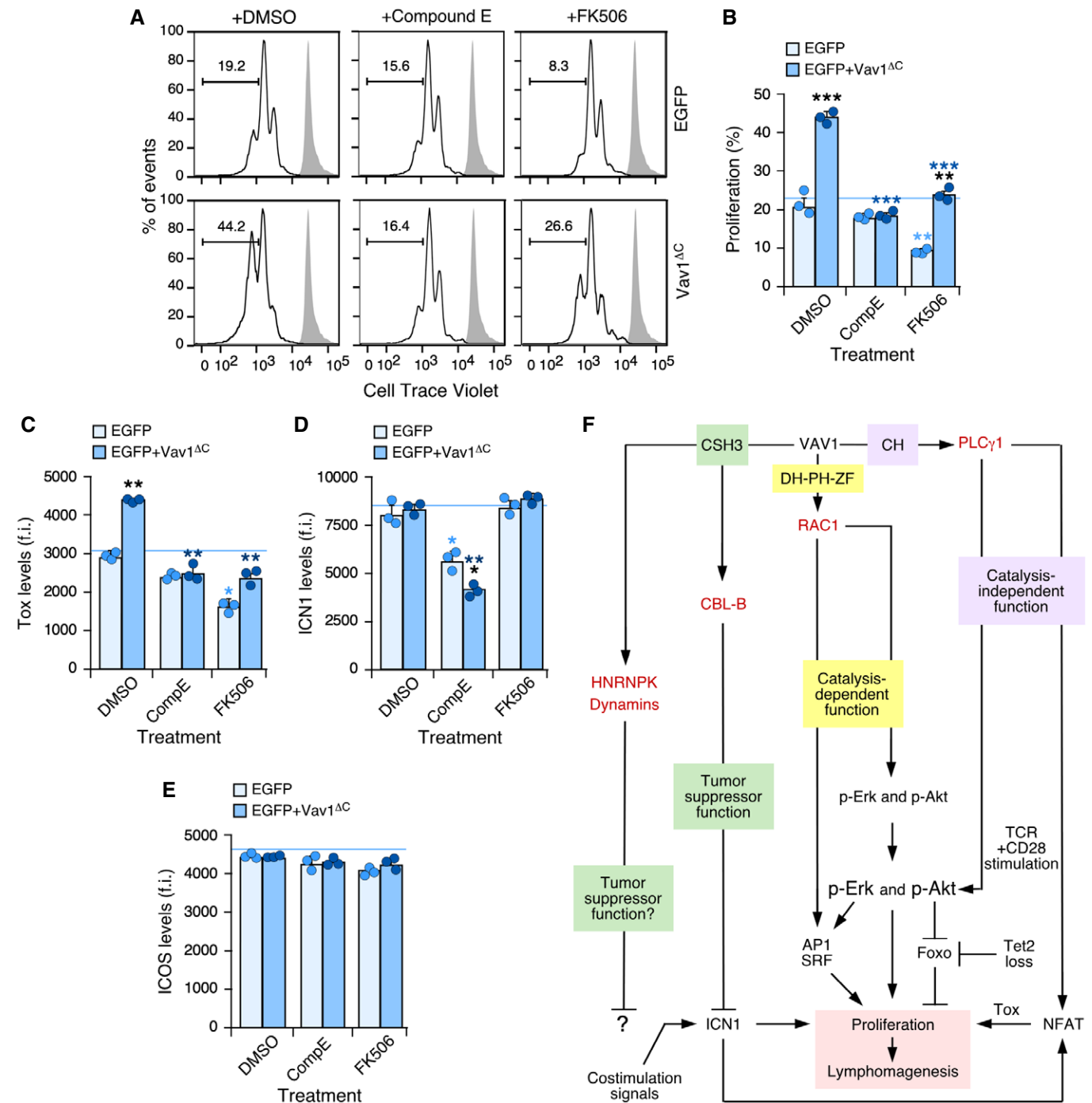

Figure 7.

Figure 7. **Vav1$^{\Delta C}$-driven CD4$^+$ T-cell proliferation requires ICN1 and proper calcineurin signaling.**

A, B   Representative FACS plots (A) and quantification (B) of the EGFP$^+$ CD4$^+$ T-cell proliferation in the different experimental groups (right) and indicated experimental conditions (top) using the Cell Trace Violet detection method. In A, gray shaded histograms represent the fluorescence obtained from nonstimulated CD4$^+$ T cells before stimulation and retroviral transduction. n = 3 independent experiments.

C–E   Flow cytometry determination of intracellular Tox (C), intracellular ICN1 (D), and surface ICOS (E) levels in EGFP$^+$ CD4$^+$ T cells expressing the indicated Vav1 proteins. f.i., mean fluorescence intensity relative to the isotype-matched control antibody. n = 3 independent experiments.

F   Summary of the Vav1-regulated signaling pathways that contribute to promote the proliferation of primary CD4$^+$ T cells that have been unveiled in this work. The other downstream effectors and pathways of Vav1 are indicated. The main primary effectors as shown in red.

Data information: In panels (B, C, D, and E), values are shown as means ± SEM from three independent experiments. *P*-values are given relative to nontreated (light blue asterisks) and treated (dark blue asterisks) EGFP$^+$ cells. We also include *P*-values for the values exhibited by each experimental group relative to those obtained in nontreated condition (black asterisks). *$P \leq 0.05$; **$P \leq 0.01$; ***$P \leq 0.001$ (Mann–Whitney U-test). Source data are available online for this figure.

also indicate that the NOTCH1-derived signals will be important to provide an extra proliferative boost to the cells bearing *VAV1* mutations (Fig 7F). These results agree with the observation that the most prevalent *VAV1* mutations found in AITL belong to the trivalent and bivalent subclasses. These data also suggest that the *VAV1* mutants that deregulate single signaling branches could only drive AITL when the pathways that retain WT-like activity in those mutants become hyperactivated by convergent pathways from other mutant proteins (e.g., NOTCH1, PLCγ1) or from strong costimulation signals from adjacent lymphoid or stromal cells.

Our work has also generated a new experimental model that can be used to better understand the etiology of AITL cases lacking *TET2* LOF mutations from the earliest preneoplastic to the full-blown transformed states. An inference from our study is that most PTCL-NOS cases that are *VAV1* mutation$^+$ will likely correspond to the recently characterized T$_{FH}$ subtype (Chiba & Sakata-Yanagimoto, 2020; Fiore *et al*, 2020). These two diseases are still poorly understood due to the relatively small number of cases available for study, their complex genetic make-up, and the multiple cancer cell-extrinsic processes affecting its evolution (Fiore *et al*, 2020). The results obtained with our mouse model support, in agreement with previous observations (de Leval *et al*, 2007; Piccaluga *et al*, 2007; Cortes *et al*, 2018; Fiore *et al*, 2020), that these tumors sprout from T$_{FH}$ cells. They also indicate that the preneoplastic phase of the disease is associated with a population of chronically activated T$_{FH}$ cells that can stay in stasis for long periods of time until shifting into a phase of rapid expansion and terminal disease. This long latency is in syntony with the usual detection of this disease in elderly people (Chiba & Sakata-Yanagimoto, 2020). It is likely, however, that this process can be accelerated by concurrent genetic lesions that could develop during this latency phase of the disease. Our data also suggest that *VAV1* mutant$^+$ patients could benefit from therapies based on the inhibition of the RAC1 and NFAT signaling elements and VAV1 itself. Interestingly, we have observed that the transcriptional program found in Vav1$^{\Delta C}$-transformed cells is quite similar to that previously observed in RHOA^{G17V}-expressing *Tet2$^{-/-}$* AITL cells. This suggests that AITL patients with these distinct mutational packages will exhibit similar clinical features and overlapping therapeutic vulnerabilities such as, dependency on exacerbated Akt, Erk, and ICOS signaling.

We have not detected the development of lymphomas with T$_{H1}$ or T$_{H2}$ features in our adoptive transfer experiments even though Vav1^{WT} does play roles in these lineages (Gulbranson-Judge *et al*, 1999; Tanaka *et al*, 2005). The reason for this selectivity is unknown, although it can be connected to recent observations indicating that the polarization toward the T$_{FH}$ lineage is associated with

a Bcl6- and ICOS-dependent block in the specification of both T$_H$ and T$_{reg}$ cells (Hatzi *et al*, 2015). The lack of detection of other PTLC subtypes in our mouse models is also unclear, although it might reflect the need of cooperating genetic events that could favor the rewiring of the T$_{FH}$ phenotype toward other lymphomagenic states (e.g., viral integrations in the case of ATLL) (Fiore *et al*, 2020). Alternatively, these subtypes might require more genetic lesions to take off. In fact, in humans, the genomic complexity of AITL cases is much lower than in the case of non-T$_{FH}$ GATA3$^+$ PTCL-NOS subtype (Heavican *et al*, 2019). However, Chiba and coworkers have reported during the elaboration of this work that transgenic mice expressing oncogenic Vav1 can develop GATA3$^+$ PTCL-NOS-like tumors when combined with full *Trp53* ablation (Fukumoto *et al*, 2020). The reason for the different spectra of tumors found in the transgenic mice and our adoptive transfer experiments is at present unclear. A plausible explanation is that the GATA3$^+$ PTCL-NOS tumors could have arisen by the combination of very high levels of expression of the Vav1 mutants and the *Trp53* null background in the transgenic animals. In this context, it is worth noting that the loss of *TP53* is usually associated with GATA$^+$ PTCL-NOS in humans (Heavican *et al*, 2019). Although with very limited numbers of patients scored, *VAV1* mutations have not been found so far in GATA3$^+$ PTCL-NOS patients (Heavican *et al*, 2019).

Future studies will be required to expand our understanding of the role of *VAV1* oncogenic mutations both autonomously and in synergy with other genetic lesions in AITL, PTCL, and other tumors such as NSCLC. Given that VAV1 is not expressed under physiological conditions in the lung epithelium (Bustelo *et al*, 1993), it is likely that the contribution of the mutant protein to tumorigenic processes in these cells will require genetic or epigenetic events that will trigger the spurious expression of the *VAV1* locus as previously described in cell lines (Ilan & Katzav, 2012). This might explain the low frequency of VAV1 mutations in NSCLC when compared to PTCL cases. The adoptive transfer experiments described here will also represent an ideal tool for testing preclinically new therapies against AITL, a disease whose poor prognosis has not significantly improved in the last 30 years (Chiba & Sakata-Yanagimoto, 2020; Fiore *et al*, 2020).

Materials and Methods

Ethics statement

All mouse experiments were performed according to protocols approved by the Bioethics Committee of the University of

Salamanca and the animal experimentation authorities of the autonomous Government of Castilla y León (Spain). We have not utilized patients or patient-derived samples in this work. No statistical methods were used to determine sample size. In all cases, we have used at least five mice per experiment. The exact sample size used in each experiment is indicated in the appropriate figure legend of the manuscript. Experimental groups were allocated randomly by a technician that was blind to the hypothesis to be tested.

3D structures

Three-dimensional structures were generated and analyzed in MacPyMol software using the Protein Data Bank-stored structure files for the Vav1 CH-Ac-DH-PH-C1 (PCD ID: 3KY9), the Vav1 DH-PH-ZF cassette bound to Rac1 (PCD ID: 2VRW), the Vav1 SH2 bound to the Syk phospho-peptide (PCD ID: 2MC1), and the Vav1 CSH3 (PCD ID: 2KBT) regions.

Plasmids

Most constructs used in this work used the mouse version of Vav1 when interrogating mutations in conserved residues between the human and mouse homologs. When this conservation did not occur (D^{26} and H^{399}), we used the plasmids encoding the human VAV1 protein. Plasmids encoding human VAV1^{WT} (pJRV58), mouse Vav1^{WT} (pJLZ52), and mouse Vav1^{Y174E} (pMB123) have been previously described (Zugaza *et al*, 2002; Abate *et al*, 2017; Barreira *et al*, 2018). Plasmids encoding human versions of the activated forms of RHO GTPases (RAC1^{Q61L}, RHOA^{Q63L}, and CDC42^{Q61L}) were a gift from P. Crespo (IBBTEC, CSIC-University of Cantabria, Santander, Spain). Mammalian expression vectors encoding the appropriate mutants were generated using either the pJLZ52 or the pJRV58 vectors as a template utilizing *in situ* mutagenesis techniques (QuikChange Mutagenesis Kit, Cat. No. 200518, Agilent Technologies). Oligonucleotides used in the mutagenesis steps are listed in Appendix Table S1. To generate the retroviral vectors encoding the different mouse Vav1 mutants plus EGFP protein, the *Vav1* cDNA was PCR amplified (NZYProof DNA polymerase, Cat. No. 14601; NZYTech) using the pJLZ52 plasmid as template, digested with BamHI and XhoI, and ligated into the pMIG-II vector (Cat. No. 52107, Addgene). The oligonucleotide primers used included those for Vav1^{WT} (pLFN119): 5′-CTG ACA GGA TCC GCC ACC ATG GAG CTC TGG CGA CAG TGC ACC CAC-3′ (forward, BamHI site underlined) and 5′-CTG ACA CTC GAG CGC TCA GCA ATA TTC GGA ATA GTC TTC CTC-3′ (reverse, XhoI site underlined); Vav1$^{Δ1-189}$ (pLFN120): 5′-CTG ACA GGA TCC GCC ACC ATG ACA GAG TAT GAT AAG CGC TGC TGC-3′ (forward; BamHI site underlined) and 5′-CTG ACA CTC GAG CGC TCA GCA ATA TTC GGA ATA GTC TTC CTC-3′ (reverse; XhoI site underlined) and Vav1$^{Δ835-845}$ (pLFN121): 5′-CTG ACA GGA TCC GCC ACC ATG GAG CTC TGG CGA CAG TGC ACC CAC-3′ (forward; BamHI site underlined) and 5′-CTG ACA CTC GAG CGC TCA AGA AGG GAA CCA GCC GAT CCG GCC-3′ (reverse; XhoI site underlined). All newly generated plasmids were subjected to DNA sequence analysis at the CIC Genomics Unit to confirm both the presence of the targeted mutations and absence of off-target ones.

The pNFAT-Luc plasmid was obtained from Addgene (Cat. No. 17870) whereas the pSRE-luc (Cat. number 219081), the pFR-Luc (Cat. number 219050), and pFA2-cJun (Cat. number 219053) plasmids were obtained from Stratagene. The pRL-SV40 plasmid was obtained from Promega (Cat. number E2231). The pGEX-4T3 plasmid was a gift from C. Guerrero (Cancer Research Center, CSIC, Salamanca, Spain). The pCL-Eco (Cat. No. 12371) and pMIG-II (Cat. No. 52107) plasmids were obtained from Addgene.

The pGEX vectors encoding the GST-CSH3^{WT} (pMB33) and GST-CSH3^{P833L} (pMB35) have been described before (Barreira *et al*, 2014). The rest of pGEX vectors encoding Vav1 CSH3 mutant versions were generated using pMB33 as template. Oligonucleotides used for these mutagenesis steps are also listed in Appendix Table S1.

Cell lines

All cells were obtained from the ATCC and authenticated periodically in the lab. COS1, HEK293, and NIH3T3 cells were grown in DMEM supplemented with 10% fetal calf serum, 1% L-glutamine, penicillin (10 μg/ml), and streptomycin (100 μg/ml). Jurkat cells were grown in RPMI-1640 medium supplemented with 10% fetal calf serum, 1% L-glutamine, penicillin (10 μg/ml), and streptomycin (100 μg/ml). All tissue culture reagents were obtained from Gibco-Thermo Fisher Scientific. All cell lines were maintained at 37°C in a humidified, 5% CO_2 atmosphere.

Luciferase reporter assays

In the case of SRF experiments, COS1 cells exponentially growing in 10-cm plates were transfected with liposomes (Lipofectamine 2000, Cat. No. 11668019, Thermo Fisher Scientific) with 1 μg of the pSRE-Luc, 1 ng of pRL-SV40 encoding the *Renilla* luciferase, and 1 μg of the appropriate experimental vectors. After 24 h, cells were lysed with Passive Lysis Buffer (Cat No. E1960, Promega) and luciferase activities determined using the Dual Luciferase Assay System (Cat No. E1960, Promega). In the case of JNK assays, 2×10^7 of exponentially growing Jurkat cells were electroporated (250 mV, 950 μF) with 20 μg of the appropriate expression vectors, the pRL-SV40 (5 ng) plus 10 and 5 μg of the pFR-Luc and pFA2-cJun, respectively. 36 h post-transfection, cells were either left nonstimulated or stimulated with antibodies to human CD3 (UCHT1 clone, Cat. No. 217570, Calbiochem, 5 μg/ml) for 7 h. Cells were then lysed with Passive Lysis Buffer (5×) and luciferase activities determined using the Dual Luciferase Assay System. In the case of NFAT assays, 2×10^7 of exponentially growing Jurkat cells were coelectroporated with 20 μg of the appropriate Vav1-encoding experimental vectors, the pNFAT-luc reporter vector (10 μg) and pRL-SV40 (5 ng). 36 h post-transfection, cells were either left nonstimulated or stimulated with antibodies to human CD3 and luciferase activities determined as above. In all cases, the values of firefly luciferase activity obtained in each experimental point were normalized considering the activity of the *Renilla* luciferase obtained in each experimental sample. In addition, we analyzed aliquots of the same lysates by Western blot to assess the appropriate expression of the ectopically expressed proteins interrogated in the experiments. Values are represented in graphs as the *n*-fold change in the experimental sample relative to the activity shown by mock-transfected cells (which was given an arbitrary value of 1 in each case). For heatmap representation, we used the heatmap3 R package including all Vav1-

dependent activities analyzed in this study (assigning to the values obtained with Vav1^{WT} an arbitrary number of 1). Adjusted *P*-values for multiple comparisons were calculated applying the Benjamini–Hochberg correction (FDR).

Western blot analyses

To determine abundance of proteins, cells were extensively washed with phosphate-buffered saline solution and broken in lysis buffer 1 (10 mM Tris–HCl [pH 8.0], 150 mM NaCl, 1% Triton X-100, 1 mM Na$_3$VO$_4$, 10 mM β-glycerophosphate, and a cocktail of protease inhibitors [Cømplete, Cat. No. 05056489001, Roche]). Cellular extracts were precleared by centrifugation at 20,000 *g* for 10 min at 4°C, denatured by boiling in 2× SDS–PAGE sample buffer, separated electrophoretically, and transferred onto nitrocellulose filters (Cat. No. 2022-04-26, Thermo Fisher) using the iBlot Dry Blotting System (Thermo Fisher). Membranes were blocked in 5% bovine serum albumin (Cat. No. A4503, Sigma-Aldrich) in TBS-T (25 mM Tris–HCl [pH 8.0], 150 mM NaCl, 0.1% Tween-20) for at least 1 h and then incubated overnight with the appropriate antibodies. Membranes were then washed three times with TBS-T, incubated with the appropriate secondary antibody (GE Healthcare) for 30 min at room temperature, and washed twice as above. Immunoreacting bands were visualized using a chemiluminescent method (ECL, Cat. No. RPN2209, Amersham). Primary antibodies used included those to the Vav1 DH (homemade, 1:10,000 dilution), tubulin α (Cat. No. CP06-100UG, Calbiochem; 1:2,000 dilution), CBL-B (Cat No. 9498, Cell Signaling Technologies; 1:1,000 dilution), DNM2 (Cat. No. ab65556, Abcam; 1:1,000 dilution), HNRNPK (Cat. No. sc-28380, Santa Cruz; 1:1,000 dilution), phospho-Vav1 (p-Tyr^{174}) (homemade, 1:10,000 dilution), phosphotyrosine residues (Cat. No. sc-7020, Santa Cruz; 1:1,000 dilution), Tp53 (Cat. No. 2524, Cell Signaling Technologies; 1:1,000 dilution), phospho-PKD/PKCμ (p-Ser$^{744/748}$) (Cat. No. 2054, Cell Signaling Technologies; 1:1,000 dilution), phospho-Akt (p-Ser^{473}) (Cat. No. 4051, Cell Signaling Technologies; 1:1,000 dilution), Akt (Cat. No. 2920, Cell Signaling Technologies; 1:1,000 dilution), phospho-Erk1/2 (p-Thr^{202} and p-Tyr^{204}) (Cat. No. 4370, Cell Signaling Technologies; 1:1,000 dilution), Erk1/2 (Cat. No. 4695, Cell Signaling Technologies; 1:1,000 dilution), β-actin (Cat. No. sc-47778, Santa Cruz; 1:2,000 dilution), and GFP (Cat. No. MMS-118P, Covance; 1:2,000 dilution).

RAC1, RHOA, and CDC42 GTPase activation assays

Exponentially growing COS1 and Jurkat cells were transfected with 1 μg and 20 μg of the appropriate experimental expression vector as above, respectively. Thirty-six hours post-transfection, the cells were washed with chilled phosphate-buffered solution and lysed in RIPA buffer [10 mM Tris–HCl (pH 8.0), 150 mM NaCl, 1% Triton X-100, 1 mM Na$_3$VO$_4$ (Sigma-Aldrich, Catalog No. S6508), 1 mM NaF (Sigma-Aldrich, Catalog No. S7920), and Cømplete] at 4°C. Extracts were precleared by centrifugation at 20,000 *g* for 10 min at 4°C and snap-frozen. Upon thawing and determination of total protein concentration (Bradford reactive, Cat. No. 5000006, Bio-Rad), extracts were analyzed using G-LISA Assay Kits according to the manufacturer's instructions (Cat. No. BK135, Cytoskeleton). Values are represented as the *n*-fold change in the experimental sample relative to the activity shown by mock-transfected cells (which was given an arbitrary value of 1 in each case). For heatmap

representation, we used the heatmap3 R package including all GTPase activities analyzed in this study (assigning to the values obtained with Vav1^{WT} an arbitrary number of 1). Adjusted *P*-values for multiple comparisons were calculated as above.

Purification of GST proteins

The expression of indicated GST proteins was induced *E. coli* using isopropyl β-D-1-thiogalactopyranoside (Cat. No. I5502, Sigma) and purified with glutathione-coated Sepharose beads (Cat. No. 17-0756-01, GE Healthcare Life Biosciences) (Barreira *et al*, 2014). Eluted proteins were dialyzed in phosphate-buffered saline solution and stored until use at −70°C.

Immunoprecipitations

A 2 × 10^6 of exponentially growing Jurkat cells were transfected with 20 μg of the appropriate expression vector (diluted in 100 μl of R buffer; Cat No. MPK10096, Life Technologies) using two 20-ms electroporation cycles at 1.7 mV in the Neon system (Life Technologies). Electroporated cells were then maintained in standard culture media for 36 h and disrupted in lysis buffer 1. Upon elimination of cell debris by centrifugation, cellular extracts were incubated for 2 h at 4°C with a primary antibody to Vav1. Immunocomplexes were collected with Gammabind G-Sepharose beads (Cat. No. 17-0885-01, GE Healthcare), washed three times in lysis buffer 1, resuspended in SDS–PAGE buffer, boiled for 5 min, electrophoresed, and subjected to immunoblot analyses with the appropriate antibodies.

GST pull-down experiments

A 1 × 10^7 of exponentially growing Jurkat cells were washed with phosphate-buffered saline solution and disrupted in lysis buffer 2 (20 mM Tris–HCl [pH 7.5], 150 mM NaCl, 5 mM MgCl$_2$, 0.5% Triton X-100, 5 mM β-glycerophosphate [Cat. No. 50020, Sigma-Aldrich], 1 mM dithiothreitol, and Cømplete). After eliminating cellular debris by centrifugation at 20,000 *g* for 10 min at 4°C, lysates were incubated for 2 h at 4°C with ≈ 20 μg of the indicated GST proteins. Protein complexes were trapped with glutathione-coated Sepharose beads, washed thrice in lysis buffer, resuspended in SDS–PAGE sample buffer, fractionated electrophoretically, and subjected to immunoblotting using antibodies to CBL-B, DNM2, and HNRNPK. To detect the GST proteins used in the pull-downs, the nitrocellulose filters containing the complexes were stained with a Ponceau solution before the Western blotting step. Aliquots of the same cell lysates that were used for the pull-down experiments were fractionated electrophoretically and subjected to immunoblot analyses to determine the total amount of endogenous protein present in each sample.

CD4$^+$ T-cell isolation and activation

Single cell suspensions were generated by mechanical homogenization of spleen and lymph nodes in 3 ml of phosphate-buffered saline solution supplemented with 2% bovine serum albumin and 0.5 mM EDTA (referred to hereafter as cell extraction buffer). Cells obtained were washed once by low-speed centrifugation, resuspended in cell extraction buffer, subjected to a 0.17 M NH$_4$Cl lysis step to eliminate erythrocytes, and filtered with a cell strainer (nylon mesh with 40-μm

pores, Cat. No. 352340, Falcon) to remove debris. Naïve CD4+ T cells were then purified by negative selection using the EasySep™ Mouse CD4+ T Cell Isolation Kit (Cat. No. 19852, StemCell Technologies) according to the manufacturer's protocol. 1×10^6 of purified CD4+ T cells were then cultured on goat-anti-hamster IgG (Cat. No. 31115, Invitrogen)-coated plate for 16–24 h in RPMI-1640 media containing 10% fetal bovine serum, glutamine, 50 μM 2-mercaptoethanol, antibodies to CD3 (Cat. No. 100202, BioLegend; 1 μg/ml), and antibodies to CD28 (Cat. No. 102102, BioLegend; 0.5 μg/ml). The quality of the purification step was always confirmed by flow cytometry.

Production of retroviral particles

To generate infectious retroviral particles, we transfected the retroviral plasmids together with the pCL-Eco packaging vector into HEK293T cells using the JetPEI transfection reagent (Cat. No. 101-10N, Polyplus). Retrovirus-containing supernatants were collected and concentrated using Lenti-X™ concentrator (Cat. No. 631231, Takara) by centrifugation at 2,000 g for 1 h at 4°C. Concentrated retroviruses were resuspended and tittered using infection of NIH3T3 cells and scoring GFP-positive cells by flow cytometry. Viruses with high titers were aliquoted and stored in −80°C for up to 2 months.

Ectopic expression of Vav1 mutants in CD4+ T cells

CD4+ T cells stimulated with antibodies to CD3 and CD28 for 16 h as indicated above were infected in the presence of polybrene (6 μg/ml; Cat. No. H9268-5G, Sigma-Aldrich) with retroviruses encoding the indicated proteins, pelleted by centrifugation (2,000 g at 32°C for 90 min), and treated with interleukin 2 (Cat. No. 200-02, PeproTech; 50 U/ml). The transduction efficiency was examined by flow cytometry 48 h after transduction. Transduced cells were then used either for adoptive T-cell transfer experiments or for short-term cell cultures as indicated below.

Adoptive T-cell transfer experiments

A 24–48 h after the retroviral transduction step, the EGFP+ CD4+ T cells were collected by centrifugation (2,000 g for 10 min) and resuspended in phosphate-buffered saline solution at a concentration of 1×10^4 cells/μl. A 100 μl of the cell resuspension was then introduced by retro-orbital injection into 6- to 8-week-old $Vav1^{-/-}$; $Vav2^{-/-}$; $Vav3^{-/-}$ recipient mice (Menacho-Marquez et al, 2013; Lorenzo-Martín et al, 2020). This lymphopenic mouse strain was used to minimize the potential rejection of the transplanted cells due to neoantigen expression (Lorenzo-Martín et al, 2020). Mice were then examined weekly until showing obvious physical signs of sickness. Aliquots of peripheral blood (100 μl) were analyzed by flow cytometry to detect changes in immune populations. Upon euthanasia, the indicated tissues and peripheral blood were collected for histological processing, flow cytometry analyses, and extraction of either total cellular proteins or RNAs.

Flow cytometry determinations of surface and intracellular proteins

Isolated cells were washed once in cell extraction buffer, resuspended in standard phosphate-buffered saline solution, and stained

following standard procedures with combinations of fluorescein isothiocyanate- (FITC, Cat. No. 553729), allophycocyanin- (APC, Cat. No. 553051), APC-Cy7- (Cat. No. 560181), or V500-labeled (Cat. No. 560783) antibodies to CD4; FITC- (Cat. No. 553031), Pacific blue- (PB, Cat. No. 558106), or phycoerythrin-labeled (PE, Cat. No. 553032) antibodies to CD8; APC- (Cat. No. 558643) or PE-Cy7-labeled (Cat. No. 552880) antibodies to CD25; peridinin chlorophyll-cyanin 5.5-labeled (PerCP-Cy5.5) antibody to B220 (Cat. No. 45-0452-82; eBiosciences); PE-labeled antibody to TCRβ (Cat. No. 12-5961-82, eBiosciences); FITC-labeled antibody to GL7 (Cat. No. 144603; BioLegend); PE-labeled antibody to PD1 (Cat. No. 12-9985-82; eBiosciences); PE-Cy7-labeled antibody to CXCR5 (Cat. No. 25-9185-42; eBiosciences); APC-labeled antibody to ICOS (Cat. No. 17-9949-82; eBiosciences); APC-labeled antibody to CD95 (Cat. No. 17-0951-82; eBiosciences), and a V450-labeled antibody to CD69 (Cat. No. 560690).

For intracellular Tox and ICN1 staining, cells were fixed with Cytofix/Cytoperm (Cat. No. 554714, BD Bioscience) for 10 min and stained with PE-labeled antibodies to Tox (Cat. No. 12-6502-82; eBiosciences; 1:50 dilution) or ICN1 (mN1A, Cat. No. 552768; 1:50 dilution) for 1 h at room temperature in phosphate-buffered saline solution supplemented with 5% fetal bovine serum and 10% saponin. For flow cytometry detection of phosphorylated intracellular proteins, cells were fixed with 2% formaldehyde, permeabilized with 90% ice-cold methanol, and incubated with antibodies to p-Erk1/2 (p-Thr^{202}/p-Tyr^{204}) (Cat. No. 4377, Cell Signaling Technologies; 1:200 dilution) and p-Akt (p-Ser^{473}) (Cat. No. 4060, Cell Signaling Technologies; 1:400 dilution). Cells were then stained with an Alexa-648-labeled secondary antibody to rabbit immunoglobulins (Cat. No. A21443, Invitrogen; 1:500 dilution). Unless otherwise stated, the antibodies used were from BD Biosciences. Antibody-stained cells were run in a FACSAria III flow cytometer (BD Biosciences) and data analyzed using the FlowJo software.

Determination of mRNA abundance

Total RNA was extracted from cells using NZYol (Cat. No. MB18501, NZYtech) and mRNAs purified using RNeasy Mini Kit (Cat. No. 74106, QIAGEN) following the manufacturer's protocol. mRNAs were analyzed by qRT–PCR using the iScript One-Step RT–PCR kit with SYBR green (Cat. No. 1708892, Bio-Rad) and the StepOnePlus Real-Time PCR System (Applied BioSystems). Raw qRT–PCR data were analyzed using the StepOne software v2.1 (Applied Biosystems), using the abundance of the endogenous *Actb* as internal normalization control. Primers used were 5′-ATG TGG GTC CGG CAG GTA CCC TGG-3′ (forward, *Pdcd1*), 5′-TCA AAG AGG CCA AGA ACA ATG TCC-3′ (reverse, *Pdcd1*), 5′-CTC GGC CGA TCA TAG GAT GT-3′ (forward, *Icos*), 5′-CTC CAC TAA GGT TCC TTT CTT-3′ (reverse, *Icos*), 5′-TGG CCT TCT ACA GTA ACA GCA-3′ (forward, *Cxcr5*), 5′-GCA TGA ATA CCG CCT TAA AGG AC-3′ (reverse, *Cxcr5*), 5′-CCT GCA ACT GGA AGA AGT ATA AG-3′ (forward, *Bcl6*), 5′-AGT ATG GAG GCA CAT CTC TGT AT-3′ (reverse, *Bcl6*), 5′-TCA TCA TTG ACC TCG TGG CCC-3′ (forward, *il21*), 5′-ATC GTA CTT CTC CAC TTG CAA TCC C-3′ (reverse, *il21*), 5′-GGC CAG CTG ATA TAA TGG AGA AAA-3′ (forward, *Hes1*), 5′-TCC ATG ATA GGC TTT GAT GAC TT-3′ (reverse, *Hes1*), 5′-CAC TGG CCC TGT CCA CCC AGC CTT GGC AGG-3′ (forward, *Dtx1*), 5′-ATG CGA ATT CGG GAA GGC GGG CAA CTC AGG-3′ (reverse, *Dtx1*), 5′-TCA

GGT GTC AGG CTC TAC CA-3′ (forward, *Ptcra*), 5′-ACC AGA CAG GGT TGT CAA GG-3′ (reverse, *Ptcra*), 5′-AGT AGG ACT GAG AAG GGA AAG T-3′ (forward, *Tet2*), 5′-CGG TTG TGC TGT CAT TTG TTT-3′ (reverse, *Tet2*), 5′-GTA TTT CAC CCT CAA GAT CC-3′ (forward, *Trp53*), 5′-TGG GCA TCC TTT AAC TCT A-3′ (reverse, *Trp53*), 5′-GTC CCT CAC CCT CCC AAA AG-3′ (forward, *Actb*), and 5′-GCT GCC TCA ACA CCT CAA CCC-3′ (reverse, *Actb*).

Gene expression profiling

These experiments included cells purified from both the spleen and lymph nodes to assess the potential contribution of each niche to the transcriptome of the cancer cells. To this end, total RNAs from control and Vav1$^{\Delta C}$-expressing EGFP$^+$ CD4$^+$ T cells from those two tissues were isolated using the RNAeasy Mini Kit (Qiagen, Catalog No. 74104) to be analyzed using Affymetrix platform (Clariom™ S Assay HT) at the CIC Genomics Core Facility according to the manufacture's recommendations.

Bioinformatics of microarray data

R version 3.6.3 was used for statistical analyses along with Python version 3.9 for text file processing. Signal intensity values were obtained from expression microarray CEL files after robust multi-chip average (RMA). Principal component analyses were generated using the factoextra R package. Differentially expressed genes were identified using linear models for microarray data (limma). Adjusted *P*-values for multiple comparisons were calculated applying the Benjamini–Hochberg correction (FDR). Gene Ontology and KEGG pathways enrichment analyses were performed using DAVID (https://david.ncifcrf.gov). Expression heatmaps were generated using the heatmap3 R package. Volcano plots were generated using the Glimma R package. GSEAs were performed with described gene sets using gene set permutations ($n = 1,000$) for the assessment of significance and signal-to-noise metric for ranking genes. The data-sets used were those for: AP1 (Gustems *et al*, 2014), SRF (Selvaraj & Prywes, 2004), ICN1 (Li *et al*, 2008), the Molecular Signatures Database (MSigDB v7.2, for E2F, G_2/M checkpoint, Myc and Foxo), T_{FH} cells (Weinstein *et al*, 2014), Tox (Scott *et al*, 2019), and SJL mice (Jain *et al*, 2015). To evaluate the Vav1$^{\Delta C}$-associated gene signature fitness across the mouse *Rhoa*^{G17V} and *Tet2* mutant CD4$^+$ T-cell signatures (Zang *et al*, 2017), SJL mice (Jain *et al*, 2015), and human PTCL (Maura *et al*, 2019), the enrichment scores for both the upregulated and downregulated signatures found in Vav1$^{\Delta C}$-transformed AITL cells were calculated using single-sample GSEA. The difference between the two normalized enrichment scores yielded the fit score, a measure of the enrichment and depletion of the upregulated and downregulated signatures, respectively. The Vav1$^{\Delta C}$-specific gene signature was established by comparing the full Vav1$^{\Delta C}$-associated gene signature with the differential transcriptomes of *Tet2*$^{-/-}$, *Rhoa*^{G17V}, and *Tet2*$^{-/-}$; *Rhoa*^{G17V} CD4$^+$ T cells (Zang *et al*, 2017).

Evaluation of short-term effects of proteins in CD4$^+$ T cells

Splenic and lymph node CD4$^+$ T cells purified as above were stained with Cell Trace Violet (Cat. No. C34557, Life Technologies) following the manufacturer's protocol. T cells were then cultured on goat-

anti-hamster IgG-coated plates for 16–24 h in RPMI-1640 media as above to stimulate them. Upon activation, cells were infected with the indicated retroviral particles in the presence of interleukin 2 (Cat. No. 200-02, PeproTech; 50 U/ml) and, three days later, were processed to measure the indicated biological and signaling parameters by flow cytometry. In the case of experiments using drug inhibitors, the CD4$^+$ T cells were isolated, activated, and infected as above and, 24 h after infection, treated with 200 nM Compound E (Cat. No. ALX-270-415-C250, Enzo Life Sciences), 10 μM FK506 (Cat. No. tlrl-fk5, Invitrogen), or solution control (DMSO). Three days later, cells were collected for flow cytometry experiments as indicated above.

Statistics

Calculations were performed using Microsoft Excel 2020 and GraphPad Prism software (version 6.0). The number of biological replicates (n), the type of statistical tests performed, and the statistical significance are indicated for each experiment in the figure legends as well as the Results section of this document. Parametric and nonparametric distributions were analyzed using Student's t-test and Mann–Whitney test, respectively. Chi-squared tests were used to determine the significance of the differences between expected and observed frequencies. Tukey's honest significance difference test was used to identify groups showing differential enrichment of the indicated signatures. Statistical analyses of the immunoblot-generated data were carried out using the GraphPad Prism software (version 6.0). In all cases, values were considered significant when $P \leq 0.05$. Data obtained are given as the mean $\pm$ SEM.

Data availability

A Source Data file is provided with this paper. All relevant data are available from the corresponding author upon reasonable request. Microarray data reported in this paper have been deposited in the GEO database (https://www.ncbi.nlm.nih.gov/geo/) under the accession number GSE165006.

Author contributions

JR-V participated in all experimental work, analyzed data, and contributed to both artwork design and manuscript writing. LF-N and ENA-S carried out experimental work related to the characterization of the biological activity of Vav1 mutants. MC and AA helped in animal model-based experiments. LFL-M and RC carried out the *in silico* analyses. IF-P collaborated in the adoptive transfer experiments. SR-F contributed to the characterization of the SH2 mutants. XRB conceived the work, analyzed data, wrote the manuscript, and carried out the final editing of figures.

Conflict of interest

The authors declare that they have no conflict of interest.

References

Abate F, da Silva-Almeida AC, Zairis S, Robles-Valero J, Couronne L, Khiabanian H, Quinn SA, Kim M-Y, Laginestra MA, Kim C *et al* (2017) Activating mutations and translocations in the guanine exchange factor VAV1 in peripheral T-cell lymphomas. *Proc Natl Acad Sci U S A* 114: 764−769

Aghazadeh B, Lowry WE, Huang XY, Rosen MK (2000) Structural basis for relief of autoinhibition of the Dbl homology domain of proto-oncogene Vav by tyrosine phosphorylation. *Cell* 102: 625−633

Barreira M, Fabbiano S, Couceiro JR, Torreira E, Martínez-Torrecuadrada JL, Montoya G, Llorca O, Bustelo XR (2014) The C-terminal SH3 domain contributes to the intramolecular inhibition of Vav family proteins. *Sci Signal* 7: ra35

Barreira M, Rodriguez-Fdez S, Bustelo XR (2018) New insights into the Vav1 activation cycle in lymphocytes. *Cell Signal* 45: 132−144

Boddicker RL, Razidlo GL, Dasari S, Zeng YU, Hu G, Knudson RA, Greipp PT, Davila JI, Johnson SH, Porcher JC *et al* (2016) Integrated mate-pair and RNA sequencing identifies novel, targetable gene fusions in peripheral T-cell lymphoma. *Blood* 128: 1234−1245

Bustelo XR (2014) Vav family exchange factors: an integrated regulatory and functional view. *Small GTPases* 5: e973757

Bustelo XR, Barbacid M (1992) Tyrosine phosphorylation of the vav proto-oncogene product in activated B cells. *Science* 256: 1196−1199

Bustelo XR, Dosil M (2016) The Vav family. In: *Encyclopedia of signaling molecules*, Choi S (ed.), pp. 1−15. New York, NY: Springer

Bustelo XR, Ledbetter JA, Barbacid M (1992) Product of vav proto-oncogene defines a new class of tyrosine protein kinase substrates. *Nature* 356: 68−71

Bustelo XR, Rubin SD, Suen KL, Carrasco D, Barbacid M (1993) Developmental expression of the vav protooncogene. *Cell Growth Differ* 4: 297−308

Bustelo XR, Suen KL, Michael WM, Dreyfuss G, Barbacid M (1995) Association of the vav proto-oncogene product with poly(rC)-specific RNA-binding proteins. *Mol Cell Biol* 15: 1324−1332

Campbell JD, Alexandrov A, Kim J, Wala J, Berger AH, Pedamallu CS, Shukla SA, Guo G, Brooks AN, Murray BA *et al* (2016) Distinct patterns of somatic genome alterations in lung adenocarcinomas and squamous cell carcinomas. *Nat Genet* 48: 607−616

Chiba S, Sakata-Yanagimoto M (2020) Advances in understanding of angioimmunoblastic T-cell lymphoma. *Leukemia* 34: 2592−2606

Chrencik JE, Brooun A, Zhang H, Mathews II, Hura GL, Foster SA, Perry JJP, Streiff M, Ramage P, Widmer H *et al* (2008) Structural basis of guanine nucleotide exchange mediated by the T-cell essential Vav1. *J Mol Biol* 380: 828−843

Clipstone NA, Crabtree GR (1992) Identification of calcineurin as a key signalling enzyme in T-lymphocyte activation. *Nature* 357: 695−697

Cortes JR, Ambesi-Impiombato A, Couronne L, Quinn SA, Kim CS, da Silva Almeida AC, West Z, Belver L, Martin MS, Scourzic L *et al* (2018) RHOA[G17V] Induces T follicular helper cell specification and promotes lymphomagenesis. *Cancer Cell* 33: 259−273.e257

Couceiro JR, Martin-Bermudo MD, Bustelo XR (2005) Phylogenetic conservation of the regulatory and functional properties of the Vav oncoprotein family. *Exp Cell Res* 308: 364−380

Crescenzo R, Abate F, Lasorsa E, Tabbo' F, Gaudiano M, Chiesa N, Di Giacomo F, Spaccarotella E, Barbarossa L, Ercole E *et al* (2015) Convergent mutations and kinase fusions lead to oncogenic STAT3 activation in anaplastic large cell lymphoma. *Cancer Cell* 27: 516−532

Crespo P, Schuebel KE, Ostrom AA, Gutkind JS, Bustelo XR (1997) Phosphotyrosine-dependent activation of Rac-1 GDP/GTP exchange by the vav proto-oncogene product. *Nature* 385: 169−172

de Leval L, Rickman DS, Thielen C, Reynies AD, Huang Y-L, Delsol G, Lamant L, Leroy K, Brière J, Molina T *et al* (2007) The gene expression profile of nodal peripheral T-cell lymphoma demonstrates a molecular link between angioimmunoblastic T-cell lymphoma (AITL) and follicular helper T (TFH) cells. *Blood* 109: 4952−4963

Fiore D, Cappelli LV, Broccoli A, Zinzani PL, Chan WC, Inghirami G (2020) Peripheral T cell lymphomas: from the bench to the clinic. *Nat Rev Cancer* 20: 323−342

Fujikawa K, Miletic AV, Alt FW, Faccio R, Brown T, Hoog J, Fredericks J, Nishi S, Mildiner S, Moores SL *et al* (2003) Vav1/2/3-null mice define an essential role for Vav family proteins in lymphocyte development and activation but a differential requirement in MAPK signaling in T and B cells. *J Exp Med* 198: 1595−1608

Fukumoto K, Sakata-Yanagimoto M, Fujisawa M, Sakamoto T, Miyoshi H, Suehara Y, Nguyen TB, Suma S, Yanagimoto S, Shiraishi Y *et al* (2020) VAV1 mutations contribute to development of T-cell neoplasms in mice. *Blood* 136: 3018−3032

Gallardo M, Lee H, Zhang X, Bueso-Ramos C, Pageon L, McArthur M, Multani A, Nazha A, Manshouri T, Parker-Thornburg J *et al* (2015) hnRNP K is a haploinsufficient tumor suppressor that regulates proliferation and differentiation programs in hematologic malignancies. *Cancer Cell* 28: 486−499

Gomez TS, Hamann MJ, McCarney S, Savoy DN, Lubking CM, Heldebrant MP, Labno CM, McKean DJ, McNiven MA, Burkhardt JK *et al* (2005) Dynamin 2 regulates T cell activation by controlling actin polymerization at the immunological synapse. *Nat Immunol* 6: 261−270

Gulbranson-Judge A, Tybulewicz VL, Walters AE, Toellner KM, MacLennan IC, Turner M (1999) Defective immunoglobulin class switching in Vav-deficient mice is attributable to compromised T cell help. *Eur J Immunol* 29: 477−487

Gustems M, Woellmer A, Rothbauer U, Eck SH, Wieland T, Lutter D, Hammerschmidt W (2014) c-Jun/c-Fos heterodimers regulate cellular genes via a newly identified class of methylated DNA sequence motifs. *Nucleic Acids Res* 42: 3059−3072

Hatzi K, Nance JP, Kroenke MA, Bothwell M, Haddad EK, Melnick A, Crotty S (2015) BCL6 orchestrates Tfh cell differentiation via multiple distinct mechanisms. *J Exp Med* 212: 539−553

Heavican TB, Bouska A, Yu J, Lone W, Amador C, Gong Q, Zhang W, Li Y, Dave BJ, Nairismägi M-L *et al* (2019) Genetic drivers of oncogenic pathways in molecular subgroups of peripheral T-cell lymphoma. *Blood* 133: 1664 − 1676

Ilan L, Katzav S (2012) Human Vav1 expression in hematopoietic and cancer cell lines is regulated by c-Myb and by CpG methylation. *PLoS One* 7: e29939

Jain S, Chen J, Nicolae A, Wang H, Shin D-M, Adkins EB, Sproule TJ, Leeth CM, Sakai T, Kovalchuk AL *et al* (2015) IL-21-driven neoplasms in SJL mice mimic some key features of human angioimmunoblastic T-cell lymphoma. *Am J Pathol* 185: 3102 − 3114

Kataoka K, Nagata Y, Kitanaka A, Shiraishi Y, Shimamura T, Yasunaga J-I, Totoki Y, Chiba K, Sato-Otsubo A, Nagae G *et al* (2015) Integrated molecular analysis of adult T cell leukemia/lymphoma. *Nat Genet* 47: 1304 − 1315

Katzav S, Martin-Zanca D, Barbacid M (1989) Vav, a novel human oncogene derived from a locus ubiquitously expressed in hematopoietic cells. *EMBO J* 8: 2283 − 2290

Kopan R, Ilagan MX (2009) The canonical Notch signaling pathway: unfolding the activation mechanism. *Cell* 137: 216 − 233

Kuhne MR, Ku G, Weiss A (2000) A guanine nucleotide exchange factor-independent function of Vav1 in transcriptional activation. *J Biol Chem* 275: 2185 − 2190

Li X, Gounari F, Protopopov A, Khazaie K, von Boehmer H (2008) Oncogenesis of T-ALL and nonmalignant consequences of overexpressing intracellular NOTCH1. *J Exp Med* 205: 2851 − 2861

Lopez-Lago M, Lee H, Cruz C, Movilla N, Bustelo XR (2000) Tyrosine phosphorylation mediates both activation and downmodulation of the biological activity of Vav. *Mol Cell Biol* 20: 1678 − 1691

Lorenzo-Martín LF, Fernández-Parejo N, Menacho-Márquez M, Rodríguez-Fdez S, Robles-Valero J, Zumalave S, Fabbiano S, Pascual G, García-Pedrero JM, Abad A *et al* (2020) VAV2 signaling promotes regenerative proliferation in both cutaneous and head and neck squamous cell carcinoma. *Nat Commun* 11: 4788

Manning BD, Toker A (2017) AKT/PKB signaling: navigating the network. *Cell* 169: 381 − 405

Martinez GJ, Hu JK, Pereira RM, Crampton JS, Togher S, Bild N, Crotty S, Rao A (2016) Cutting edge: NFAT transcription factors promote the generation of follicular helper T cells in response to acute viral infection. *J Immunol* 196: 2015 − 2019

Maura F, Agnelli L, Leongamornlert D, Bolli N, Chan WC, Dodero A, Carniti C, Heavican TB, Pellegrinelli A, Pruneri G *et al* (2019) Integration of transcriptional and mutational data simplifies the stratification of peripheral T-cell lymphoma. *Am J Hematol* 94: 628 − 634

Menacho-Marquez M, Garcia-Escudero R, Ojeda V, Abad A, Delgado P, Costa C, Ruiz S, Alarcon B, Paramio JM, Bustelo XR (2013) The Rho exchange factors Vav2 and Vav3 favor skin tumor initiation and promotion by engaging extracellular signaling loops. *PLoS Biol* 11: e1001615

Mhaidly R, Krug A, Gaulard P, Lemonnier F, Ricci JE, Verhoeyen E (2020) New preclinical models for angioimmunoblastic T-cell lymphoma: filling the GAP. *Oncogenesis* 9: 73

Mitra A, Shanthalingam S, Sherman HL, Singh K, Canakci M, Torres JA, Lawlor R, Ran Y, Golde TE, Miele L *et al* (2020) CD28 signaling drives notch ligand expression on CD4 T cells. *Front Immunol* 11: 735

Moon CS, Reglero C, Cortes JR, Quinn SA, Alvarez S, Zhao J, Lin WW, Cooke AJ, Abate F, Soderquist CR *et al* (2021) FYN-TRAF3IP2 induces NF-κB signaling-driven peripheral T cell lymphoma. *Nat Cancer* 2: 98 − 113

Movilla N, Bustelo XR (1999) Biological and regulatory properties of Vav-3, a new member of the Vav family of oncoproteins. *Mol Cell Biol* 19: 7870 − 7885

Muller MR, Rao A (2010) NFAT, immunity and cancer: a transcription factor comes of age. *Nat Rev Immunol* 10: 645 − 656

Palaga T, Miele L, Golde TE, Osborne BA (2003) TCR-mediated Notch signaling regulates proliferation and IFN-gamma production in peripheral T cells. *J Immunol* 171: 3019 − 3024

Park J, Yang J, Wenzel AT, Ramachandran A, Lee WJ, Daniels JC, Kim J, Martinez-Escala E, Amankulor N, Pro B *et al* (2017) Genomic analysis of 220 CTCLs identifies a novel recurrent gain-of-function alteration in RLTPR (p. Q575E). *Blood* 130: 1430 − 1440

Piccaluga PP, Agostinelli C, Califano A, Carbone A, Fantoni L, Ferrari S, Gazzola A, Gloghini A, Righi S, Rossi M *et al* (2007) Gene expression analysis of angioimmunoblastic lymphoma indicates derivation from T follicular helper cells and vascular endothelial growth factor deregulation. *Cancer Res* 67: 10703 − 10710

Rapley J, Tybulewicz VL, Rittinger K (2008) Crucial structural role for the PH and C1 domains of the Vav1 exchange factor. *EMBO Rep* 9: 655 − 661

Robles-Valero J, Lorenzo-Martin LF, Menacho-Marquez M, Fernandez-Pisonero I, Abad A, Camos M, Toribio ML, Espinosa L, Bigas A, Bustelo XR (2017) A paradoxical tumor-suppressor role for the Rac1 exchange factor Vav1 in T cell acute lymphoblastic leukemia. *Cancer Cell* 32: 608 − 623.e609

Rodriguez-Fdez S, Bustelo XR (2019) The Vav GEF family: an evolutionary and functional perspective. *Cells* 8: E465

Rodríguez-Fdez S, Fernández-Nevado L, Lorenzo-Martín LF, Bustelo XR (2020) Lysine acetylation reshapes the downstream signaling landscape of Vav1 in lymphocytes. *Cells* 9: 609

Schuebel KE, Movilla N, Rosa JL, Bustelo XR (1998) Phosphorylation-dependent and constitutive activation of Rho proteins by wild-type and oncogenic Vav-2. *EMBO J* 17: 6608 − 6621

Scott AC, Dündar F, Zumbo P, Chandran SS, Klebanoff CA, Shakiba M, Trivedi P, Menocal L, Appleby H, Camara S *et al* (2019) TOX is a critical regulator of tumour-specific T cell differentiation. *Nature* 571: 270 − 274

Selvaraj A, Prywes R (2004) Expression profiling of serum inducible genes identifies a subset of SRF target genes that are MKL dependent. *BMC Mol Biol* 5: 13

Steinbuck MP, Arakcheeva K, Winandy S (2018) Novel TCR-mediated mechanisms of notch activation and signaling. *J Immunol* 200: 997 − 1007

Tanaka Y, So T, Lebedeva S, Croft M, Altman A (2005) Impaired IL-4 and c-Maf expression and enhanced Th1-cell development in Vav1-deficient mice. *Blood* 106: 1286 − 1295

Vallois D, Dobay MPD, Morin RD, Lemonnier F, Missiaglia E, Juilland M, Iwaszkiewicz J, Fataccioli V, Bisig B, Roberti A *et al* (2016) Activating mutations in genes related to TCR signaling in angioimmunoblastic and other follicular helper T-cell-derived lymphomas. *Blood* 128: 1490 − 1502

Weinstein JS, Lezon-Geyda K, Maksimova Y, Craft S, Zhang Y, Su M, Schulz VP, Craft J, Gallagher PG (2014) Global transcriptome analysis and enhancer landscape of human primary T follicular helper and T effector lymphocytes. *Blood* 124: 3719 − 3729

Wu J, Katzav S, Weiss A (1995) A functional T-cell receptor signaling pathway is required for p95vav activity. *Mol Cell Biol* 15: 4337 − 4346

Xu W, Zhao X, Wang X, Feng H, Gou M, Jin W, Wang X, Liu X, Dong C (2019) The transcription factor Tox2 drives T follicular helper cell development via regulating chromatin accessibility. *Immunity* 51: 826 − 839.e825

Yoo HY, Sung MK, Lee SH, Kim S, Lee H, Park S, Kim SC, Lee B, Rho K, Lee J-E *et al* (2014) A recurrent inactivating mutation in RHOA GTPase in angioimmunoblastic T cell lymphoma. *Nat Genet* 46: 371 − 375

Yu B, Martins IR, Li P, Amarasinghe GK, Umetani J, Fernandez-Zapico ME, Billadeau DD, Machius M, Tomchick DR, Rosen MK (2010) Structural and energetic mechanisms of cooperative autoinhibition and activation of Vav1. *Cell* 140: 246–256

Zang S, Li J, Yang H, Zeng H, Han W, Zhang J, Lee M, Moczygemba M, Isgandarova S, Yang Y *et al* (2017) Mutations in 5-methylcytosine oxidase TET2 and RhoA cooperatively disrupt T cell homeostasis. *J Clin Invest* 127: 2998–3012

Zhang Z, Chen C, Guo W, Zheng S, Sun Z, Geng X (2016) DNM3 attenuates hepatocellular carcinoma growth by activating P53. *Med Sci Monit* 22: 197–205

Zugaza JL, Lopez-Lago MA, Caloca MJ, Dosil M, Movilla N, Bustelo XR (2002) Structural determinants for the biological activity of Vav proteins. *J Biol Chem* 277: 45377–45392

Expanded View Figures
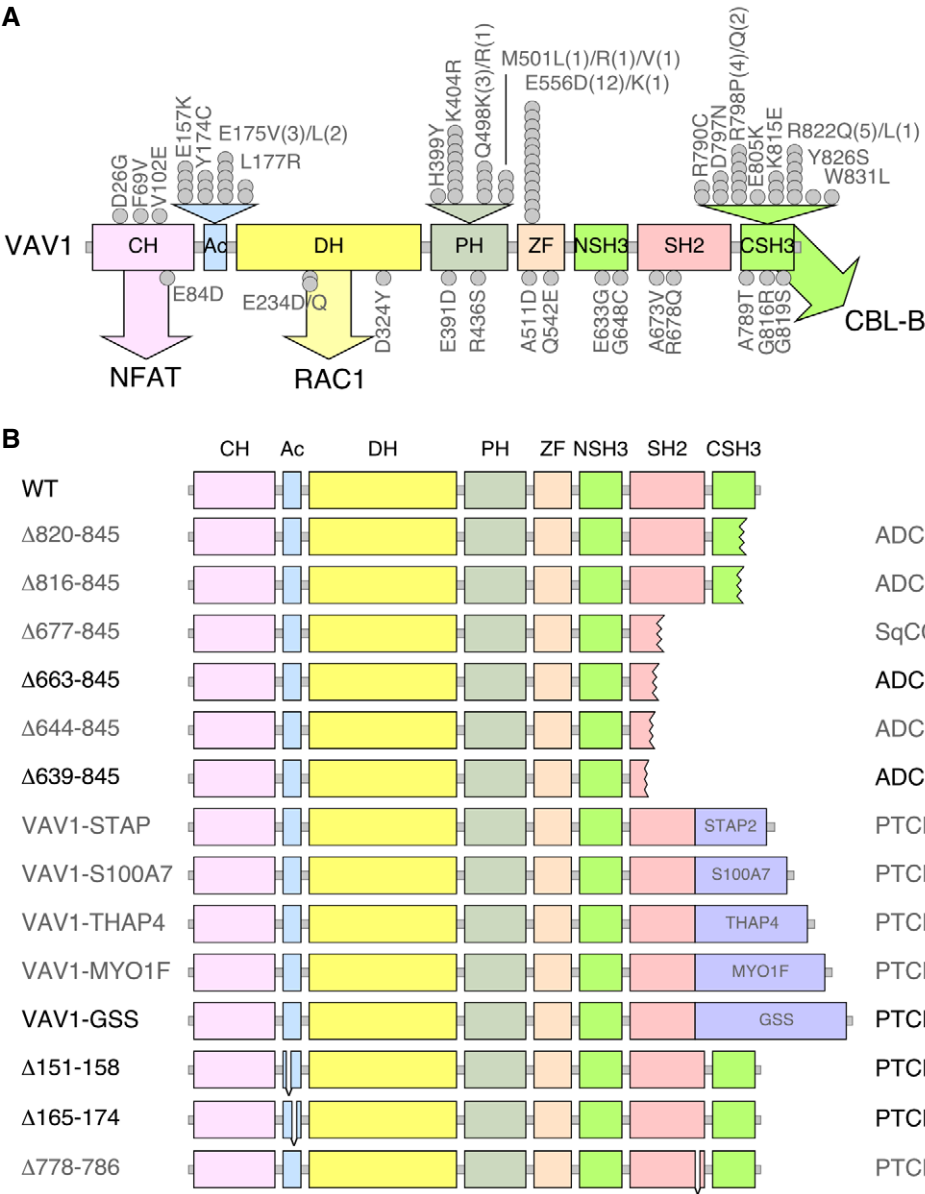
Figure EV1. Tumor-associated *VAV1* mutations.

A   Localization of *VAV1* missense mutations identified in PTCL (top) and NSCLC (bottom) in the primary structure of the protein. Each dot represents one patient. Abbreviations for domains have been described in main text. Mutations analyzed in this study are shown in gray color. The main pathways activated by the VAV1 domains are indicated. CH, calponin homology; Ac, acidic; DH, Dbl homology; PH, pleckstrin homology; ZF, zinc finger; NSH3, most N-terminal SH3 domain; CSH3, most C-terminal SH3.

B   Examples of C-terminal truncations (top, proteins 1 to 6), translocations affecting the C-terminal end (middle, proteins 7 to 11, fused protein indicated as a violet box), and internal gene deletions (bottom, proteins 12 to 14) found in human patients. Mutations analyzed in this study are shown in gray font. Those not tested are in black font.

Figure EV2. CSH3 mutations alter the interaction between VAV1 and binding partners.

A   Co-immunoprecipitation of indicated Vav1 proteins with CBL-B in Jurkat cells ectopically expressing the indicated combinations of proteins (top). Amount of immunoprecipitated CBL-B was assessed by reblotting the same filter with antibodies to CBL-B (second panel from top). Expression of ectopic VAV1 proteins (third panel from top) and endogenous tubulin α (loading control, bottom panel) was determined by immunoblotting using aliquots of the total cellular lysates used in the immunoprecipitation step. The color code of the mutant residues follows the criteria used in Fig 1C and D.

B–D   Representative examples of the interactions found in Jurkat cells among GST-tagged proteins fused to the indicated CSH3 versions of Vav1 and the endogenous CBL-B, Dynamin 2, and HNRNPK proteins. In all cases, the relative amount of bait used in the pull-down assays is shown in the fourth panel from top. Expression of the endogenous proteins was determined by immunoblotting using aliquots of the total cellular lysates used in the pull-down step. Asterisks in the second and fourth panels in the total cellular lysate panels pinpoint the CBL-B and HNRNPK immunoreactive bands from the previous immunoblot of the same filter, respectively. In (D), asterisk in the first panel in the pull-down panels indicates the Dynamin 2 band from the previous immunoblot of the same filter. Similar results were obtained in three additional experiments. GST-VAV1^{P833L}, negative control of interaction (it bears a mutation that inactivates the binding properties of the domain). The color code of the mutant residues follows the criteria used in Fig 1C and D.

E   Summary of binding alterations found in the Vav1 CSH3 mutants. Proper binding is shown as green boxes and arrows. Lack of binding is shown as blue boxes and arrows. The activation of NOTCH1 signaling is depicted as a red box. The percentage of each mutant subclass (relative to all CSH3 mutants tested) is indicated at the top of each functional subgroup.
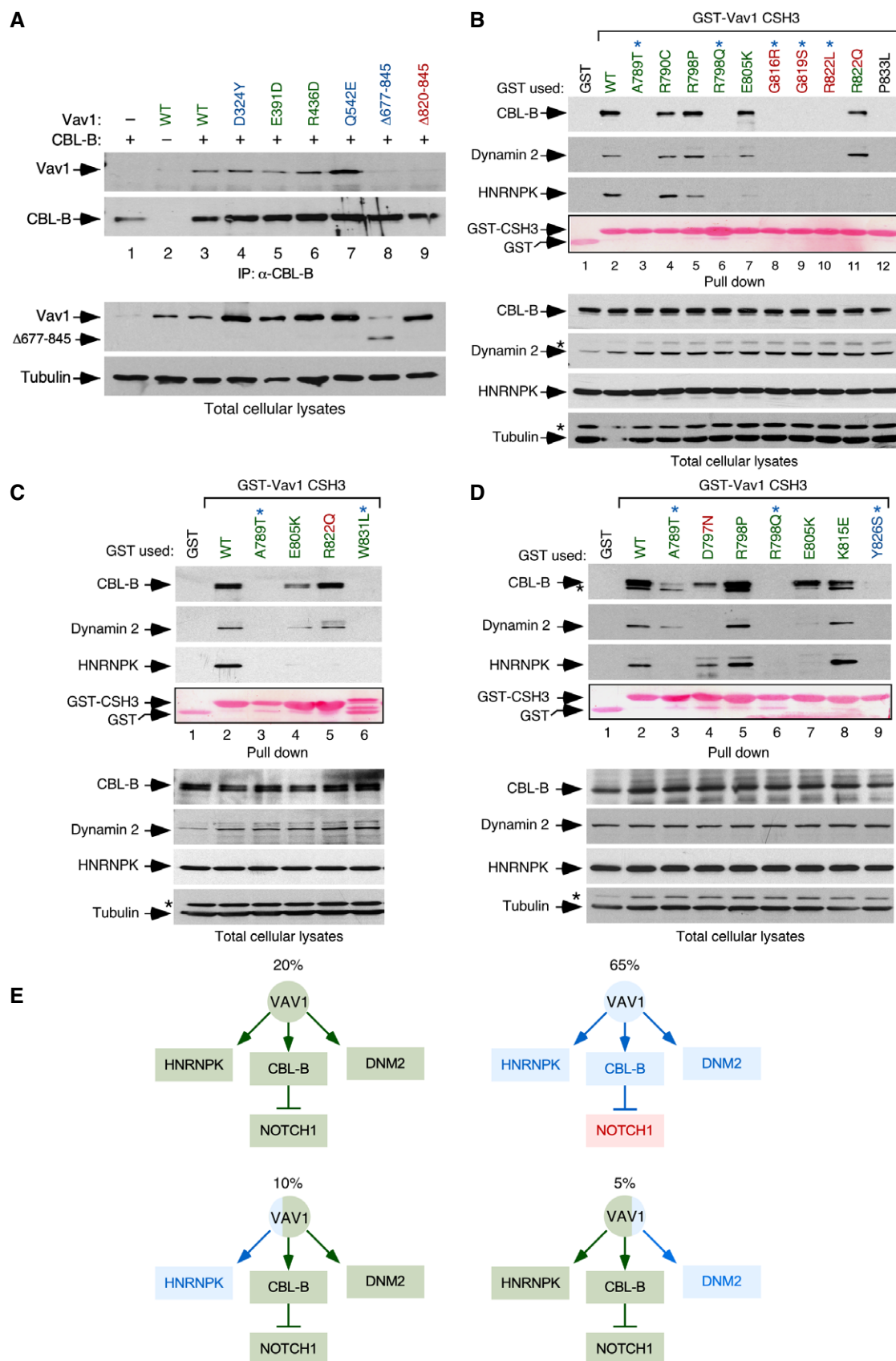
Source data are available online for this figure.

Figure EV2.

Figure EV3. New regulatory layers unveiled by the VAV1 mutations.

A   Depiction of the main intramolecular interactions that mediate the inactivation of VAV family proteins in the nonphosphorylated state. The interactions of the CH, Ac, and CSH3 domains with the catalytic cassette are shown in pink, blue, and purple lanes, respectively. The phosphorylation sites involved in the activation step are indicated. PTKs, protein tyrosine kinases involved in the tyrosine phosphorylation-mediated activation step of VAV family proteins.

B, C   Depiction of areas of interaction between the CH-Ac and the catalytic cassette. The side chains of the residues whose mutation leads to GOF effects are shown in red. The main regulatory phosphosites are shown in blue. The CH, Ac, and DH region are colored in purple, blue, and yellow, respectively.

D, E   Depiction of the area of the catalytic cassette containing the α_{11} DH helix, the PH, and the ZF regions in the context of the crystallized CH-Ac-DH-PH-ZF (D) and the CH-PH-ZF (E) fragments of human and mouse Vav1, respectively. Residues whose mutation leads to GOF and LOF effects are colored in red and blue, respectively. The CH, Ac, DH, PH, and ZF regions are colored in purple, blue, yellow, green, and brown, respectively.

F   Zoom of the Vav1 α_{11} DH helix-PH-ZF region showing the interactions established by the indicated residues. Residues and domains are depicted as in above panels.

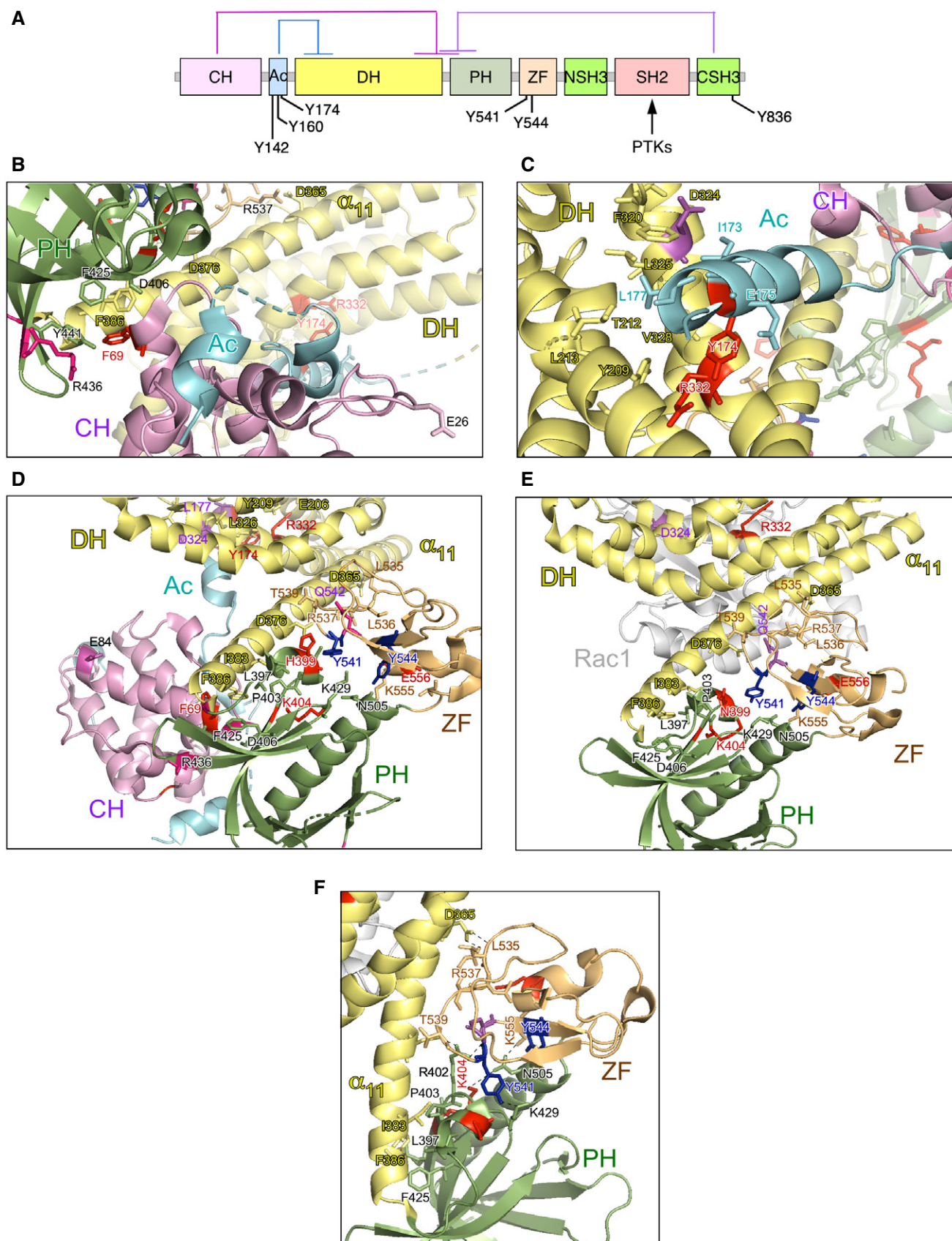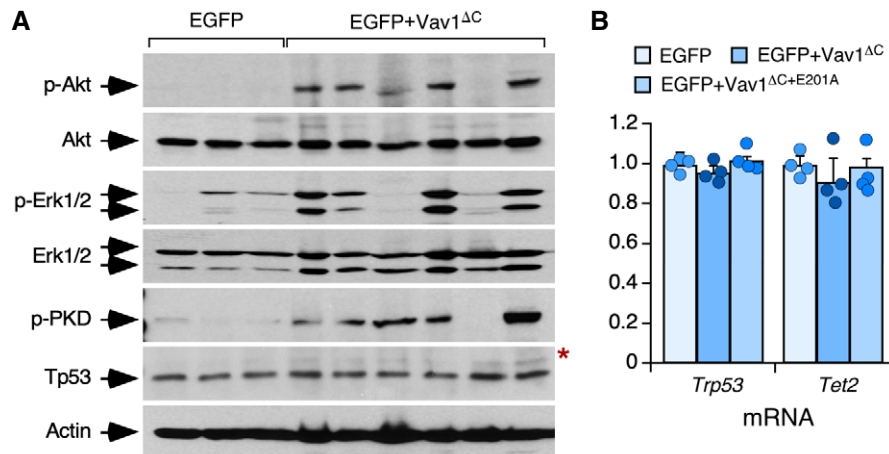Figure EV3.

A

B

Figure EV4. Status of signal transduction pathways in Vav1$^{\Delta C}$-transformed cells.

A Western blot showing the levels of phosphorylated and total proteins in spleen extracts from control and tumor-bearing recipient mice that had been transplanted with the indicated retrovirally transduced CD4$^+$ T cells (top). Total levels of Akt, Erk1/2, and actin were used as loading controls. The red asterisk indicates a panel that has been generated using an independent filter but the same tissue lysates.

B Abundance of indicated transcripts (bottom) in splenic cells from control (EGFP$^+$), tumor-bearing mice (expressing EGFP and Vav1$^{\Delta C}$), and mice transplanted with cells transduced with the catalytically dead version of Vav1$^{\Delta C}$ (expressing EGFP and Vav1$^{\Delta C+E201A}$). Values are given relative to the expression of each transcript in samples obtained from EGFP controls (which was given an arbitrary value of 1). $n = 4$ animals per class analyzed. a.u., arbitrary unit. Data represent the mean $\pm$ SEM. Statistical values obtained using the Student's t are given relative to control EGFP$^+$ cells.

Source data are available online for this figure.

Figure EV5. Vav1$^{\Delta C}$ triggers a vast proliferative program in transformed T$_{FH}$ cells.

A Main functional pathways upregulated in the Vav1$^{\Delta C}$-dependent transcriptome according to unbiased GSEAs. For all of them, q-val < 0.05.

B Principal component analysis showing the enrichment of the Vav1$^{\Delta C}$-dependent signature across the indicated tumor-associated transcriptomes. cSCC, cutaneous squamous cell carcinoma; oSCC, oral squamous cell carcinoma; T-ALL, T-cell acute lymphoblastic leukemia.

C GSEA for the Vav1$^{\Delta C}$-tumor gene expression matrix using as gene set the differentially expressed genes by the FOXO pathway. The expression profile of the top 25 leading-edge genes in the transcriptome of CD4$^+$ T cells from healthy and Vav1$^{\Delta C}$ tumor-bearing mice is shown. The normalized enrichment scores (NES) and false discovery rate values (FDR, using q values) are indicated inside the GSEA graph. Relative changes in abundance are shown in color gradients according to the color scale shown at the bottom. q-val, q value.

D GSEAs for the Vav1$^{\Delta C}$-tumor gene expression matrix using as gene set the differentially expressed genes by the SJL mouse model. The NES and FDR (using q values) are indicated inside the GSEA graph as in C. q-val, q value.

E Dot plot of the Vav1$^{\Delta C}$-dependent gene signature fit score in the indicated experimental groups (bottom). Dots represent values from an individual sample. Bars represent the mean enrichment value $\pm$ SEM for the overall sample set. ***$P \le 0.001$ (according to Tukey's honest significance difference test).

F Main functional categories encoded by the Vav1$^{\Delta C}$-specific gene subset described in the main text. Up (red); down (blue). For all of categories, $P \le 0.001$ (Fisher's exact test).

G Fraction of upregulated (left) and downregulated (right) Vav1$^{\Delta C}$-driven transcriptome showing conservation with the expression programs identified in human AITL patients. Relative changes in abundance are shown in color gradients according to the color scale shown on the right. Healthy, CD4$^+$ T cells from healthy patients (green box). AITL, human AITL (red color boxes).

H Venn diagrams representing the number of up- (top) and downregulated (bottom) genes from the Vav1$^{\Delta C}$-dependent transcriptome that are shared with the AITL patient dataset used in panel G.

I Enrichment of indicated Vav1$^{\Delta C}$-driven gene signatures that are shared with the AITL patient dataset used in panel G.

J Heatmaps showing the expression profiles of human and mouse differentially expressed genes (DEG) belonging to the indicated functional categories (indicated on the left of each panel). Each row represents 1 DEG identified in the indicated AITL models (top). Each column represents 1 sample. The number of genes of each functional category is indicated. Relative changes in abundance are shown in color gradients according to the color scale shown on the bottom right. Green boxes, healthy individuals (in the case of human data), and WT mice. Red boxes, AITL samples from either patients or the indicated mouse models.
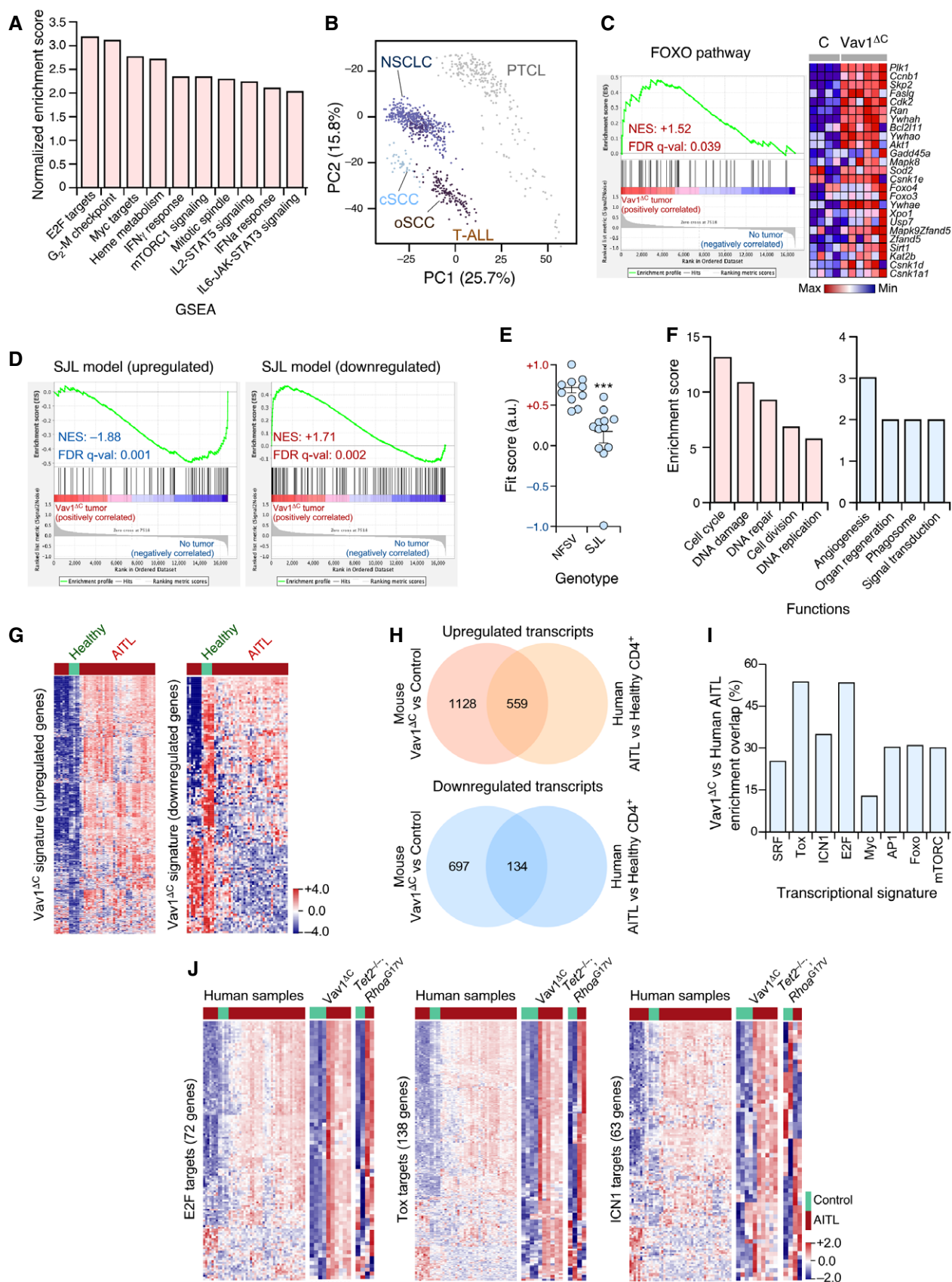
Figure EV5.

Appendix for

CANCER-ASSOCIATED MUTATIONS IN *VAV1* TRIGGER VARIEGATED SIGNALING OUTPUTS AND T CELL LYMPHOMAGENESIS

by

Javier Robles-Valero *et al*.

This PDF file includes:

Appendix Figures S1 to S9 and legends

Appendix Table S1
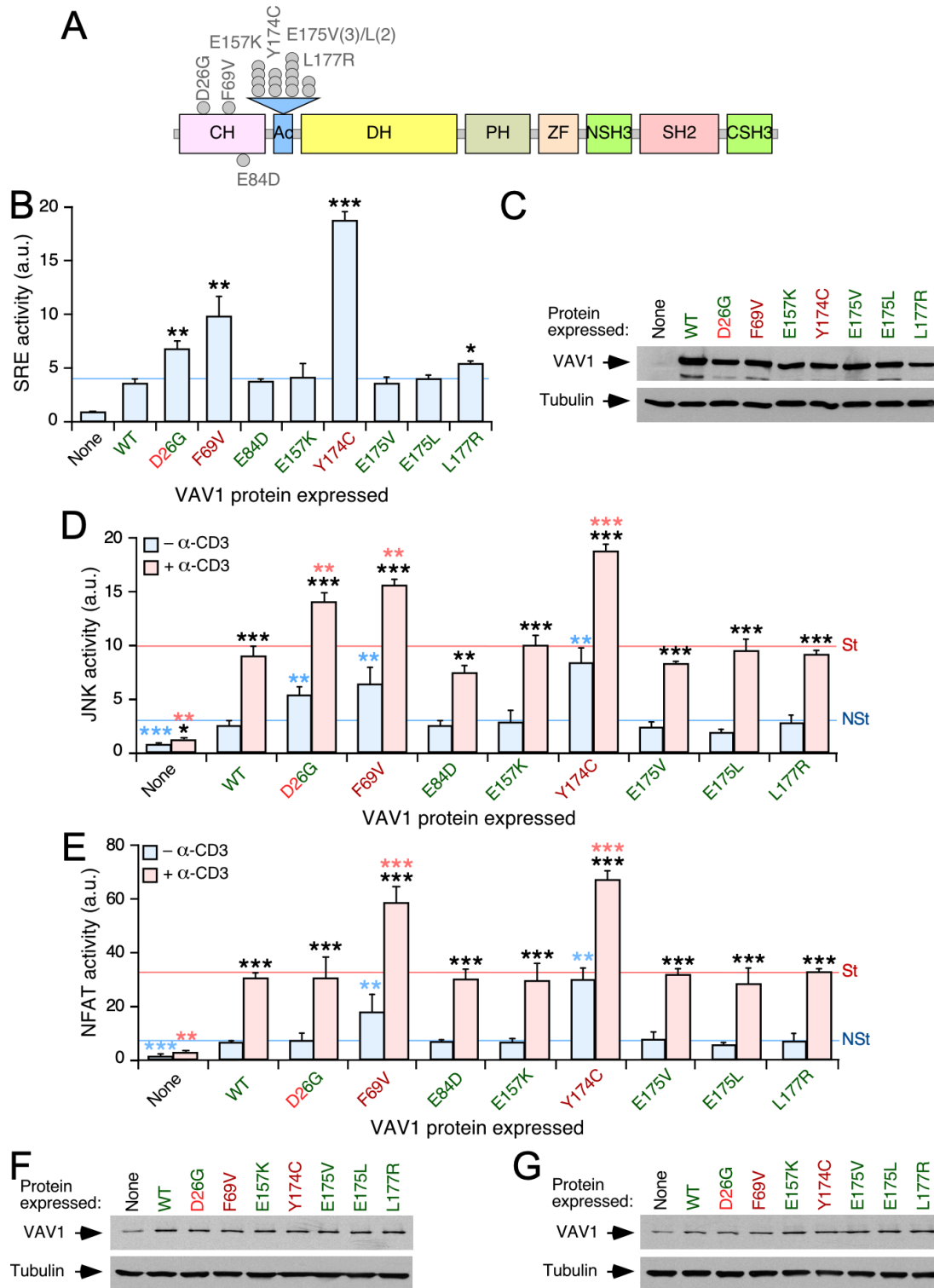
APPENDIX FIGURE S1. Effect of *VAV1* mutations located in the CH and acidic domains in the canonical pathways of the protein

(A) Localization of the *VAV1* missense mutations found in PTCL (top) and NSCLC (bottom) that have been tested in the assays shown in this figure. Each circle depicts one patient (same notation will be used in the rest of figures of this file).

(B) SRE promoter activity of COS cells expressing the indicated Vav1 mutant proteins (bottom). Mutations have been labeled as in **Figure 1C** to indicate the functional subclass (this labelling will be used in the rest of figures shown in this Supplemental Information file). *, $P \leq 0.05$; **, $P \leq 0.01$; ***, $P \leq 0.001$ using the Mann–Whitney U test. n = 3 independent experiments, each performed in triplicate.

(C) Representative immunoblot showing the abundance of the indicated VAV1 proteins in the transfected cells used in panel B. Endogenous tubulin α has been used as loading control.

(D and E) Activation of JNK (D) and NFAT (E) by the indicated ectopically expressed Vav1 proteins in Jurkat cells under nonstimulation (blue bars) and anti-CD3-stimulation (red bars) conditions. NSt, nonstimulated; St, stimulated. *P* values are given relative to nonstimulated (blue asterisks) and stimulated (red asterisks) cells expressing Vav1^{WT} in the same cell line. We also included *P* values for the values exhibited by each Vav1 mutant protein relative to those obtained in nonstimulated condition (black asterisks). We have not included statistics in mock-transfected cells (none) for the sake of simplicity. *, $P \leq 0.05$; **, $P \leq 0.01$; ***, $P \leq 0.001$ (Mann-Whitney U test). n = 3 independent experiments, each performed in triplicate.

(F and G) Representative immunoblots showing the abundance of the ectopic Vav1 proteins in the transfected cells used in panels D (F) and E (G), respectively. Endogenous tubulin α has been used as loading control in all the cases.

In B, D and E, values are shown as means ± SEM from three independent experiments (each performed in triplicate).
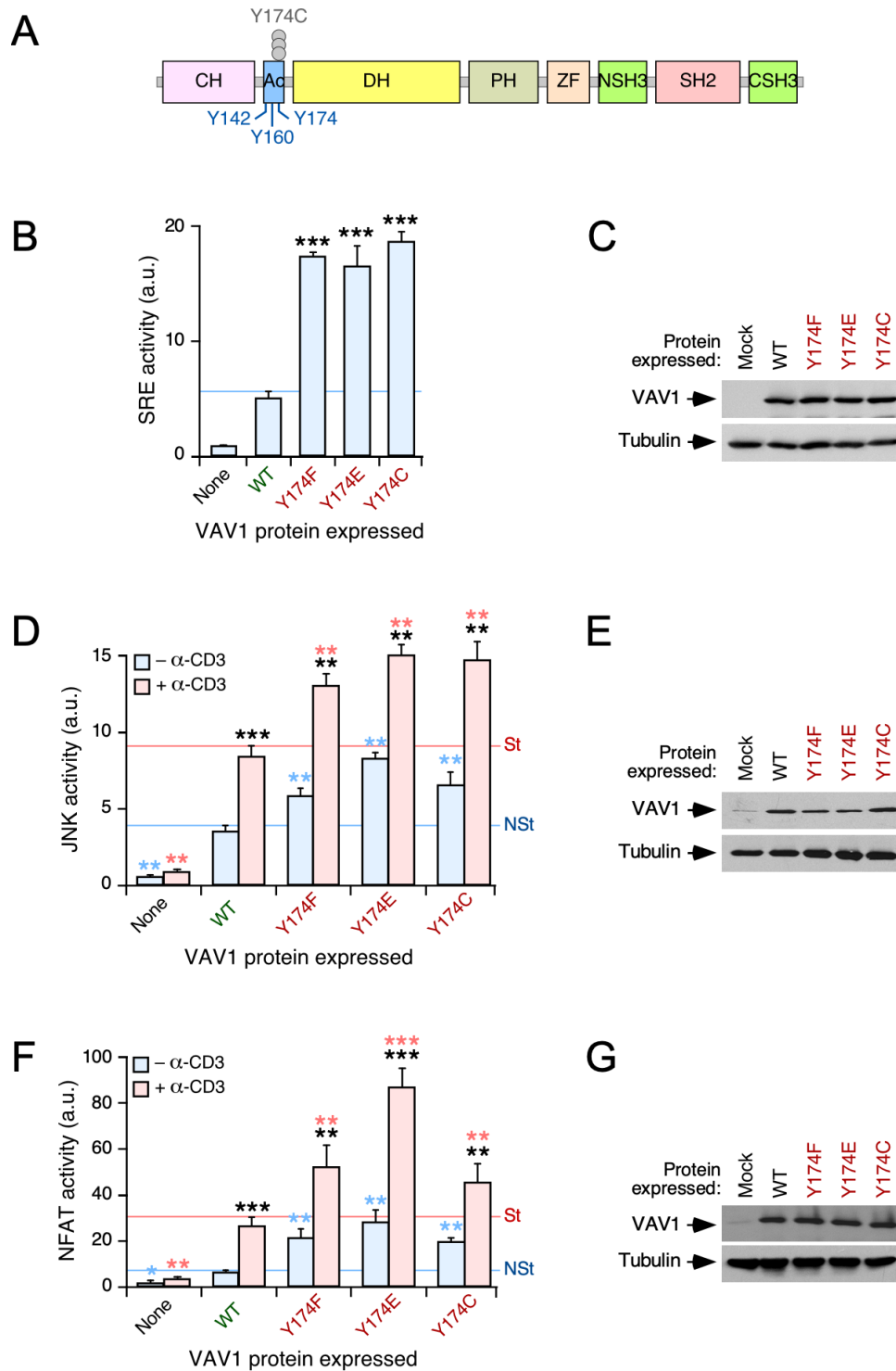
APPENDIX FIGURE S2. Functional impact of the mutations in the regulatory Y^{174} VAV1 phosphosite in the canonical pathways of the protein

(A) Localization of the *VAV1* missense mutations found in PTCL that have been tested in the assays shown in this figure. The regulatory phosphosites of Vav1 are indicated at the bottom in blue.

(B) Levels of stimulation of SRE triggered by the indicated VAV1 proteins in COS cells. ***, $P \leq 0.001$ using the Mann-Whitney U test of indicated experimental values compared to Vav1^{WT}-expressing cells (n = 3 independent experiments, each performed in triplicate).

(C) Representative immunoblot showing the abundance of the ectopic Vav1 proteins and endogenous tubulin α in the experiment shown in B.

(D and F) Activation of JNK (D) and NFAT (F) by the indicated Vav1 mutants in Jurkat cells under nonstimulation (blue bars) and anti-CD3-stimulation (red bars) conditions. Data and P values are depicted as in **Appendix Figures S1D** and **S1E**. *, $P \leq 0.05$; **, $P \leq 0.01$; ***, $P \leq 0.001$ (Mann-Whitney U test).

(E and G) Representative immunoblots showing the abundance of the ectopic Vav1 proteins in the transfected cells used in D (E) and F (G), respectively. Endogenous tubulin α has been used as loading control in all the cases.

In B, D and F, values are shown as means ± SEM from three independent experiments (each performed in triplicate).
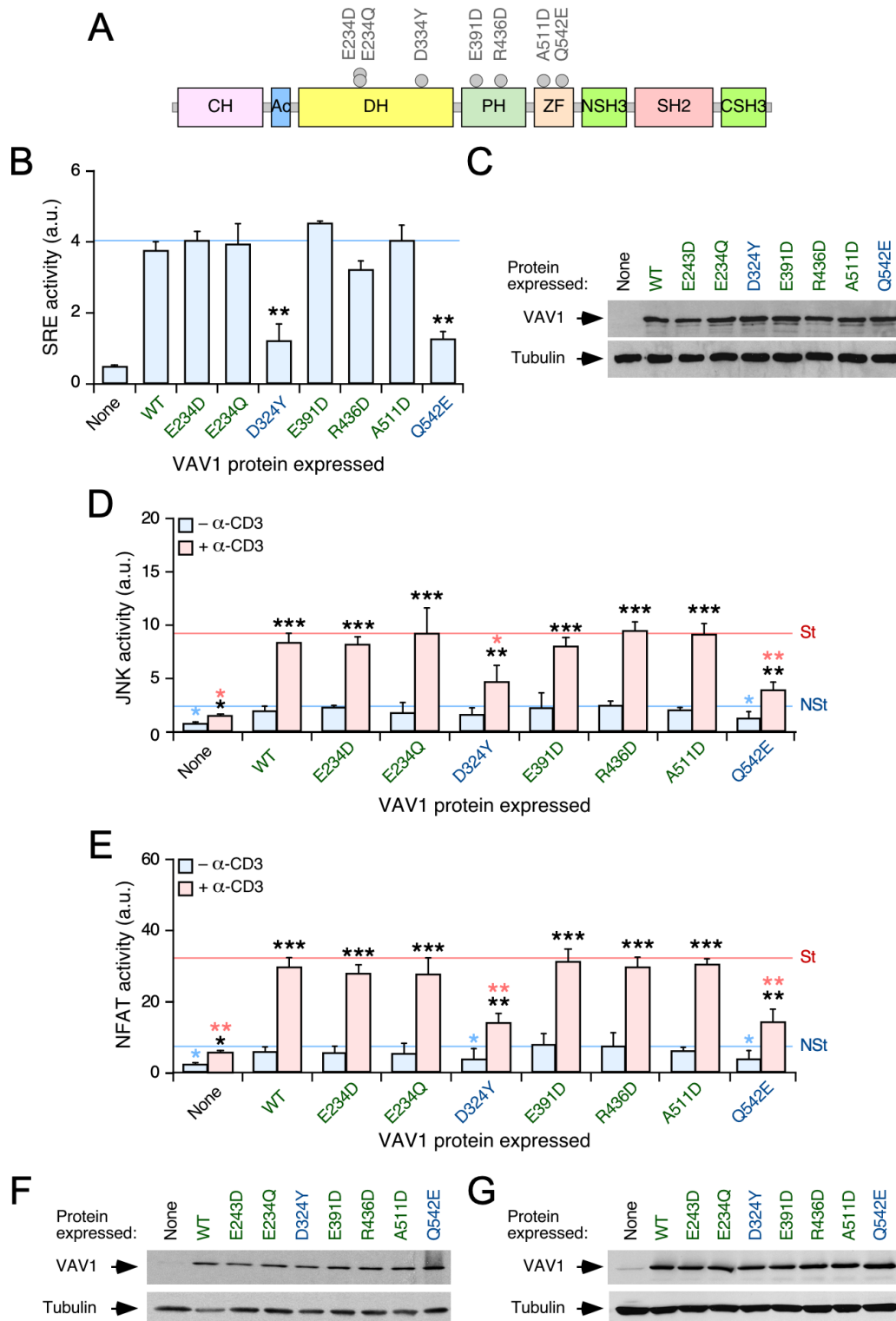
APPENDIX FIGURE S3. Effect of the lung-tumor detected mutations located in the VAV1 catalytic core (DH-PH-ZF) in the canonical pathways of the protein

(A) Localization of the *VAV1* missense mutations found in NSCLC that have been tested in the assays shown in this figure.

(B) SRE promoter activity of COS cells expressing the indicated Vav1 mutant proteins (bottom). Data and *P* values are depicted as in **Appendix Figure S1B**. **, $P \leq 0.01$. Statistical values were obtained using the Mann-Whitney U test.

(C) Representative immunoblot showing the abundance of the indicated Vav1 proteins in the transfected cells used in B. Endogenous tubulin α has been used as loading control.

(D and E) JNK (D) and NFAT (E) activity elicited by the indicated Vav1 proteins in Jurkat cells under nonstimulation (blue bars) and anti-CD3-stimulation (red bars) conditions. Data and *P* values are depicted as in **Appendix Figure S1D** and **S1E** (*n* =3 independent experiments, each performed in triplicate). *, $P \leq 0.05$; **, $P \leq 0.01$; ***, $P \leq 0.001$ (Mann-Whitney U test).

(F and G) Representative immunoblots showing the abundance of the ectopic Vav1 proteins and the endogenous tubulin α in the experiments used in D (F) and E (G), respectively.

In B, D and E, values are shown as means ± SEM from three independent experiments (each performed in triplicate).

APPENDIX FIGURE S4. Effect of *VAV1* mutations found in the catalytic core of the protein in the canonical pathways of the protein

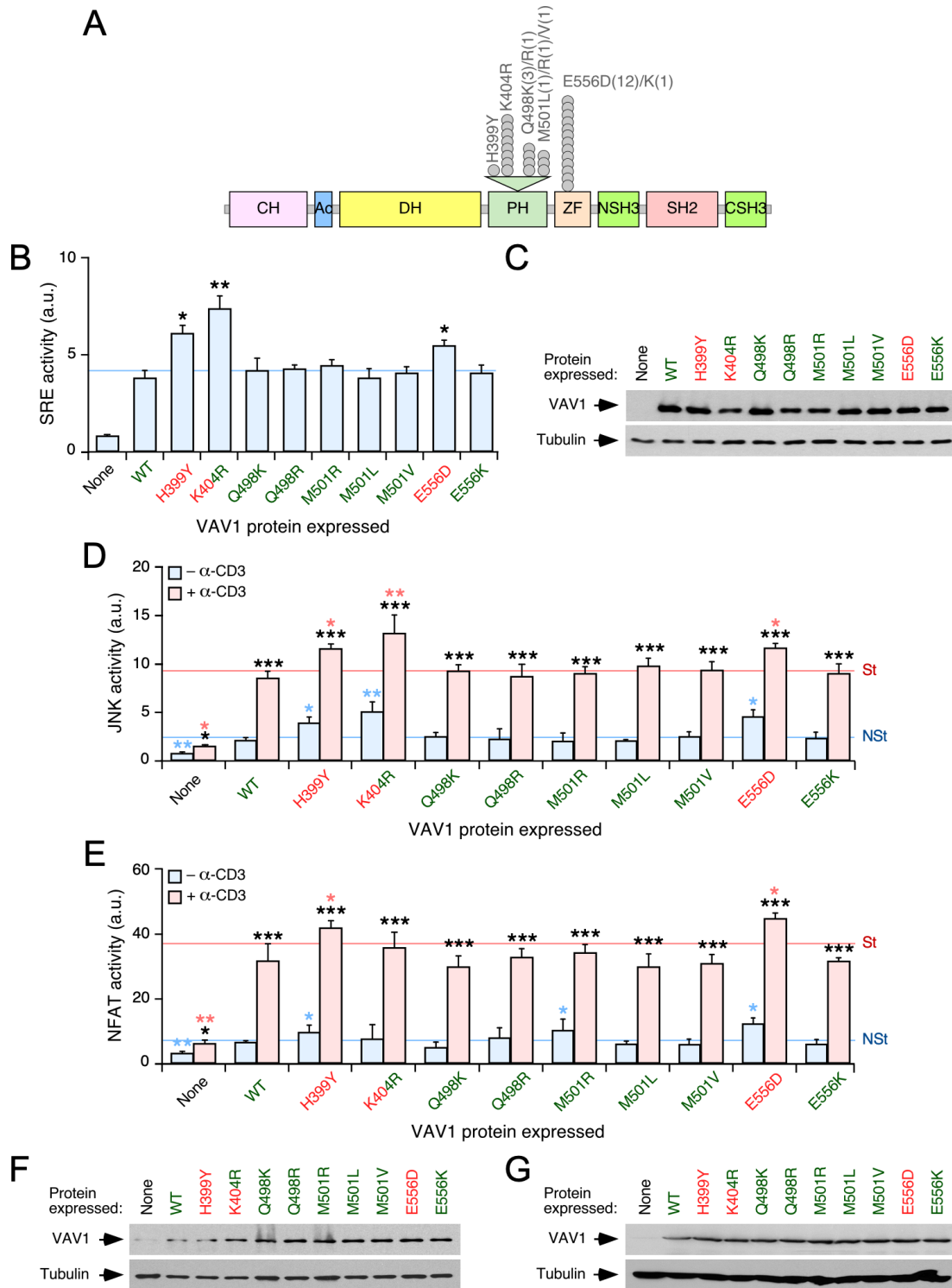**(A)** Localization of the *VAV1* missense mutations found in PTCL that target the PH and ZF domains of the protein.

(B) SRE promoter activity of COS cells expressing the indicated VAV1 mutant proteins. Data and *P* values are depicted as in **Appendix Figure S1B**. *, $P \le 0.05$; **, $P \le 0.01$ (Mann–Whitney U test).

(C) Representative immunoblot showing the abundance of the indicated Vav1 proteins in the transfected cells used in B. Endogenous tubulin α has been used as loading control.

(D and E) JNK (D) and NFAT (E) activity showed by indicated Vav1 proteins in nonstimulated (blue bars) and anti-CD3-stimulated (red bars) Jurkat cells. Data and P values are depicted as in Appendix **Figures S1D** and **S1E**. *, $P \leq 0.05$; **, $P \leq 0.01$; ***, $P \leq 0.001$ (Mann-Whitney U test).

(F and G) Representative immunoblots showing the abundance of the ectopic Vav1 proteins in the transfected cells used in D (F) and E (G), respectively. Endogenous tubulin α has been used as loading control in all the cases.

In B, D and E, values are shown as means ± SEM from three independent experiments (each performed in triplicate).
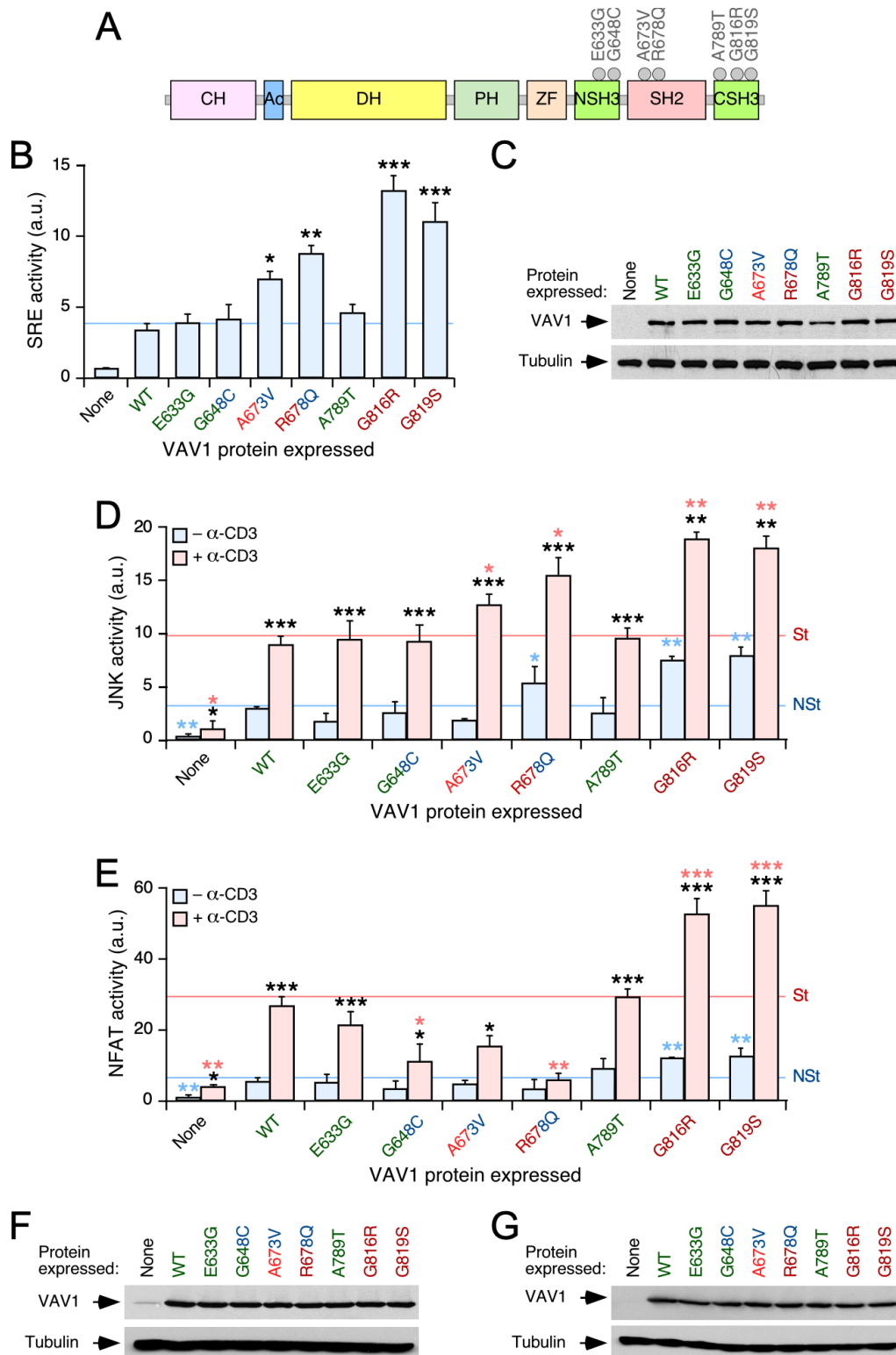
APPENDIX FIGURE S5. Functional impact of *VAV1* gene mutations located in the NSH3, SH2 and CSH3 in the canonical activities of the protein

(A) Localization of the mutations targeting the VAV1 SH3-SH2-SH3 cassette found in lung tumor patients.

Robles-Valero et al. (2021)

10

(B) SRE promoter activity elicited by Vav1 mutant proteins in COS cells. Data and *P* values are depicted as in **Appendix Figure S1B**. *, $P \leq 0.05$; **, $P \leq 0.01$; ***, $P \leq 0.001$ (Mann-Whitney U test).

(C) Representative immunoblot showing the abundance of the indicated Vav1 proteins in the transfected cells used in B. Endogenous tubulin α has been used as loading control.

(D and E) Activation of JNK (D) and NFAT (E) by the indicated Vav1 proteins in Jurkat cells under nonstimulation (blue bars) and anti-CD3-stimulation (red bars) conditions. Data and *P* values are depicted as in **Appendix Figures S1D** and **S1E**. *, $P \leq 0.05$; **, $P \leq 0.01$; ***, $P \leq 0.001$ (Mann-Whitney U test).

(F and G) Representative immunoblots showing the abundance of the ectopic Vav1 proteins in the transfected cells used in D (F) and E (G), respectively. Endogenous tubulin α has been used as loading control.

In B, D and E, values are shown as means ± SEM from three independent experiments (each performed in triplicate).
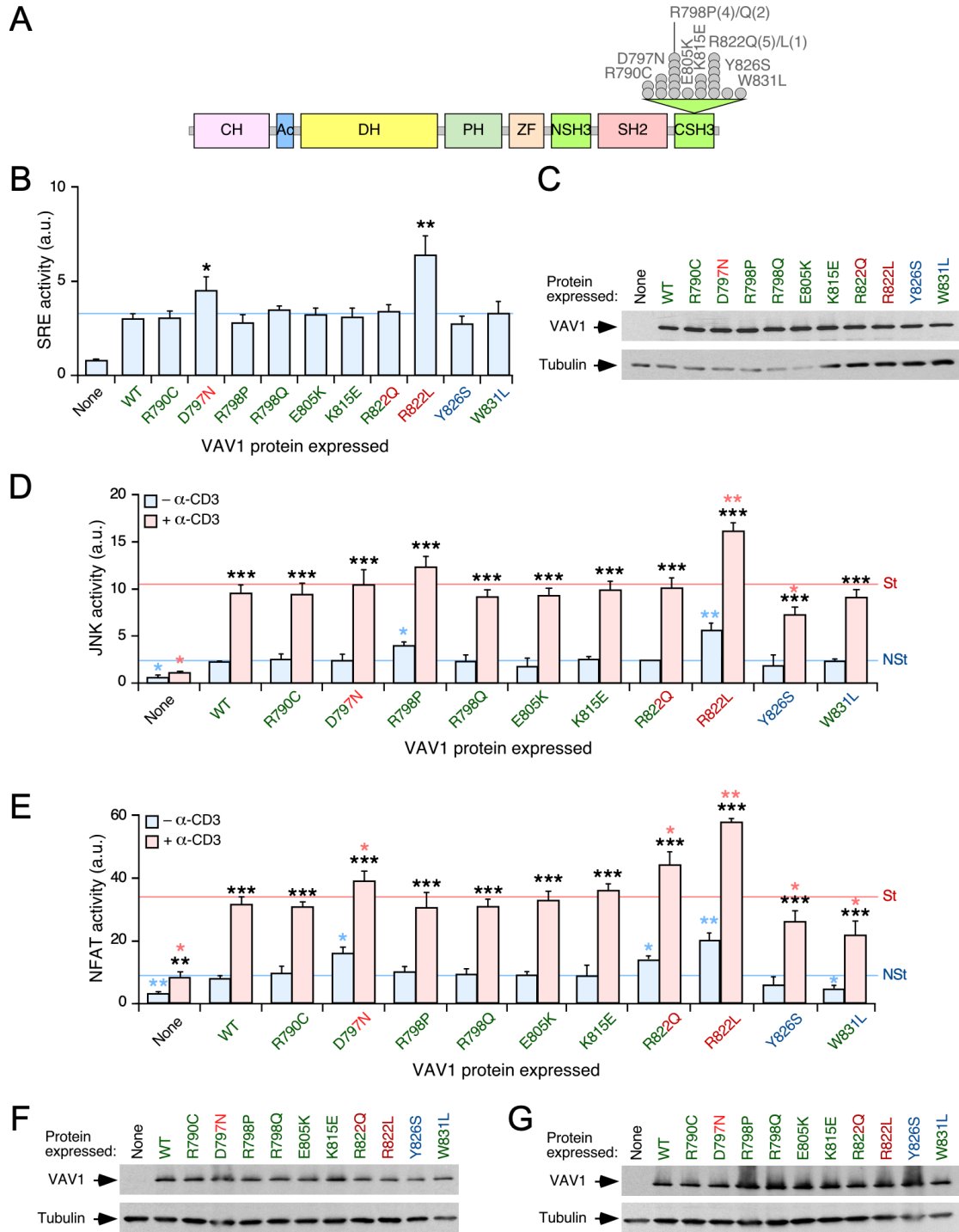
APPENDIX FIGURE S6. Functional characterization of *VAV1* mutations found in the CSH3 domain in PTCL patients

(A) Localization of the mutations.

(B) SRE promoter activity of COS cells expressing the indicated Vav1 mutant proteins. *, $P \leq 0.05$; **, $P \leq 0.01$ (Mann-Whitney U test).

(C) Representative immunoblot showing the abundance of the indicated Vav1 proteins in the transfected cells used in B. Endogenous tubulin α has been used as loading control.

(D and **E)** Activation of JNK (D) and NFAT (F) by the indicated Vav1 proteins in nonstimulated (blue bars) and anti-CD3-stimulated (red bars) Jurkat cells. *, $P \le 0.05$; **, $P \le 0.01$; ***, $P \le 0.001$ (Mann-Whitney U test).

(F and **G)** Representative immunoblots showing the abundance of the ectopic Vav1 proteins and endogenous tubulin α (loading control) in the transfected cells used in D (F) and E (G), respectively.

In B, D and E, values are shown as means ± SEM from three independent experiments (each performed in triplicate).
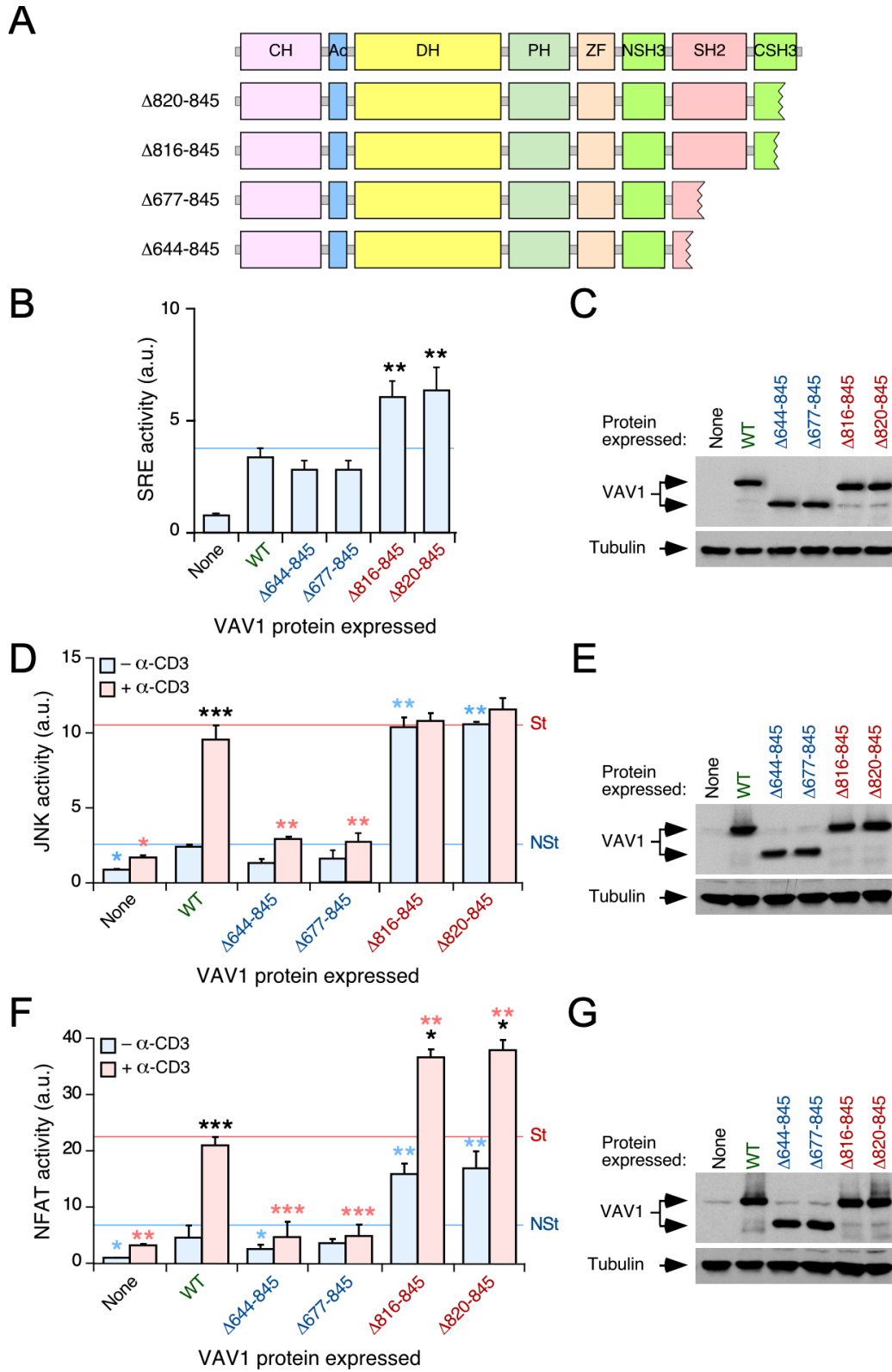
APPENDIX FIGURE S7. Effect of *VAV1* gene truncations in the canonical pathways of the protein

(A) Depiction of the inframe stop mutations identified in the C-terminal domains of VAV1 in NSCLC.

(B) SRE promoter activity triggered by VAV1 mutant proteins in COS cells. *, $P \leq 0.05$; **, $P \leq 0.01$ (Mann-Whitney U test).

(C) Representative immunoblot showing the abundance of the indicated Vav1 proteins and endogenous tubulin α in the transfected cells used in B.

(D and F) Activation of JNK (D) and NFAT (E) by the indicated Vav1 proteins in Jurkat cells under nonstimulation (blue bars) and anti-CD3-stimulation (red bars) conditions. *, $P \leq 0.05$; **, $P \leq 0.01$; ***, $P \leq 0.001$ (Mann-Whitney U test).

(E and G) Representative immunoblots showing the abundance of the ectopic Vav1 proteins in the transfected cells used in D (E) and F (G), respectively. Endogenous tubulin α has been used as loading control.

In B, D and F, values are shown as means ± SEM from three independent experiments (each performed in triplicate).
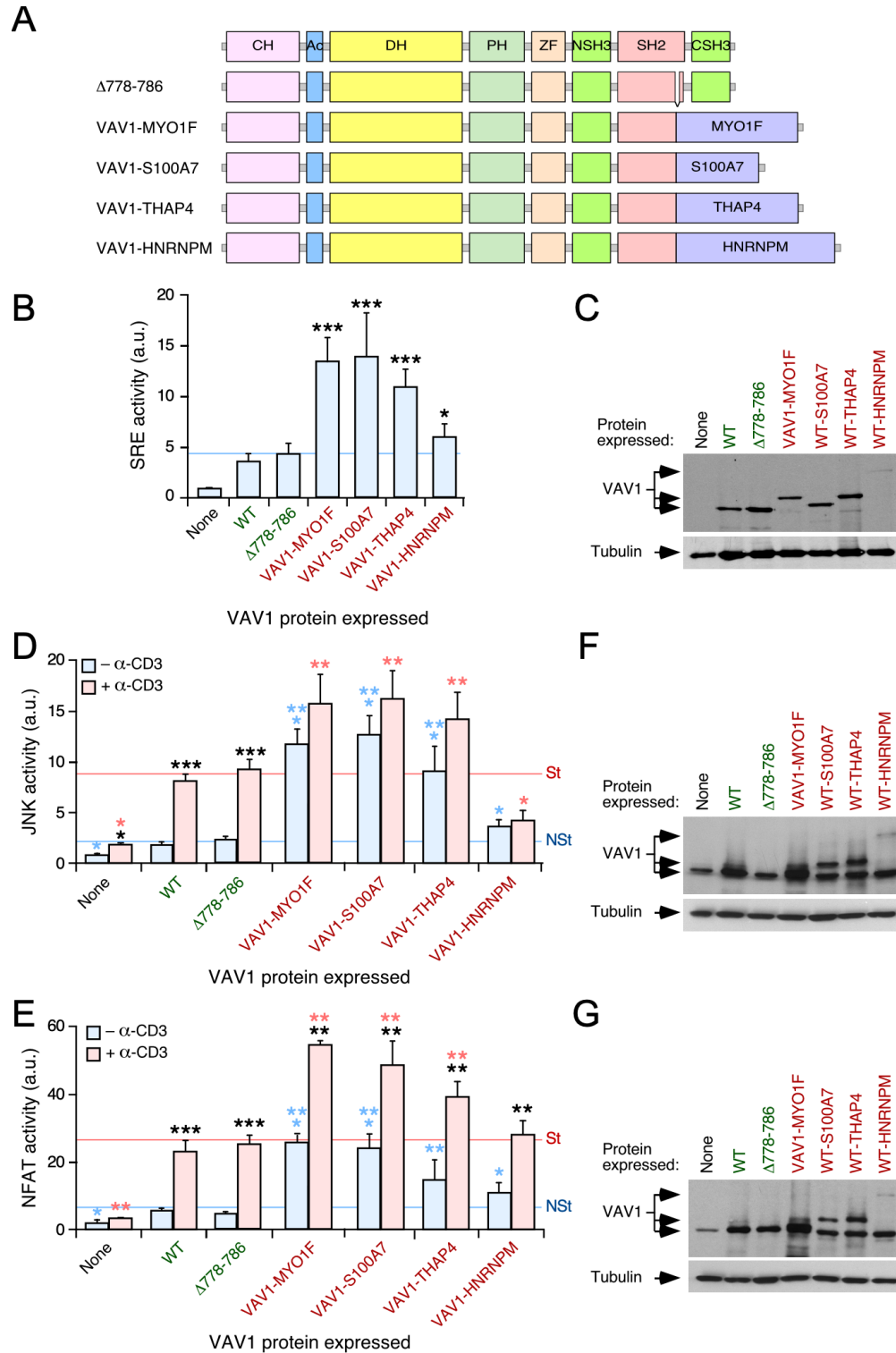
APPENDIX FIGURE S8. Functional impact of internal focal deletions and *VAV1* fusion genes found in PTCLs

(A) Depiction of the Vav1 mutant proteins used in these experiments.

(B) Levels of stimulation of SRE elicited by the indicated Vav1 proteins in COS cells. *, $P \le 0.05$, ***, $P \le 0.001$ (Mann-Whitney U test).

(C) Representative immunoblot showing the abundance of the ectopic Vav1 proteins and endogenous tubulin α in the experiment shown in B.

(D and E) Activation of JNK (D) and NFAT (F) by ectopically expressed Vav1 proteins in Jurkat cells under nonstimulation (blue bars) and anti-CD3-stimulation (red bars) conditions. *, $P \leq 0.05$; **, $P \leq 0.01$; ***, $P \leq 0.001$ (Mann-Whitney U test).

(F and G) Representative immunoblots showing the abundance of the ectopic Vav1 proteins in the transfected cells used in D (F) and E (G), respectively. Endogenous tubulin α has been used as loading control in all the cases.

In B, D and E, values are shown as means ± SEM from three independent experiments (each performed in triplicate).
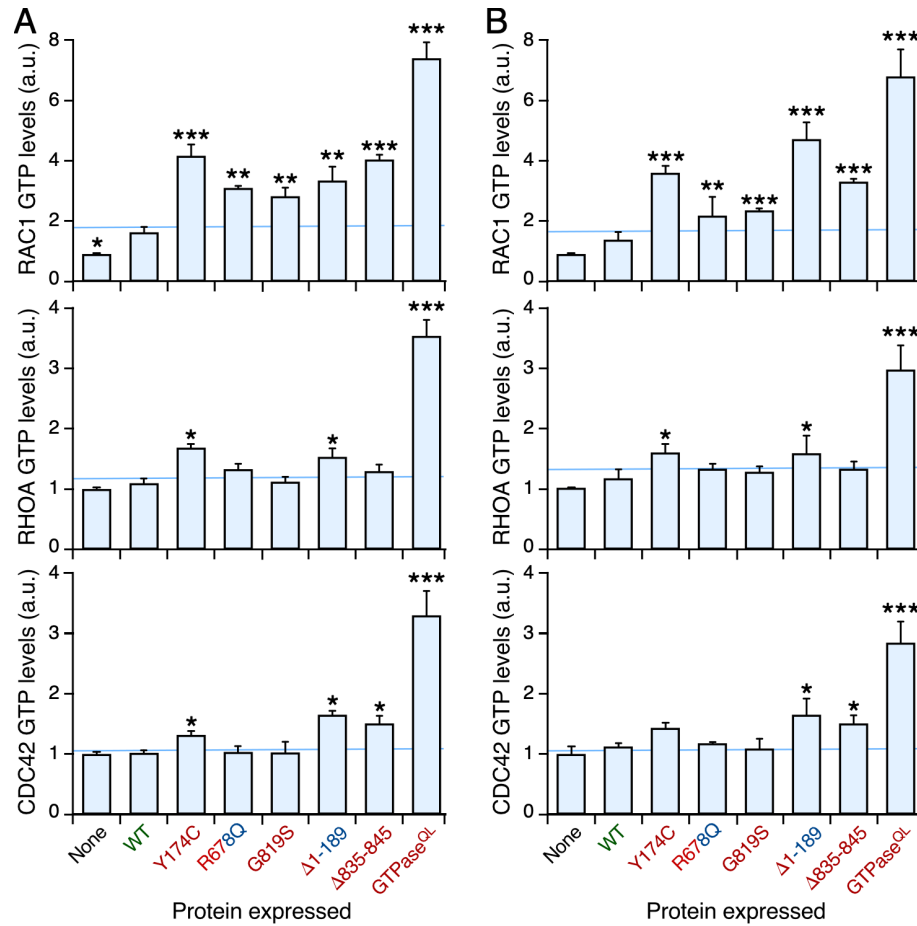
APPENDIX FIGURE S9. Functional impact of indicated proteins in the activation of RHO family proteins

(A and B) Levels of GTP-bound RAC1 (A,B; upper panels), RHOA (A,B; middle panels) and CDC42 (A,B; bottom panels) in COS1 (A) and Jurkat (B) cells transiently transfected with the indicated proteins (bottom). Data are shown as means ± SEM from three independent experiments (each performed in duplicate). As positive control, we used the active versions (GTPase^{QL}) of the indicated GTPases as well as the Vav1$^{\Delta1-189}$ protein. *, $P \leq 0.05$; **, $P \leq 0.01$; ***, $P \leq 0.001$ using the Mann-Whitney U test.

APPENDIX TABLE S1. List of primers used in this study. Fw, forward; Rv, reverse

Mouse *Vav1* (NM_011691)	
Primer	**Sequence**
E26G_Fw	5'-AGCCACCGTGTGACCTGGGGGGGGGGCCCAGGTGTGT-3'
E26G_Rv	5'-ACACACCTGGGCCCCCCCCCAGGTCACACGGTGGCT-3'
F69V_Fw	5'-CGGCCCCAGATGTCCCAGGTCCTTTGTCTTAAGAACATT-3'
F69V_Rv	5'-AATGTTCTTAAGATAAAGGACCTGGGACATCTGGGGCCG-3'
E84D_Fw	5'-ACCTTCCTGTCTACTTGCTGTGACAAGTTCGGCCTCAAGCGCAGT-3'
E84D_Rv	5'-ACTGCGCTTGAGGCCGAACTTGTCACAGCAAGTAGACAGGAAGGT-3'
E157K_Fw	5'-GACACCGCAGAGGAAGACAAGGACCTTTATGACTGCGTG-3'
E157K_Rv	5'-CACGCAGTCATAAAGGTCCTTGTCTTCCTCTGCGGTGTC-3'
Y174C_Fw	5'-GAGGCAGAGGGGGACGAGATCTGCGAGGACCTAATGCGCTTGGAG-3'
Y174C_Rv	5'-CTCCAAGCGCATTAGGTCCTCGCAGATCTCGTCCCCCTCTGCCTC-3'
E175V_Fw	5'-GCAGAGGGGGACGAGATCTACGTGGACCTAATGCGCTTGGAGTCG-3'
E175V_Rv	5'-CGACTCCAAGCGCATTAGGTCCACGTAGATCTCGTCCCCCTCTGC-3'
E175L_Fw	5'-GCAGAGGGGGACGAGATCTACTTGGACCTAATGCGCTTGGAGTCG-3'
E175L_Rv	5'-CGACTCCAAGCGCATTAGGTCCAAGTAGATCTCGTCCCCCTCTGC-3'
L177R_Fw	5'-GACGAGATCTACGAGGACCGAATGCGCTTGGAGTCGGTG-3'
L177R_Rv	5'-CACCGACTCCAAGCGCATTCGGTCCTCGTAGATCTCGTC-3'
E201A_Fw	5'-CGCTGCTGCTGCCTGCGGGCGATCCAGCAGACGGAGGAG-3'
E201A_Rv	5'-CTCCTCCGTCTGCTGGATCGCCCGCAGGCAGCAGCAGCG-3'
E234D_Fw	5'-GAGACCATCTTTGTCAACATTGACGAGCTGTTCTCTGTGCATACC-3'
E234D_Rv	5'-GGTATGCACAGAGAACAGCTCGTCAATGTTGACAAAGATGGTCTC-3'
E234Q_Fw	5'-GAGACCATCTTTGTCAACATTCAGGAGCTGTTCTCTGTGCATACC-3'
E234Q_Rv	5'-GGTATGCACAGAGAACAGCTCCTGAATGTTGACAAAGATGGTCTC-3'
D324Y_Fw	5'-GGCCGATTCACCCTACGGTATCTGCTGATGGTACCTATG-3'
D324Y_Rv	5'-CATAGGTACCATGCAGATACCGTAGGGTGAATCGGCC-3'
H337Y_Fw	5'-ATGCAGCGGGTGCTGAAGTACTACCTCCTTCTCCAGGAGCTAGTG-3'
H337Y_Rv	5'-CACTAGCTGGAGAAGGAGGTAGTACTTCAGCACCCGCTGCAT-3'
E391D_Fw	5'-AACTTTCAGCTGTCCATTGACAACCTGGACCAGTCTCTG-3'
E391D_Rv	5'-CAGAGACTCGGTCCAGGTTGTCAATGGACAGCTGAAAGTT-3'
N399Y_Fw	5'-CTGGACCAGTCTCTGGCTTACTATGGCCGGCCCAAGATT-3'
N399Y_Rv	5'-AATCTTGGGCCGGCCATAGTAAGCCAGAGACTGGTCCAG-3'
K404R_Fw	5'-GCTAACTATGGCCGGCCCAGGATTGACGGTGAGCTCAAG-3'
K404R_Rv	5'-CTTGAGCTCACCGTCAATCCTGGGCCGGCCATAGTTAGC-3'
R436D_Fw	5'-TCACTGCTCATCTGTAAAAGCCGCGGGGACTCTTACGAC-3'
R436D_Rv	5'-GTCGTAAGAGTCCCCGCGGCTTTTACAGATGAGCAGTGA-3'
Q498K_Fw	5'-CTGAAGAAGAAGTGGATGGAAAAGTTCGAAATGGCCATCTCCAAC-3'
Q498K_Rv	5'-GTTGGAGATGGCCATTTCGAACTTTTCCATCCACTTCTTCTTCAG-3'
Q498R_Fw	5'-CTGAAGAAGAAGTGGATGGAACGGTTCGAAATGGCCATCTCCAAC-3'
Q498R_Rv	5'-GTTGGAGATGGCCATTTCGAACCGTTCCATCCACTTCTTCTTCAG-3'
M501R_Fw	5'-GTGGATGGAACAGTTCGAACGGGCCATCTCCAACATTTACC-3'
M501R_Rv	5'-GGTAAATGTTGGAGATGGCCCGTTCGAACTGTTCCATCCAC-3'
M501L_Fw	5'-GTGGATGGAACAGTTCGAATTGGCCATCTCCAACATTTACC-3'
M501L_Rv	5'-GGTAAATGTTGGAGATGGCCAATTCGAACTGTTCCATCCAC-3'
M501V_Fw	5'-GTGGATGGAACAGTTCGAAGTGGCCATCTCCAACATTTACC-3'
M501V_Rv	5'-GGTAAATGTTGGAGATGGCCACTTCGAACTGTTCCATCCAC-3'
A511D_Fw	5'-TACATTTACCCAGAGAATGAAACAGCCAATGGGCATGAT-3'
A511D_Rv	5'-ATCATGCCCATTGGCTGTTTCATTCTCTGGGTAAATGTA-3'
Q542E_Fw	5'-CTCAGAGGCACATTCTACGAGGGATATCGCTGTTACAGG-3'
Q542E_Rv	5'-CCTGTAACAGCGATATCCCTCGTAGAATGTGCCTCTGAG-3'

E556D_Fw	5'-GCCGGGCACCTGCACACAAGGATTGTCTGGGGAGAGTGCCTCC-3'
Mouse *Vav1* (NM_011691)	
E556D_Rv	5'-GGAGGCACTCTCCCCAGACAATCCTTGTGTGCAGGTGCCCGGC-3'
E556K_Fw	5'-GCCGGGCACCTGCACACAAGAAGTGTCTGGGGAGAGTGCCTCC-3'
E556K_Rv	5'-GGAGGCACTCTCCCCAGACACTTCTTGTGTGCAGGTGCCCGGC-3'
E633G_Fw	5'-GAGCTCACTAAGGCAGAGGCTGGGCACAACTGGTGGGAGGGAAGG-3'
E633G_Rv	5'-CCTTCCCTCCCACCAGTTGTGCCCAGCCTCTGCCTTAGTGAGCTC-3'
G648C_Fw	5'-GCTACAAATGAAGTCTGCTGGTTTCCCTGTAAC-3'
G648C_Rv	5'-GTTACAGGGAAACCAGCAGACTTCATTTGTAGC-3'
A673V_Fw	5'-CAGAGGGTGAAAGATACAGTGGAGTTCGCCATCAGCATT-3'
A673V_Rv	5'-AATGCTGATGGCGAACTCCACTGTATCTTTCACCCTCTG-3'
R678Q_Fw	5'-TATGCGGGCCCTATGGAACAAGCAGGCGCTGAGGGCATC-3'
R678Q_Rv	5'-GATGCCCTCAGCGCCTGCTTGTTCCATAGGGCCCGCATA-3'
A789T_Fw	5'-TATTTTGGCACTGCCAAAACCCGCTACGACTTCTGTGCC-3'
A789T_Rv	5'-GGCACAGAAGTCGTAGCGGGTTTTGGCAGTGCCAAAATA-3'
R790C_Fw	5'-GGCACTGCCAAAGCCTGCTACGACTTCTGTGCC-3'
R790C_Rv	5'-GGCACAGAAGTCGTAGCAGGCTTTGGCAGTGCC-3'
D797N_Fw	5'-CGCTACGACTTCTGTGCCCGGGAAACGTCGGAACTGTCCCTTAAG-3'
D797N_Rv	5'-CTTAAGGGACAGTTCCGACGTTTCCCGGGCACAGAAGTCGTAGCG-3'
R798P_Fw	5'-GACTTCTGTGCCCGGGACCCGTCGGAACTGTCCCTTAAG-3'
R798P_Rv	5'-CTTAAGGGACAGTTCCGACGGGTCCCGGGCACAGAAGTC-3'
R798Q_Fw	5'-GACTTCTGTGCCCGGGACCAGTCGGAACTGTCCCTTAAG-3'
R798Q_Rv	5'-CTTAAGGGACAGTTCCGACTGGTCCCGGGCACAGAAGTC-3'
E805K_Fw	5'-AGGTCGGAACTGTCCCTTAAGAAGGGTGATATCATCAAGATCCTC-3'
E805K_Rv	5'-GAGGATCTTGATGATATCACCCTTCTTAAGGGACAGTTCCGACCT-3'
K815E_Fw	5'-CATCAAGATCCTCAATAAGGAGGGACAGCAAGGCTGGTGGC-3'
K815E_Rv	5'-GCCACCAGCCTTGCTGTCCCTCCTTATTGAGGATCTTGATG-3'
G816R_Fw	5'-TGGCGTGGGGAGATCTACTGACGGATCGGCTGGTTCCCT-3'
G816R_Rv	5'-AGGGAACCAGCCGATCCGTCAGTAGATCTCCCCACGCCA-3'
G819S_Fw	5'-GAGATCTACGGCCGGATCAGCTGGTTCCCTTCTAACTAT-3'
G819S_Rv	5'-ATAGTTAGAAGGGAACCAGCTATCCGGCCGTAGATCT-3'
R822Q_Fw	5'-GGACAGCAAGGCTGGTGGCAAGGGGAGATCTACGGCCGG-3'
R822Q_Rv	5'-CCGGCCGTAGATCTCCCCTTGCCACCAGCCTTGCTGTCC-3'
R822L_Fw	5'-GGACAGCAAGGCTGGTGGCTTGGGGAGATCTACGGCCGG-3'
R822L_Rv	5'-CCGGCCGTAGATCTCCCCAAGCCACCAGCCTTGCTGTCC-3'
Y826S_Fw	5'-GGCTGGTGGCGTGGGGAGATCTCCGGCCGGATCGGCTGGTTCCCT-3'
Y826S_Rv	5'-AGGGAACCAGCCGATCCGGCCGGAGATCTCCCCACGCCACCAGCC-3'
W831L_Fw	5'-GAGATCTACGGCCGGATCGGCTTGTTCCCTTCTAACTATGTGGAG-3'
W831L_Rv	5'-CTCCACATAGTTAGAAGGGAACAAGCCGATCCGGCCGTAGATCTCT-3'
Δ644_Fw	5'-GAGGGAAGGAATACTGCTTAAAATGAAGTCGGCTGGTTT-3'
Δ644_Rv	5'-AAACCAGCCGACTTCATTTTAAGCAGTATTCCTTCCCTC-3'
Δ677_Fw	5'-TGGTATGCGGGCCCTATGTAACGAGCAGGCGCTGAGGGC-3'
Δ677_Rv	5'-GCCCTCAGCGCCTGCTCGTTACATAGGGCCCGCATACCA-3'
Δ816_Fw	5'-TGGCGTGGGGAGATCTACTGACGGATCGGCTGGTTCCCT-3'
Δ816_Rv	5'-AGGGAACCAGCCGATTCAGCCGTAGATCTCCCCACGCCA-3'
Δ820_Fw	5'-ATCTACGGCCGGATCGGCTGATTCCCTTCTAACTATGTG-3'
Δ820_Rv	5'-CACATAGTTAGAAGGGAATCAGCCGATCCGGCCGTAGAT-3'

Human *VAV1* (NM_005428)	
Primer	**Sequence**
D26G_Fw	5'-AGCCACCGCGTGACCTGGGGGGGGGCTCAGGTGTGT-3'
D26G_Rv	5'-ACAACACCTGAGCCCCCCCCCAGGTCACGCGGTGGCT-3'
H399Y_Fw	5'-CTGGACCAGTCTCTGGCTTACTATGGCCGGCCCAAGATC-3'

| H399Y_Rv | 5'-GATCTTGGGCCGGCCATAGTAAGCCAGAGACTGGTCCAG-3' |

Cancer-associated mutations in *VAV1* trigger variegated signaling outputs and T cell lymphomagenesis

Javier Robles-Valero, Lucia Fernandez-Nevado, L. Francisco Lorenzo-Martin, Myriam Cuadrado, Isabel Fernandez-Pisonero, Sonia Rodriguez-Fdez, Elsa Astorga-Simon, Antonio Abad, Ruben Caloto, and Xose Bustelo
DOI: 10.15252/embj.2021108125

Corresponding author(s): Xose Bustelo (xbustelo@usal.es)

Review Timeline:

Editor: Daniel Klimmeck

Transaction Report:

Dear Dr Bustelo,

Thank you for the submission of your manuscript (EMBOJ-2021-108125) to The EMBO Journal. Please accept my apologies for the unusual delay with the peer-review of your work due to protracted referee input and detailed discussions in the team. Your manuscript has been sent to three reviewers and we have received reports from all of them, which I enclose below.

As you will see, the referees acknowledge the potential interest and novelty of your resource catalogue and functional results on the roles of mutant VAV1 in cancer, although they also express a number of major issues that will have to be conclusively addressed before they can be supportive of publication of your manuscript in The EMBO Journal. In more detail, referee #3 points to substantial concerns on the importance of additional Rho GTPase family members and asks you to address RAC1 function more directly (ref#3, pts 2,4). This referee also states that the methods annotation and data display need improvement (ref#3, pts 1,5,6). In line, referees #1 and #2 find that the manuscript is too dense currently and needs restructuring and suggest to emphasize the trivalent mutant data and related messages more. These experts also point to additional experiments and controls required to resolve data inconsistencies.

Given the referees' overall positive recommendations, I would like to invite you to submit a revised version of the manuscript, addressing the comments of all three reviewers.

In light of the extensive requests requested by the reviewers i.p. on the manuscript and data organisation, I would appreciate if you could contact me during the next weeks via e.g. a video call to discuss your perspective on the comments and potential plan for the manuscript revision.

We generally allow three months as standard revision time. As a matter of policy, competing manuscripts published during this period will not negatively impact on our assessment of the conceptual advance presented by your study. However, we request that you contact the editor as soon as possible upon publication of any related work, to discuss how to proceed. Should you foresee a problem in meeting this three-month deadline, please let us know in advance and we may be able to grant an extension.

I this context I also want to point to our adjusted GTA We are aware that many laboratories cannot function at full efficiency during the current COVID-19/SARS-CoV-2 pandemic and have therefore extended our 'scooping protection policy' to cover the period required for a full revision to address the experimental issues highlighted in the editorial decision letter. Please contact us at any time to discuss an adapted revision plan for your manuscript should you need additional time, and also if you see a paper with related content published elsewhere.

Thank you for the opportunity to consider your work for publication. I look forward to your revision.

Kind regards,

Daniel Klimmeck

Daniel Klimmeck, PhD

Senior Editor
The EMBO Journal

Instructions for preparing your revised manuscript:

Please make sure you upload a letter of response to the referees' comments together with the revised manuscript.

Please also check that the title and abstract of the manuscript are brief, yet explicit, even to non-specialists.

When assembling figures, please refer to our figure preparation guideline in order to ensure proper formatting and readability in print as well as on screen:
https://bit.ly/EMBOPressFigurePreparationGuideline

IMPORTANT: When you send the revision we will require
- a point-by-point response to the referees' comments, with a detailed description of the changes made (as a word file).
- a word file of the manuscript text.
- individual production quality figure files (one file per figure)
- a complete author checklist, which you can download from our author guidelines
(https://www.embopress.org/page/journal/14602075/authorguide).
- Expanded View files (replacing Supplementary Information)
Please see out instructions to authors
https://www.embopress.org/page/journal/14602075/authorguide#expandedview

Please remember: Digital image enhancement is acceptable practice, as long as it accurately represents the original data and conforms to community standards. If a figure has been subjected to significant electronic manipulation, this must be noted in the figure legend or in the 'Materials and Methods' section. The editors reserve the right to request original versions of figures and the original images that were used to assemble the figure.

Further information is available in our Guide For Authors:
https://www.embopress.org/page/journal/14602075/authorguide

The revision must be submitted online within 90 days; please click on the link below to submit the revision online before 27th Jun 2021.

https://emboj.msubmit.net/cgi-bin/main.plex

Referee #1:

This manuscript presents new data about oncogenic functions of Vav1 mutations and rearrangements in peripheral T cell lymphomas and selected other malignancies. The authors deserve a lot of credit for investigating systematically more than 50 Vav1 mutations identified in patients through a battery of assays that dissect the different pathways operating downstream of Vav1, including pathways that do and do not require the catalytic function of Vav1, as well as a new tumor suppressor pathway operating via Cbl-b/Notch that the authors reported recently. Most relevant is the identification of recurrent genetic events that create what the authors refer to as "trivalent effects" on Rac1 activation and NFAT activation while also increasing Notch activity through decreased Notch degradation. These "triple hit" Vav1 genetic events are highly enriched in ALCL, AITL and PTCL-NOS, but importantly other families of mutations are also identified with more selective effects on downstream pathways, and systematically catalogued here as a resource for the field. The paper is dense but generally well organized and presented. Structural and biochemical considerations are also a major plus in interpreting the impact of individual mutations. Of note, the authors also present a new in vivo assay leading to PTCL in mice with Tfh characteristics by overexpressing a C-terminal truncation mutant of Vav1 in mature CD4+ T cells. Given the paucity of PTCL models in mice, this could also be a useful resource.

Specific comments:

1) In Fig. 1C-D and 2A, the authors choose a heatmap strategy to graphically display a large amount of experimental data about individual Vav1 mutations (with primary data presented in the supplement). This is a clever strategy to provide a synthetic overview of the findings. However, for the JNK+aCD3 and NFAT+aCD3 readouts, the heatmap system documents the increased activity as compared to that of JNK and NFAT readouts alone, but as a result to not clearly display the impact of individual mutations in these conditions. Could the authors consider normalizing the data to that found with the WT Vav1 construct in these conditions? This would better represent changes introduced by individual mutants compared to wild-type Vav1.
2) In Fig. 5, the authors use an adoptive transfer system to transfer mature CD4+ T cells transduced with retroviral constructs expressing GFP, a C-terminal deletion mutant of Vav1 or the same mutant with a point mutation in Vav1's catalytic site. It appears that the system relies on transfer into lymphopenic Vav1/2/3 TKO recipients, a context that could impact the transforming potential of this strategy. I would recommend to disclose more prominently the unique features of this system in the text, figures and legends (rather than only mentioning it in the Methods section).
3) In Fig. 5M and/or Fig. 6, information about expression of canonical Notch target genes would be useful.
4) In the short-term culture assays presented in Fig. 7-8, it is unclear how much Notch signaling can be delivered to mature T cells cultured in the absence of a defined source of Notch ligands. This limitation should at least be acknowledged. Thus, whether the effects of compound E are fully on target remains not entirely clear. Along the same lines of thought, the anti-Notch1 antibodies used in Fig. 7J and 8D are not specific for the cleaved form of Notch1 (which is classically detected by antibodies reactive with a Val1744 epitope revealed by gamma-secretase cleavage. Such a strategy would provide more specific and definitive information about Notch pathway activation in this system.
5) In Fig. 9, a significant limitation is that the analysis is performed in steady-state conditions rather than after an immunization challenge that triggers a strong Tfh response (and ideally a GC reaction) Thus, conclusions about the physiological role of Vav1/3 in the generation of normal Tfh cells may not be definitive.

Referee #2:

EMBOJ- Robles-Valero et al.-2021-108125

Robles-Valero et al. systematically characterized the functional impacts of cancer-associated VAV1 mutations on the three main VAV1 signaling branches. This includes 51 different VAV1 mutations and definition of a classification based on their impact the downstream signaling branches. They demonstrated the most frequent VAV1 mutant subtype with a truncated CSH3 (that alleviates auto-repression and activates RAC1 and NFAT but lacks CBL-B mediated suppressor activity) specifically drives PTCL formation in mice via the cooperation of the polarization, chronic activation, and transformation of follicular helper T cells.

Overall, while the study is of significance and the conclusions are important for understanding peripheral T cell lymphomagenesis, the presented data is difficult to follow. Figures are very packed, with multiple abbreviations and color codding that make the reading very complex. The thinking process and the reason for each experiment are not clearly presented and can seem random at times. For example, there's no clear reason as to why Lung SH2 mutations are presented in figure 1E; 3D structures presented in figure 2C and 4D-E don't seem to add any information or there's no clear explanation as to why it is being shown to the reader. Figure 3 seems like a repetition of figures 1 and 2 with some added information from other tumors, again with no clear reason. Figures 5-9 seem like a completely different manuscript and go from studying VAV1 mutational landscape to validating in vivo the effects of a specific VAV1 mutation.

Overall, the manuscript as currently organized in nearly incomprehensible due to the density of the data and the fact that the results and discussion sections jump from one figure to the other and to supplementary which contributes to the difficulty in reading.

The manuscript would perhaps be better off being split into two separate papers, one with analysis of VAV1 mutational landscape and its functional impact and the other showing in vivo validation of VAV1ΔC in mouse T cells. A general additional suggestion is that the authors should only show the detailed in vitro assays of the T-cell neoplasm-related VAV1 mutations in the main figures and focus the unique features of the trivalent VAV1 mutations (one of which was functionally validated in the following mouse model). Most data in Figure 1, 2, 3 and 4 can either go to the supplemental data or can be used for another manuscript. Then maybe there would be the space to better describe the reasoning and results of each experiment.

Other specific comments:

1. Figure 1D: R678Q was defined as a "LOF" mutation, but still showed activation on SRF assay. It will be informative to verify whether this mutation affects the RAC activity or not by pull-down assay. This information will help to explain whether the activation on SRF assay is RAC1 dependent or not.

2. Figure 5C, did the mice in the Vav1dC+E201A group which died show any PTCL phenotypes?

3. Figure 5M, the authors should also show the gene expression data of EGFP+Vav1dC+E201A control samples.

4. Figure 6L, the authors should focus the overlapping genes between VavC-dependent genes and other PTCL models, not the overlapping genes between Tet2 loss and RhoAG17V.

5. Figure 7C, the ectopic expression level of different Vav1 mutant protein is different, and this may cause different biological effects. The authors should address this.

6. Figure 7L, the increased p-Akt in Vav1dC+E201A infected cells shown here is not consistent with the data shown in Figure 5N.

7. Figure 8. The authors should include the EGFP+Vav1dC+E201A as a control for all the inhibitor treatment experiments.

8. Figure 9E, the difference shown here between Vav1-/- and Vav1-/-, Vav2-/-, Vav3-/- samples suggests Vav2 and Vav3 may also play a role in the proliferation, is this due to the differential

expression of Myc?

Referee #3:

This is a comprehensive tour-de-force analysis of 51 VAV1 mutants found in two human cancer types, PTCL and NSCLC, which is a very valuable resource for both cancer researchers and cell signaling researchers. By using a range of complementary assays following expression of the mutants in cultured cells, the authors choose a functional mutation that they then test extensively in a mouse model in T cells in vivo, as well as cultured mouse T cells.
One concern with the interpretation of their results is that they assume that VAV1 DH-PH only activates RAC1, whereas in some circumstances it can act on other Rho GTPase family members. The indirect luciferase assays they are using could equally be activated by multiple other pathways. These assays are useful for high throughput and rapid screening through the mutants, but not so informative about which pathway(s) are feeding in upstream.

The following points need to be addressed in a revised manuscript:
1. Overall, the text and figures are very dense in information; some careful re-writing would help to get the main messages across without getting lost in the detail.
2. The Introduction should mention that VAV1 has also been reported to be a GEF for RHOA and CDC42 under some cellular contexts. This is particularly relevant for RHOA, since frequent mutations in RHOA are found in the same groups of PTCL as have VAV1 mutations (this should be introduced in more detail and discussed more extensively in the Discussion; e.g. Fujisawa et al., Leukemia 2018), and because SRF activation is most frequently linked to RHOA rather than RAC1 activation. Moreover, some of the LOF mutations in VAV1 could equate to similar LOF/DN mutations of RHOA in some PTCLs.
3. There are some mutants that activated JNK but not SRF signaling, or that have a much stronger effect on one or the other, in the luciferase read-outs, which provides additional evidence that the two assays measure different upstream signals and not simply 'RAC activity'. The authors should revise their interpretation of these results throughout.
4. The authors have not measured RAC1 activation directly for any of the mutants. They need to include some example RAC1 activity assays for at least a subset of relevant mutations (and simultaneously test for RHOA activation, see point 1).
5. Fig. 1: panel B - information on how each pathway was assayed should be provided here (e.g. SRE-Luc), because some of the assays are quite indirect (e.g. JNK activity is not being assayed directly); panels C, D; it would help to add asterisks or similar mark to indicate the positive control mutants (Y174 mutants) because these heat maps contain so many different mutants.
6. Fig 3A, B: the color coding in these figures is very complex and not intuitive to follow. It would be easier if all pathways that are unchanged are in green, and pathways that are changed are in a different color (red/pink for up, blue for down). The naming of the subclasses is also difficult to follow in the text - adding a diagram of VAV1 domains again with the subclasses indicated on it would help interpretation here (or just forget all the subclasses).
7. Fig. 5, Fig. 6 and accompanying text: it is not possible to compare the mouse studies carried here with those from a different group using different genetic changes (Zang et al., 2017). This can be put in the discussion but not stated as fact when the authors have not repeated the same experiment for direct comparison. The text and figure legend for Fig. 6 also need to make it clear that they are comparing gene expression results from Zang et al. with their own results. This information is only hidden in the Methods section.
8. This sentence does not make sense: 'For example, it is known that the bivalent F69V GOF

mutation targets a CH residue contributes to the autoinhibited structure of nonphosphorylated VAV1……'

9. Use g not rpm throughout the methods section (g is the relevant unit; rpm is centrifuge type-dependent).

COMMENTS TO REFEREES

MANUSCRIPT EMBOJ-2021-108125

REVIEWER #1:

General Comment. *This manuscript presents new data about oncogenic functions of Vav1 mutations and rearrangements in peripheral T cell lymphomas and selected other malignancies. The authors deserve a lot of credit for investigating systematically more than 50 Vav1 mutations identified in patients through a battery of assays that dissect the different pathways operating downstream of Vav1, including pathways that do and do not require the catalytic function of Vav1, as well as a new tumor suppressor pathway operating via Cbl-b/Notch that the authors reported recently. Most relevant is the identification of recurrent genetic events that create what the authors refer to as "trivalent effects" on Rac1 activation and NFAT activation while also increasing Notch activity through decreased Notch degradation. These "triple hit" Vav1 genetic events are highly enriched in ALCL, AITL and PTCL-NOS, but importantly other families of mutations are also identified with more selective effects on downstream pathways, and systematically catalogued here as a resource for the field. The paper is dense but generally well organized and presented. Structural and biochemical considerations are also a major plus in interpreting the impact of individual mutations. Of note, the authors also present a new in vivo assay leading to PTCL in mice with Tfh characteristics by overexpressing a C-terminal truncation mutant of Vav1 in mature CD4+ T cells. Given the paucity of PTCL models in mice, this could also be a useful resource.*

Authors' response: We thank this Referee for her/his comments. We also appreciate it very much her/his technical comments, which have helped us improving quite significantly our work.

Specific Point #1. *In Fig. 1C-D and 2A, the authors choose a heatmap strategy to graphically display a large amount of experimental data about individual Vav1 mutations (with primary data presented in the supplement). This is a clever strategy to provide a synthetic overview of the findings. However, for the JNK+aCD3 and NFAT+aCD3 readouts, the heatmap system documents the increased activity as compared to that of JNK and NFAT readouts alone, but as a result to not clearly display the impact of individual mutations in these conditions. Could the authors consider normalizing the data to that found with the WT Vav1 construct in these conditions? This would better represent changes introduced by individual mutants compared to wild-type Vav1.*

Authors' response: Agree. Thanks for pinpointing this issue. To avoid this problem, we have reformatted the heatmaps originally presented in **Figures 1C,D** and **2A** (now, **new Fig. 1F**). In this new version, we have expanded the color scale to avoid the saturation at the extremes. With this change, we believe we have significantly improved both the resolution and the variations seen in the case of the CD3 stimulation conditions. There was another option: removing the data from stimulated cells. However, we believe that it is important to present the effect of the interrogated mutants under both basal and stimulation conditions. This is particularly important to identify the mutants that show full constitutive, phosphorylation-independent activity. However, if this Reviewer feels otherwise, we can eliminate them in the final version of the manuscript.

Specific Point #2. *In Fig. 5, the authors use an adoptive transfer system to transfer mature CD4+ T cells transduced with retroviral constructs expressing GFP, a C-terminal deletion mutant of Vav1 or the same mutant with a point mutation in Vav1's catalytic site. It appears that the system*

1

relies on transfer into lymphopenic Vav1/2/3 TKO recipients, a context that could impact the transforming potential of this strategy. I would recommend to disclose more prominently the unique features of this system in the text, figures and legends (rather than only mentioning it in the Methods section).

Authors' response: Agree. As indicated in the original **Methods** section, we have used the compound *Vav1^{-/-};Vav2^{-/-};Vav3^{-/-}* mice as recipient for these T cell adoptive experiments. The rationale for using this mouse strain is that, due to its lymphopenia, it offers a cheaper model than the standard immunocompromised strains to carry out this type of experiments. Indeed, we have shown before that this model is even suited to carry out xenotransplants with human cancer cells (Lorenzo-Martin et al. *Nat Commun* 2020, PMID: 32963234). From a methodological point of view, these mice should not be that different from other immunodeficient mice that are commonly used in this type of experiments.

Having said this, we do agree that the readers require an explanation for the use of this "nonconventional" model. Accordingly, we have modified the text in the **Results** section to better explain the experimental model used (page 16): *"To this end, we infected TCR plus CD28-stimulated mouse splenic CD4^+ T cells with retroviral vectors encoding bicistronically each mutant Vav1 protein and EGFP and, subsequently, introduced them into Vav1^{-/-};Vav2^{-/-};Vav3^{-/-} mice to test the potential development of lymphomas (Fig. 4A). These recipient mice are T lymphopenic (Bustelo & Dosil, 2016; Fujikawa et al, 2003), a feature that facilitates their use in transplantation experiments involving even cells of human origin (Lorenzo-Martín et al, 2020)."* In addition, we have changed the text in the **Methods** section (pages 38-39), which now says: *"… was then introduced by retroorbital injection into 6- to 8-week-old Vav1^{-/-};Vav2^{-/-};Vav3^{-/-} recipient mice (Lorenzo-Martín et al., 2020; Menacho-Marquez et al, 2013). This lymphopenic mouse strain was used to minimize the potential rejection of the transplanted cells due to neoantigen expression (Lorenzo-Martín et al, 2020)."*

Specific Point #3. *In Fig. 5M and/or Fig. 6, information about expression of canonical Notch target genes would be useful.*

Authors' response: Agree. Following the Referee's recommendation, we now have included in the **Figure 5M** (now, **new Fig. 4M**), the expression of canonical Notch1 target genes in Vav1^{ΔC}-transformed cells using qRT-PCR determinations. We have also included in this panel expression data from cells expressing the catalytically dead mutant version of Vav1 (Vav1^{ΔC+E201A}) that has been requested by **Referee #2** (**specific point #3**). As expected, no alterations are observed in this latter case (new **Fig. 4M**). The text of the **Results** section has been changed to include this new set of data (page 17): *"In addition, they show elevated levels of canonical Notch1 target genes such as Hes1, Dtx1 and Ptcra (Fig. 4M, right panel). Most of these transformed cell isolates also display high levels of p-Akt (Fig. 3N and Fig. EV4A) and p-Erk (Fig. 4O and Fig. EV4A) when compared to EGFP^+ lymphocytes. These molecular and signaling features are not observed in cells expressing the catalytically-deficient Vav1^{ΔC+E201A} mutant protein (Fig. 4M)."*

Regarding **Figure 6** (now, **new Fig. 5**), we have already shown using *in silico* analyses that the Vav1^{ΔC}-driven transcriptome is associated with a high enrichment in gene signatures associated with ICN1 signaling according to gene set enrichment analyses (GSEA) (see **Fig. 6H** in the original manuscript, now **Fig. 5G** in the new version of the manuscript). These results agree with the new data presented in the **new Figure 4M** (see above paragraph).

Specific Point #4. *In the short-term culture assays presented in Fig. 7-8, it is unclear how much Notch signaling can be delivered to mature T cells cultured in the absence of a defined source of*

Notch ligands. This limitation should at least be acknowledged. Thus, whether the effects of compound E are fully on target remains not entirely clear. Along the same lines of thought, the anti-Notch1 antibodies used in Fig. 7J and 8D are not specific for the cleaved form of Notch1 (which is classically detected by antibodies reactive with a Val1744 epitope revealed by gamma-secretase cleavage. Such a strategy would provide more specific and definitive information about Notch pathway activation in this system.

Authors' response: Agree. Thank you for raising this important point. We believe that our short-term culture system is fully compatible with adequate Notch1 signaling. For example, previous reports using short-term culture assays have demonstrated that Notch1 expression and ICN1 production are induced upon the stimulation of CD4$^+$ T cells with a combination of antibodies to CD3 and CD28 (Palaga et al. *J Immunol* 2003, PMID: 12960327 & Steinbuck et al. *J Immunol* 2018, PMID: 29288204). A recent report has shown that both Notch1 and some of its ligands become expressed in CD4$^+$ T cells upon TCR stimulation, leading to ICN1 production (Mitra et al. *Front Immunol* 2020, PMID: 32457739). We have included this information in the new version of the manuscript (see **Results** section, page 22): *"The activation of ICN1 under these cell stimulation conditions is consistent with previous data in CD4+ T cells (Mitra et al, 2020; Palaga et al, 2003; Steinbuck et al, 2018)."*

Regarding the second issue indicated by the Referee, we have used in these experiments an antibody that does recognize the active version of Notch1 (mN1A, Cat. No. 552768, BD). In fact, the term ICN1 used in the text refers to the intracellular fragment of NOTCH1. This information is provided in the **Methods** section (pages 39-40): *"For intracellular Tox and ICN1 staining, cells were fixed with Cytofix/Cytoperm (Cat. No. 554714, BD Bioscience) for 10 min and stained with PE-labeled antibodies to Tox (Cat. No. 12-6502-82; eBiosciences; 1:50 dilution) or ICN1 (mN1A, Cat. No. 552768; 1:50 dilution) for 1 hour at room temperature in phosphate-buffered saline solution supplemented with 5% fetal bovine serum and 10% saponin".*

Specific Point #5. *In Fig. 9, a significant limitation is that the analysis is performed in steady-state conditions rather than after an immunization challenge that triggers a strong Tfh response (and ideally a GC reaction) Thus, conclusions about the physiological role of Vav1/3 in the generation of normal Tfh cells may not be definitive.*

Authors' response: Agree. Given that other Referees of this work have complained about the large amount of data contained in this manuscript, we have decided to remove this figure from the new version of the manuscript.

In any case, following the Referee's recommendation, we have performed an immunization experiment to further determine the importance of Vav proteins in T$_{FH}$ differentiation. To this end, we immunized wild-type, *Vav1$^{-/-}$* and *Vav1$^{-/-}$;Vav2$^{-/-}$;Vav3$^{-/-}$* mice using NP-keyhole limpet hemocyanin in combination with complete Freund's adjuvant and, subsequently, analyzed T and B cell numbers in the lymph nodes 12 days later. In agreement with our short-term cultures, these experiments indicate that the Vav-deficient mice are defective in the germinal center response associated with this type of immunization(see **Figure for Referee 1** below). In addition, we have found that Vav-deficient CD4$^+$ T cells express very low levels of ICOS when compared to controls under those conditions. Taken together, these data corroborate and further expand the general implication of Vav1 protein in T$_{FH}$ cell response that was presented in the first version of the manuscript.
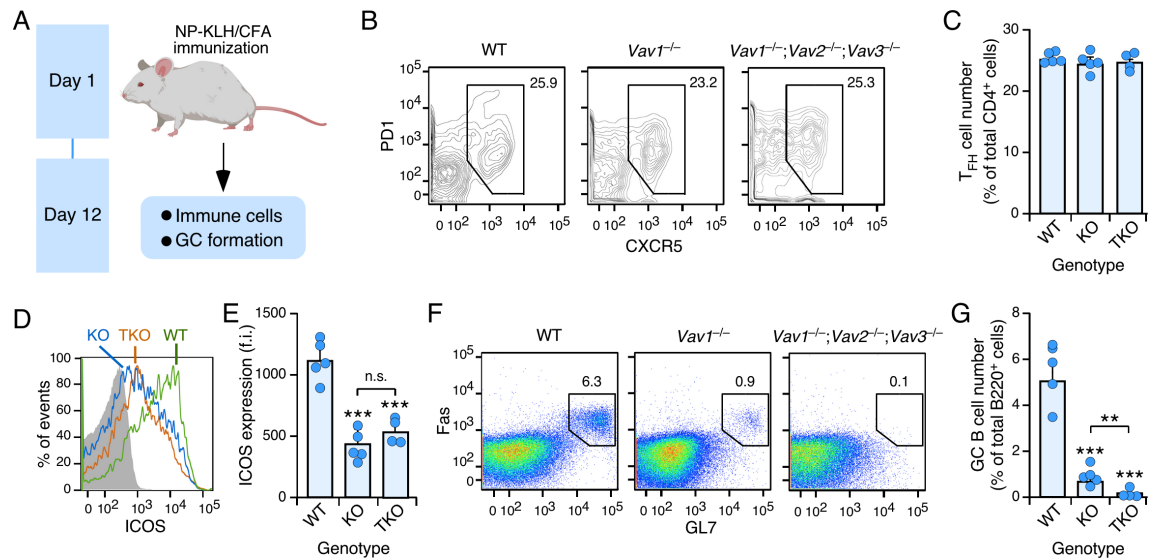
FIGURE 1 FOR REFEREES. *(A)* Schematic representation of the experiment used in panels F-J. *(B)* Flow cytometry analysis of expression of PD1 and CXCR5 in lymph node-CD4$^+$ T cells from immunized mice of indicated genotypes [(WT (n = 5), *Vav1$^{-/-}$* (n = 5) and *Vav1$^{-/-}$;Vav2$^{-/-}$;Vav3$^{-/-}$* (n = 4)]. Numbers indicate the relative percentage (%) of the cell population selected. *(C)* Quantification of the percentage of T$_{FH}$ cell numbers in lymph node-CD4$^+$ T cells from immunized mice. Each point represents the values obtained with a single experimental mouse. n as in B. *(D and E)* Example of the flow cytometry detection (D) and quantification (E) of ICOS expression in T$_{FH}$ cells from immunized mice of indicated genotypes. In E, each point represents the values obtained with a single experimental mouse. n as in B. *(F)* Flow cytometry detection of expression of Fas (CD95) and GL7 in B220$^+$-gated lymph node cells from immunized mice of indicated genotypes. Numbers indicate the relative percentage (%) of the cell population selected. n as in B. *(G)* Quantification of the percentage of germinal center (GC) B cells in B220$^+$-gated lymph node cells from the indicated mice. Each point represents the values obtained with a single experimental mouse. n as in B.

REVIEWER #2:

General Comment. *Robles-Valero et al. systematically characterized the functional impacts of cancer-associated VAV1 mutations on the three main VAV1 signaling branches. This includes 51 different VAV1 mutations and definition of a classification based on their impact the downstream signaling branches. They demonstrated the most frequent VAV1 mutant subtype with a truncated CSH3 (that alleviates auto-repression and activates RAC1 and NFAT but lacks CBL-B mediated suppressor activity) specifically drives PTCL formation in mice via the cooperation of the polarization, chronic activation, and transformation of follicular helper T cells. Overall, while the study is of significance and the conclusions are important for understanding peripheral T cell lymphomagenesis, the presented data is difficult to follow. Figures are very packed, with multiple abbreviations and color codding that make the reading very complex. The thinking process and the reason for each experiment are not clearly presented and can seem random at times. For example, there's no clear reason as to why Lung SH2 mutations are presented in figure 1E; 3D structures presented in figure 2C and 4D-E don't seem to add any information or there's no clear explanation as to why it is being shown to the reader. Figure 3 seems like a repetition of figures 1 and 2 with some added information from other tumors, again with no clear reason. Figures 5-9 seem like a completely different manuscript and go from studying VAV1 mutational landscape to validating in vivo the effects of a specific VAV1 mutation. Overall, the manuscript as currently organized in nearly incomprehensible due to the density of the data and the fact that the results and discussion sections jump from one figure to the other and to supplementary which contributes to the difficulty in reading. The manuscript would perhaps be better off being split into two separate papers, one with analysis of VAV1 mutational landscape and its functional impact and the other showing in vivo validation of VAV1ΔC in mouse T cells. A general additional suggestion is that the authors should only show the detailed in vitro assays of the T-cell neoplasm-related VAV1 mutations in the main figures and focus the unique features of the trivalent VAV1 mutations (one of which was functionally validated in the following mouse model). Most data in Figure 1, 2, 3 and 4 can either go to the supplemental data or can be used for another manuscript. Then maybe there would be the space to better describe the reasoning and results of each experiment.*

Authors' response: We thank the Referee for considering our work important for understanding peripheral T cell lymphomagenesis. We also appreciate it very much her/his constructive criticisms regarding the complexity of the work and the way in which some data are presented. Those comments have helped us in reformatting the manuscript in a more structured manner. We indicate below our comments on the issues raised by the Referee as well as the changes we have made in the new version of the manuscript to tackle them:

(1) We have eliminated the following panels in the figures (we use here to the numbers used in the first version of the manuscript): **1E** (the distribution of mutations in different tumor types), **1F** (the table with the uncoupling mutants), **2C** (3D structure of the CSH3), **3A** (the scheme of passenger mutations), **4A-C** (scheme and 3D structures), **4E** (3D structures CSH3), **6C** (expression of T_{FH} markers in the transcriptome of Vav1$^{\Delta C}$-transformed cells) and the entire **Figure 9** (role of Vav family proteins in normal T_{FH} differentiation). We have also eliminated the panels **B-G** of the old **Supplementary Figure 1** (now, **new Fig. EV1**) as indicated by the Referee (the 3D structures of all the domains).

(2) We have simplified the information given in **Figure 3** (now, **new Fig. 2**). Specifically, we removed the scheme of the passenger mutations (panel A) and we refer to the names of the tumors following the abbreviations used in the rest of the manuscript.

(3) We have simplified the information given in **Figure 4D** (now, **new Fig. 3A**) (only highlighting this time the residues that are outside the previously described inhibitory interfaces of the CSH3 domain).

(4) We have changed the place where some of the data are presented. Thus, all the data regarding the characterization of the VAV1 mutants is concentrated in **Figure 1** (leading to the elimination of **Figure 2**). In **Figure 4** (**now Fig. 3**), we have transferred panels A-C to the **Figure EV3**.

(5) We have changed some figures to reduce the number of colors used (e.g., **Figure 3**, which is now the **new Figure 2**). The rest of the figures maintain rather uniform color codes. The same applies, we believe, to the extended view and appendix figures.

(6) We have reformatted parts of the manuscript to explain better the rationale of some experiments. This has been mainly done in the section describing the functional characterization of the mutants (which was simplified, shortened, and better integrated with the information contained in former **Figure 3** (now, **new Fig. 2**), see pages 7-9), the explanation of the effect of the mutants in the context of the regulation of the activity of Vav proteins (which was also simplified and abbreviated, see pages 12-15), and the rationale for the *in vivo* experiments (pages 15-16).

(7) We reformatted the manuscript to avoid multiple calls for figures that could distract the readers.

We thank again the Referee for her/his advice on all those issues. It is obvious that we could have done a much better work in all those aspects in our original submission. However, we disagree with some of her/his comments:

(1) It is true that the manuscript has a lot of data and that most figures are composed of many panels. We believe that this is to some extent unavoidable since we aimed at: **(i)** Carrying out an extensive characterization of the mutations found in tumors (and that had to include lung tumors as well given that they have been potential hotspot *VAV1* mutations in them). **(ii)** Cataloguing these mutations in all the downstream pathways regulated by Vav1 (which is far from being monofunctional). **(iii)** Demonstrating that the most relevant mutations do act as oncogenic drivers *in vivo*. **(iv)** Dissecting the specific downstream pathways involved in that process. **(v)** Deciphering whether this transforming activity is due to *ex novo* functions or the exacerbation of the normal physiological role of the protein (this information has been removed from the current version of the manuscript). In addition, we preferred to show the data obtained and do not use "data not shown" throughout the manuscript.

(2) It is possible that we have failed in doing that, but we do believe that the data are presented in a logical way (an issue appreciated by the two other Referees). This logic follows the steps indicated in the above paragraph. Regarding the rational of the tumors used, that has been explained in the Introduction. In any case, we hope that such logic is now more apparent upon the changes made in the manuscript thanks to the input from the Referees of this work.

Specific Point #1. *Figure 1D: R678Q was defined as a "LOF" mutation, but still showed activation on SRF assay. It will be informative to verify whether this mutation affects the RAC*

Authors' response: Agree. We have carried out in the new version of the manuscript G-LISA assays in both COS1 and Jurkat cells to evaluate the impact of several VAV1 mutants (including R678Q) on the activation of the three main members of the RHO family (RHOA, RAC1 and CDC42). Our data indicate that VAV1^{R678Q} does activate RAC1 in both cell types (see **new Figs. 1E** and **Appendix S9**). This info is given in the new Results section as well (see pages 8-9 of new manuscript version): *"As a complementary avenue to the data obtained using the indirect JNK and SRF assays, we used the G-LISA method to test the direct effect of 3 VAV1 mutants belonging to the bivalent (Y174C, G819S) and signaling branch-specific (R678Q) subsets on the activation of the three main RHO family GTPases in both COS1 and Jurkat cells. As positive controls, we utilized constitutively active versions of VAV1 (Δ1-189 and Δ835-845), RAC1 (Q61L), RHOA (Q63L) and CDC42 (Q61L). When compared to VAV1^{WT}, we found that all the chosen VAV1 mutants could activate the incorporation of GTP onto RAC1 irrespectively of the functional subclass involved (Fig. 1E and Appendix Fig. S9). By contrast, they exhibited much lower activities on RHOA and CDC42 (Fig. 1E and Appendix Fig. S9). This RAC1-specificity is consistent with previous biochemical and cell-based experiments (Aghazadeh et al, 2000; Couceiro et al, 2005; Crespo et al., 1997; Rapley et al., 2008)."*

Specific Point #2. *Figure 5C, did the mice in the Vav1dC+E201A group which died show any PTCL phenotypes?*

Authors' response: Yes, we have analyzed this mouse. We could not see any evidence for the development of any tumor type in that single mouse according to anatomopathological analyses. This information has been included in the legend to this figure (now, new **Fig. 4**) (page 60): *"Note: the mouse transplanted with EGFP-transduced cells that has died in these experiments did not show any sign of tumor development according to anatomopathological analyses (data not shown)."*

Specific Point #3. *Figure 5M, the authors should also show the gene expression data of EGFP+Vav1dC+E201A control samples.*

Authors' response: Agree. We have included the requested data. As expected, we did not detect any differences in the interrogated transcripts in this case when compared to EGFP$^+$ controls (see new **Fig. 4M**). We have also modified the text in the **Results** section to include these data (see pages 17-18): *"Further buttressing the T$_{FH}$ cell-like phenotype of these tumor cells, we found using quantitative reverse transcription-PCR (qRT-PCR) that they express high levels of transcripts encoding typical follicular helper cell markers such as PD1, CXCR6, ICOS, Bcl6 and interleukin 21 (Fig. 4M, left panel). In addition, they show elevated levels of canonical Notch1 target genes such as Hes1, Dtx1 and Ptcra (Fig. 4M, right panel). Most of these transformed cell isolates also display high levels of p-Akt (Fig. 3N and Fig. EV4A) and p-Erk (Fig. 4O and Fig. EV4A) when compared to EGFP$^+$ lymphocytes. These molecular and signaling features are not observed in cells expressing the catalytically-deficient Vav1$^{ΔC+E201A}$ mutant protein (Fig. 4M)."*

Specific Point #4. *Figure 6L, the authors should focus the overlapping genes between VavΔC-dependent genes and other PTCL models, not the overlapping genes between Tet2 loss and RhoAG17V.*

Authors' response: Agree. It is important to note, however, that there is a chronic lack of a good mouse models for these tumors (reviewed in Mhaidly et al. *Oncogenesis* 2020; PMID:

32796826) and, when available, most of them do not have associated genome-wide expression data. Due to this, we have included the following datasets that are available:

(i) The AITL-like condition that develops in the SJL mouse model (Jain et al., *Am. J. Pathol.*, 2015; PMID: 26363366). As seen in the **new Figure EV5D,E**, we could not find any similarity with this transcriptome. This is indicated in two paragraphs in the **Results** section of the new manuscript version (pages 19-20): *"In addition, we have included in these in silico comparisons the transcriptome previously described in the AITL-like condition that spontaneously develops in Swiss Jim Lambert (SJL)/J mice (Jain et al, 2015; Mhaidly et al, 2020). This disease is primarily derived from the exacerbation of IL21 signaling in T_{FH} cells (Jain et al., 2015). […] We did not find any statistically significant similarity with the transcriptome previously described in the SJL/J mouse model, indicating that the similarity found between the $Vav1^{\Delta C}$ and the $RhoA^{G17V};Tet2^{-/-}$ model is specific. In fact, in the case of SJL/J mice, we found quite opposite transcriptomal patterns when using GSEAs (Fig. EV5D,E)."*

(ii) Human AITL patients. To this end, we used the two GSE6338 and GSE19069 gene expression microarray datasets that are publicly available (Piccaluga et al., *J Clin Invest*, 2007; PMID: 17304354. Iqbal et al., *Blood*, 2010; PMID: 19965671). This expression datasets are, to our knowledge, the best available in terms of: **(a)** Number of specific AITL samples contained (n = 40). **(b)** The presence of data from healthy controls (CD4$^+$ T cells). In this case, we did find a significant level of overlap with the transcriptome of our $Vav1^{\Delta C}$-driven AITL condition (see **new Fig. EV5G-J**). We have included this information in the **Results** section of the new manuscript version (page 21): *"Further in silico analyses indicated that the transcriptome of the $Vav1^{\Delta C}$-driven AITL bears high levels of similarity with the differential expression programs present in a large percentage of AITL patients (Fig. EV5G,H). Such similarity is significantly higher in the case of the $Vav1^{\Delta C}$ upregulated (49.5% of cross-species overlap) than in downregulated (19.2% of cross-species overlap) gene subset (Fig. EV5H). The overlapping transcriptomal subsets are enriched in gene signatures linked to the function of E2F and the NFAT–Tox axis, although SRF-, ICN1-, AP1-, Foxo- and mTORC-related gene expression programs are also observed (Fig. EV5I,J). As expected (Fig. 5J-K), a similar overlap is seen between the transcriptomes of human- and mouse $RhoA^{G17V};Tet2^{-/-}$ AITL samples (Fig. EV5J). However, unlike the case of the $Vav1^{\Delta C}$-driven transcriptome, we could not observe any consistent enrichment in this case in Notch1-related gene signatures (Fig. EV5J, right panel). Collectively, these data indicate significant levels of similarity of the gene expression programs of $Vav1^{\Delta C}$-transformed CD4$^+$ T cells and a significant percentage of human AITL cases."*

Specific Point #5. *Figure 7C, the ectopic expression level of different Vav1 mutant protein is different, and this may cause different biological effects. The authors should address this.*

Authors' response: Disagree. It is true that the mutant versions are expressed at lower levels than the wild-type counterpart, but this is a usual feature that is observed when using truncated versions of Vav proteins in most studies (and independently of the cell model or transfection method used). This is an advantage in this case, since it can be argued that the lack of transformation by the wild-type Vav1 cannot be due to problems associated with low levels of protein expression. The three mutants used are expressed at comparable levels. It can be in fact argued that, given its lower molecular weight, the $Vav1^{\Delta N}$ that shows reduced activity in these assays is expressed at higher levels if we consider molar ratios.

Specific Point #6. *Figure 7L, the increased p-Akt in Vav1dC+E201A infected cells shown here is not consistent with the data shown in Figure 5N.*

Authors' response: Agree. However, we do not consider that these two conditions are strictly comparable. In **Figure 7L** (now, **new Fig. 6L**)**,** we have analyzed CD4+ T cells that have been stimulated with antibodies to CD3 and CD28 in cell culture. By contrast, in **Figure 5N** (now, **new Fig. 4N**), we have analyzed CD4+ T cells directly collected in a steady-state condition from healthy spleens.

Specific Point #7. *Figure 8. The authors should include the EGFP+Vav1dC+E201A as a control for all the inhibitor treatment experiments.*

Authors' response: We respectfully disagree. We have already shown in **Figure 7** (now, **new Fig. 6**) that the catalytically dead mutant does not stimulate any of the signaling readouts used in **Figure 8** (now, **new Fig. 7**). Likewise, the effects of this mutant in cell proliferation are also quite marginal (**Fig. 7F**, now **new Fig. 6F**). Thus, the benefit of including this mutant protein in these experiments is unclear to us. It is also worth noting that repeating again all these experiments would entail the use of extra mice that, given the explanation stated above, is not very appropriate according to institutional animal experimentation procedures.

Specific Point #8. *Figure 9E, the difference shown here between Vav1-/- and Vav1-/-, Vav2-/-, Vav3-/- samples suggests Vav2 and Vav3 may also play a role in the proliferation, is this due to the differential expression of Myc?*

Authors' response: This is an interesting question indeed, although we believe that is not within the scope of the work presented in this manuscript. In any case, and as indicated above (**General Comments** section), we have decided to eliminate this part of the results to shorten the manuscript and keep with the main take-home message (the role of the mutants in tumorigenic processes *in vivo*).

REVIEWER #3:

General Comment. *This is a comprehensive tour-de-force analysis of 51 VAV1 mutants found in two human cancer types, PTCL and NSCLC, which is a very valuable resource for both cancer researchers and cell signaling researchers. By using a range of complementary assays following expression of the mutants in cultured cells, the authors choose a functional mutation that they then test extensively in a mouse model in T cells in vivo, as well as cultured mouse T cells. One concern with the interpretation of their results is that they assume that VAV1 DH-PH only activates RAC1, whereas in some circumstances it can act on other Rho GTPase family members. The indirect luciferase assays they are using could equally be activated by multiple other pathways. These assays are useful for high throughput and rapid screening through the mutants, but not so informative about which pathway(s) are feeding in upstream.*

Authors' response: We thank the Referee for her/his kind comments and for the overall positive view of the results presented. Regarding the role of other GTPases in the context of *VAV1* mutations, we will discuss this issue within the comments to her/his **Specific Points #2 to 4**.

Specific Point #1. *Overall, the text and figures are very dense in information; some careful re-writing would help to get the main messages across without getting lost in the detail.*

Authors' response: Agree. This point of concern was also raised by **Referee #2** as well. To tackle with this problem, we have done the following changes in the new version of the manuscript:

(1) We have eliminated the following panels in the figures (we use here to the numbers used in the first version of the manuscript): **1E** (the distribution of mutations in different tumor types), **1F** (the table with the uncoupling mutants), **2C** (3D structure of the CSH3), **3A** (the scheme of passenger mutations), **4A-C** (scheme and 3D structures), **4E** (3D structures CSH3), **6C** (expression of T_{FH} markers in the transcriptome of Vav1$^{\Delta C}$-transformed cells) and the entire **Fig. 9** (role of Vav family proteins in normal T_{FH} differentiation). We have also eliminated the panels **B-G** of the old **Supplementary Figure 1** (now, **new Fig. EV1**) as indicated by **Referee #2** (the 3D structures of all the domains).

(2) We have simplified the information given in **Figure 3** (now, **new Fig. 2**). Specifically, we removed the scheme of the passenger mutations (panel A) and we refer to the names of the tumors following the abbreviations used in the rest of the manuscript.

(3) We have simplified the information given in **Figure 4D** (now, **new Fig. 3A**) (only highlighting this time the residues that are outside the previously described inhibitory interfaces of the CSH3 domain).

(4) We have changed the place where some of the data are presented. Thus, all the data regarding the characterization of the VAV1 mutants is concentrated in **Figure 1** (leading to the elimination of **Figure 2**). In **Figure 4** (**now Fig. 3**), we have transferred panels A-C to the **new Figure EV3**.

(5) We have changed some figures to reduce the number of colors used (e.g., **Figure 3**, which is now the **new Figure 2**). The rest of the figures maintain rather uniform color codes. The same applies, we believe, to both the expanded view and appendix figures.

(6) We have reformatted parts of the manuscript to explain better the rationale of some experiments. This has been mainly done in the section describing the functional characterization of the mutants (which was simplified, shortened, and better integrated with the information contained in former **Figure 3** (now, **new Fig. 2**), see pages 7-9), the explanation of the effect of the mutants in the context of the regulation of the activity of Vav proteins (which was also simplified and abbreviated, see pages 12-15), and the rationale for the *in vivo* experiments (pages 15-16).

(7) We reformatted the manuscript to avoid multiple calls for figures that could distract the readers.

Specific Point #2. *The Introduction should mention that VAV1 has also been reported to be a GEF for RHOA and CDC42 under some cellular contexts. This is particularly relevant for RHOA, since frequent mutations in RHOA are found in the same groups of PTCL as have VAV1 mutations (this should be introduced in more detail and discussed more extensively in the Discussion; e.g. Fujisawa et al., Leukemia 2018), and because SRF activation is most frequently linked to RHOA rather than RAC1 activation. Moreover, some of the LOF mutations in VAV1 could equate to similar LOF/DN mutations of RHOA in some PTCLs.*

Authors' response: Partially agree. In the **Introduction**, we already indicate that *"VAV1 is a GEF for RHO GTPases, namely RAC1"*. It is true that some reports have indicated connections of VAV1 with RHOA and CDC42. However, if they exist, they must be through a catalytic-independent, indirect signaling mechanism. In this context, we have extensively shown that VAV1 uses RAC1 as main substrate and, to a much lower extent, RHOA (Crespo et al. *Nature* 1997, PMID: 8990121; Couceiro et al. *Exp Cell Res* 2005, PMID: 15950967). This is also in agreement with the biochemical activity shown by the protein *in vitro* (Crespo et al. *Nature* 1997, PMID: 8990121), an issue that has been corroborated by other groups (Rapley et al. *EMBO Rep* 2008, PMID: 18511940). For example, in that latter work, it has been estimated that the exchange rates of VAV1 towards RAC1 are 12.4- and 14.2-fold higher than those for RHOA and CDC42, respectively. This also puts into question the work by Fujisawa et al. (Leukemia 2018, PMID: 28832024), since it is unlikely that the proposed RHOA^{G17V}–VAV1 adaptor module could be assembled with such low catalytic affinities. Furthermore, it is known that exchange factors can only bind to GTPases in the nucleotide-free state, not in the GDP-bound conformation in which the RHOA^{G17V} mutant must likely exist in cells. In line with the latter issue, we have in fact a work going on in the lab in which we demonstrate that the leukemogenic activity of RHOA^{G17V} is not VAV1-dependent.

Regarding the activation of the serum response factor (SRF), it is worth noting that this event can occur upon the activation of any RHO GTPase, including of course RAC1 (Hill et al. *Cell* 1995, PMID: 7600583 & Westwick et al. *Mol Cell Biol* 1997, PMID: 9032259). In fact, any factor that would alter the G-actin/ F actin ratios in cells will do the job. Agreeing with this, it has been recently shown that the oncogenic driver function of the RAC1^{P29S} mutant is mediated, at least in part, by the activation of SRF (Lionarons et al. *Cancer Cell* 2019, PMID: 31257073).

In any case, and to satisfy the Referee's request, we have included additional experiments in the new version of the manuscript that have measured the impact of a collection of VAV1 mutants on the activation of the three main members of the RHO family (RHOA, RAC1 and CDC42). Our data, generated both in COS1 and Jurkat cells, indicate again that the main substrate of VAV1 is RAC1 (new **Figs. 1E** and **Appendix Fig. S9**). We have included proper controls to demonstrate that these assays can detect GTP-loaded RHOA and CDC42 in both cell types (new **Figs. 1E** and **Appendix Fig. S9**).

Due to the inclusion of these data, we have incorporated the following text in the Results section of the new manuscript version (pages 8-9): *"As a complementary avenue to the data obtained using the indirect JNK and SRF assays, we used the G-LISA method to test the direct effect of 3 VAV1 mutants belonging to the bivalent (Y174C, G819S) and signaling branch-specific (R678Q) subsets on the activation of the three main RHO family GTPases in both COS1 and Jurkat cells. As positive controls, we utilized constitutively active versions of VAV1 (Δ1-189 and Δ835-845), RAC1 (Q61L), RHOA (Q63L) and CDC42 (Q61L). When compared to VAV1^WT, we found that all the chosen VAV1 mutants could activate the incorporation of GTP onto RAC1 irrespectively of the functional subclass involved (Fig. 1E and Appendix Fig. S9). By contrast, they exhibited much lower activities on RHOA and CDC42 (Fig. 1E and Appendix Fig. S9). This RAC1-specificity is consistent with previous biochemical and cell-based experiments (Aghazadeh et al, 2000; Couceiro et al, 2005; Crespo et al., 1997; Rapley et al., 2008)."* The **Methods** section has also been modified to describe this new set of experiments (see page 35).

Specific Point #3. *There are some mutants that activated JNK but not SRF signaling, or that have a much stronger effect on one or the other, in the luciferase read-outs, which provides additional evidence that the two assays measure different upstream signals and not simply 'RAC activity'. The authors should revise their interpretation of these results throughout.*

Authors' response: It is difficult to compare side by side both assays since they are performed using different cell lines and transfection protocols. The cytoskeletal remodeling of these two cell lines is also different, an issue that can influence the SRF readout. In general, it is true that the SRF assays usually gives better signals when using proteins with low activity. This is probably the reason for the discrepancy observed in the color codes of the heatmap between the SRF and JNK data for some VAV1 mutants. In any case, we believe that the new data presented in our work regarding the activation of RAC1, RHOA and CDC42 by VAV1 clearly indicate that these readouts reflect primarily the effects of the mutants on RAC1 activity (new **Figs. 1E** and **Appendix Fig. S9**; see **Specific Point #2** above).

Specific Point #4. *The authors have not measured RAC1 activation directly for any of the mutants. They need to include some example RAC1 activity assays for at least a subset of relevant mutations (and simultaneously test for RHOA activation, see point 1).*

Authors' response: Agree. As indicated in **Specific Point #2**, these data have now been included in the new **Figures 1E** and **Appendix Fig. S9**.

Specific Point #5. *Fig. 1: panel B - information on how each pathway was assayed should be provided here (e.g. SRE-Luc), because some of the assays are quite indirect (e.g. JNK activity is not being assayed directly); panels C, D; it would help to add asterisks or similar mark to indicate the positive control mutants (Y174 mutants) because these heat maps contain so many different mutants.*

Authors' response: Agree. Thank you for raising those points. Following this Referee's advice, we have reformatted the way in which these experiments are indicated in the **new Figure 1B**. In addition, we have added red asterisks to indicate the positive controls used in these experiments in the **new Figure 1C,D**.

Specific Point #6. *Fig 3A, B: the color coding in these figures is very complex and not intuitive to follow. It would be easier if all pathways that are unchanged are in green, and pathways that are changed are in a different color (red/pink for up, blue for down). The naming of the subclasses*

is also difficult to follow in the text - adding a diagram of VAV1 domains again with the subclasses indicated on it would help interpretation here (or just forget all the subclasses).

Authors' response: Agree. Regarding the first part of the Referee's comment, we have changed the colors used in **Fig. 3** (now, **new Fig. 2**). Regarding the second issue, we do believe that it is important to keep the different subclasses to give all the information to the readers. In addition, the Vav1 domains targeted by the mutations are already shown in gray boxes in each subclass. We also mentioned in which tumors these mutations have been found. All this information is indicated in the legend to the **Fig. 3** (now, **new Fig. 2**).

Specific Point #7. *Fig. 5, Fig. 6 and accompanying text: it is not possible to compare the mouse studies carried here with those from a different group using different genetic changes (Zang et al., 2017). This can be put in the discussion but not stated as fact when the authors have not repeated the same experiment for direct comparison. The text and figure legend for Fig. 6 also need to make it clear that they are comparing gene expression results from Zang et al. with their own results. This information is only hidden in the Methods section.*

Authors' response: Partially agree. The information regarding how these analyses were done was already indicated in the **Methods** section. However, we acknowledge that it is perhaps better to emphasize this issue in the main text. We have done that in the new version of the manuscript (page 19). The new text says: *"Given the AITL-like phenotype exhibited by Vav1$^{\Delta C}$-transformed T$_{FH}$ cells, we next decided to investigate the level of similarity of the transcriptome of those cells with the gene expression changes previously seen associated with the deletion of Tet2 and/or the expression of a dominant negative (G17V mutation) version of the GTPase RhoA in CD4$^+$ T cells (Zang et al., 2017)."* We have also modified the legend to **Figure 6K** (now, **new Fig. 5J**) as requested (page 62): *"Dot plot of the Vav1$^{\Delta C}$-dependent gene signature fit score in the indicated experimental groups (bottom) that were retrieved from a previous work (Zang et al., 2017).*

Regarding the validity of the comparison, we have used in these analyses the GSEA (Gene Set Enrichment Analysis) algorithm. This is a thoroughly validated method with more than 26,700 citations in scientific literature (Subramanian et al. *PNAS* 2005, PMID: 16199517). This is the gold-standard tool to perform cross-comparisons of transcriptomic data from different datasets.

Specific Point #8. *This sentence does not make sense: 'For example, it is known that the bivalent F69V GOF mutation targets a CH residue contributes to the autoinhibited structure of nonphosphorylated VAV1.....'*

Authors' response: Agree. Sorry about this. We tried to indicate here that this CH residue is involved in the intramolecular inhibition of Vav1 activity. However, it is obvious that it has not been properly written. It has been modified in the new version of the manuscript (which has now been transferred to the **Appendix** file, **Appendix Supplementary Text 1**, page 2). The new sentence says: *"For example, it is likely that the F69V promotes a bivalent GOF effect through the disruption of the interactions that the F^{69} residue establishes with the PH (D^{406}), the DH α_{11} helix (F^{386}) and the first PH β strand (Y^{441})."*

Specific Point #9. *Use g not rpm throughout the methods section (g is the relevant unit; rpm is centrifuge type-dependent).*

Authors' response: Agree. Following the Referee's recommendation, we have made the appropriate changes in the **Methods** section of the new version of the manuscript.

(A) Main text:

Title page. No changes made.

Abstract. We have made minor changes (indicated in red). Total number of words: 150 words.

Introduction. Minor changes (indicated in red)

Results. They were modified to include all the new experiments, controls and comments suggested by Referees. Main changes can be found in pages 7-10, 13-17 and 19-21 of the new version of the manuscript. All changes have been highlighted in red.

Discussion. It has been modified to accommodate the points raised by Referees. Main changes can be found in page 25 of the new version of the manuscript. Changes indicated in red.

Methods. They were modified to include all the new experimental procedures. Changes indicated in red.

References. It has been modified to include new references.

Figure legends. They have been modified to incorporate the changes and new experimental data requested by the Referees. Changes indicated in red.

(B) Figures:

Old/New Figure 1. We have modified panel B to include the experimental approached used to determine each of the signaling activities of VAV1 (requested by Referee #3, Specific Point 6). We have also colored them to get correlations with each of the pathways depicted in Figure 1A. We have widened the color scale of the heatmaps in panels C and D (requested by Referee #1, Specific Point 1). We have also removed the original panels E and F. Finally, we have included two new panels: panel E (showing the effect of Vav1 mutations on the activation status of RHO proteins using G-LISA assays) and panel F (former panel A in old Figure 2).

Old Figure 2. It has been eliminated. Panel A is now in Figure 1 (panel G). Panel B is now in panel E in Figure EV2. Panel C has been eliminated.

Old Figure 3/New Figure 2. We have removed panel A (bystander mutations) and reduced the number of colors used in the new panel A (former panel B; requested by Referee #3, Specific Point 6). As a result of these changes, this figure now has 3 panels (the old version had 4 panels).

New Figure 3: It has been significantly simplified. The new figure has now 3 panels.

Old Figure 4. It is now presented as the new Figure EV3.

Old Figure 5/New Figure 4: We have included the samples from Vav1$^{\Delta C+E201A}$-expressing tumoral cells in panel M (requested by Referee #2, Specific Point 3). We have also changed panel M to include data of Notch1 target genes (right graph; requested by Referee #1, Specific Point 3). Data of *Trp53* and *Tet2* mRNA expression levels have now been transferred to the Figure EV4 (panel B).

Old Figure 6/New Figure 5: We have eliminated the original panel C.

Old Figure 7/New Figure 6: No changes.

Old Figure 8/New Figure 7: No changes.

Old Figure 9: It has been eliminated from the manuscript

(C) Appendix and Extended View files:

(C.1) Text:

Appendix text 1 (page 2). It has been modified to accommodate all changes made in the new version of the manuscript.

Figure legends. They have been modified to accommodate all changes made in the new version of the manuscript.

(C.2) Figures:

Old Figure S1/New Figure EV1. We have removed panels B-G as requested by Referee #2. As a result of these changes, this figure now has 2 panels (the old version had 8 panels).

Old/New Figures S2-S9/New Appendix Figures S1-S8. No changes made.

New Appendix Figure S9. We have included the raw data for the GTPase activity assays.

Old Figure S11/New Figure EV2. We have included the panel B from old Figure 2 as the new panel E in this supplementary figure.

Old Figure S12/New Figure EV3: We have included here some of the panels originally presented in old Figure 4.

Old Figure S13/New Figure EV4. We have included a new panel (B) originally present in old Figure 5M.

Old Figure S14/New Figure EV5. We have included five new panels showing the *in silico* analyses of the Vav1$^{\Delta C}$-dependent transcriptome with the SJL model (panels D,E) and human AITL samples (panels F-J). We included these new data to accommodate the request made by Referees #2 (point 4). As a result of these changes, this figure now has 10 panels (4 panels in the original submission).

(C.3) Tables:

Appendix Table S1. No changes.

(D). Other datasets:

Old/New SuppDataSet1. No changes.

Old/New SuppDataSet2. No changes.

Old/New SuppDataSet3. No changes.

Dear Dr Bustelo,

Thank you for submitting your revised manuscript (EMBOJ-2021-108125R) to The EMBO Journal. Please accept my apologies for the unusual protraction with the processing of your revised manuscript. Your amended study was sent back to the reviewers for re-evaluation, and we have received comments from two of them, which I enclose below.

As you will see, referees #1 and #3 stated that their issues have been comprehensively resolved and they are now broadly in favour of publication, pending minor revision.

Please note that we also had input from referee #2 who doesn't find that the revisions have address his/her concerns. However, we have received further comments on this from referee #1 who found the issues to be satisfactorily addressed.

Thus, we are pleased to inform you that your manuscript has been accepted in principle for publication in The EMBO Journal.

Please consider the remaining minor issues stated by referee #3 carefully by adjusting the text where appropriate. Further, we need you to consider a number of points related to formatting and data representation as detailed below, which should be addressed at re-submission.

Please contact me at any time if you have additional questions related to below points.

As you might have noted on our web page, every paper at the EMBO Journal now includes a 'Synopsis', displayed on the html and freely accessible to all readers. The synopsis includes a 'model' figure as well as 2-5 one-short-sentence bullet points that summarize the article. I would appreciate if you could provide this figure and the bullet points.

Thank you for giving us the chance to consider your manuscript for The EMBO Journal. I look forward to your final revision.

Again, please contact me at any time if you need any help or have further questions.

Kind regards,

Daniel Klimmeck

Daniel Klimmeck PhD
Senior Editor
The EMBO Journal

Formatting changes required for the revised version of the manuscript:

>> Limit the keywords for your manuscript to maximally five

>> Rename the current 'Competing interests' section into 'Conflict of Interest'.

>> Rename the current 'Data Resources ' section into 'Data Availability. Remove the privacy from the GEO microarray data set.

>> Add the funding information 'senior postdoc contract for J.R-V. by the Spanish Association against Cancer ; Salamanca local section of the Spanish Association against Cancer support to L.F.-N' to our manuscript onine system.

>> Nomenclature of the Dataset EV legends needs to be corrected to Dataset EV1 etc. (files and manuscript text). Dataset EV1 has 2 tabs with a Table S2, Dataset EV3 has 2 tabs with a Table S4. These tables are not called out in the manuscript and could be confusing for readers Please rename them to Table A and B to make sure there is no confusion with the regular EMBO Press nomenclature for tables.

>>Please provide source data as one zipped file per figure.

>> Add the current Appendix Supplementary text 1 to the main manuscript.

>> Please consider additional changes and comments from our production team as indicated by the .doc file enclosed and leave changes in track mode.

Please remember: Digital image enhancement is acceptable practice, as long as it accurately represents the original data and conforms to community standards. If a figure has been subjected to significant electronic manipulation, this must be noted in the figure legend or in the 'Materials and Methods' section. The editors reserve the right to request original versions of figures and the original images that were used to assemble the figure.

Further information is available in our Guide For Authors:
https://www.embopress.org/page/journal/14602075/authorguide

The revision must be submitted online within 90 days; please click on the link below to submit the revision online before 22nd Nov 2021.

https://emboj.msubmit.net/cgi-bin/main.plex

Referee #1:

The authors are presenting a revised manuscript that is further improved and adequately addresses key suggestions from the reviewers.

Referee #3:

In this revision, the authors have answered all of my points by adding extra data and changing the text. They have put a lot of effort into improving the clarity of their complex and impressive results by modifications to figures and text. The response to reviewers is also very comprehensive and clear.

I have two remaining suggestions for improving the text:

1. Introduction: 'One of the main functions of VAV1 is the catalysis of the activation step of RHO GTPases, namely RAC1'. Based on their results, I suggest rewording to 'One of the main functions of VAV1 is to catalyse the activation of the RHO GTPase RAC1'.
2. Figure 2: UNCLOUPLING should be UNCOUPLING.

Dear Dr Bustelo,

Thank you for submitting the revised version of your manuscript. I have now evaluated your amended manuscript and concluded that the remaining minor concerns have been sufficiently addressed.

Thus, I am pleased to inform you that your manuscript has been accepted for publication in the EMBO Journal.

Please note that it is EMBO Journal policy for the transcript of the editorial process (containing referee reports and your response letter) to be published as an online supplement to each paper. I would thus like to ask for your consent on keeping the additional referee figure included in this file.

Also, in case you might NOT want the transparent process file published at all, you will also need to inform us via email immediately. More information is available here: http://emboj.embopress.org/about#Transparent_Process

----

Please note that in order to be able to start the production process, our publisher will need and contact you regarding the following forms:

- PAGE CHARGE AUTHORISATION (For Articles and Resources)
http://onlinelibrary.wiley.com/journal/10.1002/(ISSN)1460-2075/homepage/tej_apc.pdf

- LICENCE TO PUBLISH (for non-Open Access)

Your article cannot be published until the publisher has received the appropriate signed license agreement. Once your article has been received by Wiley for production you will receive an email from Wiley's Author Services system, which will ask you to log in and will present them with the appropriate license for completion.

- LICENCE TO PUBLISH for OPEN ACCESS papers

Authors of accepted peer-reviewed original research articles may choose to pay a fee in order for their published article to be made freely accessible to all online immediately upon publication. The EMBO Open fee is fixed at $5,200 (+ VAT where applicable).

We offer two licenses for Open Access papers, CC-BY and CC-BY-NC-ND.
For more information on these licenses, please visit: http://creativecommons.org/licenses/by/3.0/ and http://creativecommons.org/licenses/by-nc-nd/3.0/deed.en_US

- PAYMENT FOR OPEN ACCESS papers

You also need to complete our payment system for Open Access articles. Please follow this link and select EMBO Journal from the drop down list and then complete the payment process: https://authorservices.wiley.com/bauthor/onlineopen_order.asp

Should you be planning a Press Release on your article, please get in contact with embojournal@wiley.com as early as possible, in order to coordinate publication and release dates.

On a different note, I would like to alert you that EMBO Press is currently developing a new format for a video-synopsis of work published with us, which essentially is a short, author-generated film explaining the core findings in hand drawings, and, as we believe, can be very useful to increase visibility of the work. This has proven to offer a nice opportunity for exposure i.p. for the first author(s) of the study. Please see the following link for representative examples and their integration into the article web page:
https://www.embopress.org/video_synopses
https://www.embopress.org/doi/full/10.15252/embj.2019103932

Please let me know, should you be interested to engage in commissioning a similar video synopsis for your work. According operation instructions are available and intuitive.

If you have any questions, please do not hesitate to call or email the Editorial Office.

Thank you again for this contribution to The EMBO Journal and congratulations on a successful publication! Please consider us again in the future for your most exciting work.

Kind regards,

Daniel Klimmeck

Daniel Klimmeck, PhD
Senior Editor
The EMBO Journal
EMBO
Postfach 1022-40
Meyerhofstrasse 1
D-69117 Heidelberg
contact@embojournal.org
Submit at: http://emboj.msubmit.net

** Click here to be directed to your login page: https://emboj.msubmit.net

PLEASE NOTE THAT THIS CHECKLIST WILL BE PUBLISHED ALONGSIDE YOUR PAPER

Corresponding Author Name: Xosé R. Bustelo
Journal Submitted to: EMBO Journal
Manuscript Number: EMBOJ-2021-108125

Reporting Checklist For Life Sciences Articles (Rev. June 2017)

This checklist is used to ensure good reporting standards and to improve the reproducibility of published results. These guidelines are consistent with the Principles and Guidelines for Reporting Preclinical Research issued by the NIH in 2014. Please follow the journal's authorship guidelines in preparing your manuscript.

A- Figures
1. Data
The data shown in figures should satisfy the following conditions:
➜ the data were obtained and processed according to the field's best practice and are presented to reflect the results of the experiments in an accurate and unbiased manner.
➜ figure panels include only data points, measurements or observations that can be compared to each other in a scientifically meaningful way.
➜ graphs include clearly labeled error bars for independent experiments and sample sizes. Unless justified, error bars should not be shown for technical replicates.
➜ if n< 5, the individual data points from each experiment should be plotted and any statistical test employed should be justified
➜ Source Data should be included to report the data underlying graphs. Please follow the guidelines set out in the author ship guidelines on Data Presentation.

2. Captions

Each figure caption should contain the following information, for each panel where they are relevant:

➜ a specification of the experimental system investigated (eg cell line, species name).
➜ the assay(s) and method(s) used to carry out the reported observations and measurements
➜ an explicit mention of the biological and chemical entity(ies) that are being measured.
➜ an explicit mention of the biological and chemical entity(ies) that are altered/varied/perturbed in a controlled manner.

➜ the exact sample size (n) for each experimental group/condition, given as a number, not a range;
➜ a description of the sample collection allowing the reader to understand whether the samples represent technical or biological replicates (including how many animals, litters, cultures, etc.).
➜ a statement of how many times the experiment shown was independently replicated in the laboratory.
➜ definitions of statistical methods and measures:
 • common tests, such as t-test (please specify whether paired vs. unpaired), simple χ2 tests, Wilcoxon and Mann-Whitney tests, can be unambiguously identified by name only, but more complex techniques should be described in the methods section;
 • are tests one-sided or two-sided?
 • are there adjustments for multiple comparisons?
 • exact statistical test results, e.g., P values = x but not P values < x;
 • definition of 'center values' as median or average;
 • definition of error bars as s.d. or s.e.m.

Any descriptions too long for the figure legend should be included in the methods section and/or with the source data.

B- Statistics and general methods

Please fill out these boxes ⬇ (Do not worry if you cannot see all your text once you press return)

Question	Answer
1.a. How was the sample size chosen to ensure adequate power to detect a pre-specified effect size?	No statistical methods were used to determine sample size. In general, at least three independent replicates were performed in all experiments. For experiments subjected to higher variability, such as animal-based studies, at least five animals per experiment. The sample size used for each experiment is indicated in the appropriate figure legend of the manuscript.
1.b. For animal studies, include a statement about sample size estimate even if no statistical methods were used.	OK. We have included this statement in Method section.
2. Describe inclusion/exclusion criteria if samples or animals were excluded from the analysis. Were the criteria pre-established?	No data were excluded.
3. Were any steps taken to minimize the effects of subjective bias when allocating animals/samples to treatment (e.g. randomization procedure)? If yes, please describe.	In all animal studies, groups were allocated randomly.
For animal studies, include a statement about randomization even if no randomization was used.	OK. We have included this statement in Method section
4.a. Were any steps taken to minimize the effects of subjective bias during group allocation or/and when assessing results (e.g. blinding of the investigator)? If yes please describe.	Most animal studies were coordinated by a technician in the lab, who does not have direct knowledge of the experiments and hypothesis tested.
4.b. For animal studies, include a statement about blinding even if no blinding was done	For all animal studies, the investigators were blind to group allocation. Blinding was not applicable to the rest of experiments. We have included this statement in Method section.
5. For every figure, are statistical tests justified as appropriate?	We have included all the statistical tests used in each experiment in Method section: "The number of biological replicates (n), the type of statistical tests performed, and the statistical significance are indicated for each experiment in the figure legends as well as the results section of this document. Parametric and nonparametric distributions were analyzed using Student's t-test and Mann-Whitney test, respectively. Chi-squared tests were used to determine the significance of the differences between expected and observed frequencies. The Tukey's honest significance difference test was used to identify groups showing differential enrichment of the indicated signatures. Statistical analyses of the immunoblot-generated data were carried out using the GraphPad Prism software (version 6.0). In all cases, values were considered significant when P ≤ 0.05. Data obtained are given as the mean ± SEM."
Do the data meet the assumptions of the tests (e.g., normal distribution)? Describe any methods used to assess it.	We have included all the statistical methods used in each experiment in Method section

Is there an estimate of variation within each group of data?	Yes. We have included standard deviation in each group of data
Is the variance similar between the groups that are being statistically compared?	Yes. All the groups have a similar variance

C- Reagents

6. To show that antibodies were profiled for use in the system under study (assay and species), provide a citation, catalog number and/or clone number, supplementary information or reference to an antibody validation profile. e.g., Antibodypedia (see link list at top right), 1DegreeBio (see link list at top right).	In our study we have used commercially-available antibodies that have been validated by the manufacturer for the application (immunoblot, flow cytometry) and species (mouse or human) utilized in our experiments. This information is available at each manufacturer's website and can be obtained through the catalog numbers indicated above. The homemade Vav1 antibody has been validated by us in overexpression, knockdown and knockout experiments.
7. Identify the source of cell lines and report if they were recently authenticated (e.g., by STR profiling) and tested for mycoplasma contamination.	We have included information about cell lines used in this paper in Method section. All cells were obtained from the ATCC and they are authenticated by the manufacturer. Periodic checkouts were performed at the Genomics Unit of our Center. All cell lines have tested negative for mycoplasma contamination.

* for all hyperlinks, please see the table at the top right of the document

D- Animal Models

8. Report species, strain, gender, age of animals and genetic modification status where applicable. Please detail housing and husbandry conditions and the source of animals.	Mus musculus, C57BL/10 background, 6-8 week old. The genotype (WT and Vav1–/–;Vav2–/–;Vav3–/–) and age of the animals used in each experiment is detailed in the Methods section of the manuscript. Animals were kept in ventilated rooms in pathogen–free facilities under controlled temperature (23ºC), humidity (50%), and illumination (12–hour–light/12–hour–dark cycle) conditions.
9. For experiments involving live vertebrates, include a statement of compliance with ethical regulations and identify the committee(s) approving the experiments.	This information is included in Methods, section Ethics Statment: "All mouse experiments were performed according to protocols approved by the Bioethics Committee of the University of Salamanca and the animal experimentation authorities of the autonomous Government of Castilla y León (Spain). We have not utilized patients or patient-derived samples in this work."
10. We recommend consulting the ARRIVE guidelines (see link list at top right) (PLoS Biol. 8(6), e1000412, 2010) to ensure that other relevant aspects of animal studies are adequately reported. See author guidelines, under 'Reporting Guidelines'. See also: NIH (see link list at top right) and MRC (see link list at top right) recommendations. Please confirm compliance.	We have complied with all relevant ethical regulations and include a statement affirming this in the manuscript.

E- Human Subjects

11. Identify the committee(s) approving the study protocol.	NA
12. Include a statement confirming that informed consent was obtained from all subjects and that the experiments conformed to the principles set out in the WMA Declaration of Helsinki and the Department of Health and Human Services Belmont Report.	NA
13. For publication of patient photos, include a statement confirming that consent to publish was obtained.	NA
14. Report any restrictions on the availability (and/or on the use) of human data or samples.	NA
15. Report the clinical trial registration number (at ClinicalTrials.gov or equivalent), where applicable.	NA
16. For phase II and III randomized controlled trials, please refer to the CONSORT flow diagram (see link list at top right) and submit the CONSORT checklist (see link list at top right) with your submission. See author guidelines, under 'Reporting Guidelines'. Please confirm you have submitted this list.	NA
17. For tumor marker prognostic studies, we recommend that you follow the REMARK reporting guidelines (see link list at top right). See author guidelines, under 'Reporting Guidelines'. Please confirm you have followed these guidelines.	NA

F- Data Accessibility

18: Provide a "Data Availability" section at the end of the Materials & Methods, listing the accession codes for data generated in this study and deposited in a public database (e.g. RNA-Seq data: Gene Expression Omnibus GSE39462, Proteomics data: PRIDE PXD000208 etc.) Please refer to our author guidelines for 'Data Deposition'. Data deposition in a public repository is mandatory for: a. Protein, DNA and RNA sequences b. Macromolecular structures c. Crystallographic data for small molecules d. Functional genomics data e. Proteomics and molecular interactions	Microarray data presented in this paper has been deposited in GEO database (https://www.ncbi.nlm.nih.gov/geo/) under the accession number GSE165006.
19. Deposition is strongly recommended for any datasets that are central and integral to the study; please consider the journal's data policy. If no structured public repository exists for a given data type, we encourage the provision of datasets in the manuscript as a Supplementary Document (see author guidelines under 'Expanded View' or in unstructured repositories such as Dryad (see link list at top right) or Figshare (see link list at top right).	A Source Data and an unprocessed WBs files were provided with this paper.
20. Access to human clinical and genomic datasets should be provided with as few restrictions as possible while respecting ethical obligations to the patients and relevant medical and legal issues. If practically possible and compatible with the individual consent agreement used in the study, such data should be deposited in one of the major public access-controlled repositories such as dbGAP (see link list at top right) or EGA (see link list at top right).	NA
21. Computational models that are central and integral to a study should be shared without restrictions and provided in a machine-readable form. The relevant accession numbers or links should be provided. When possible, standardized format (SBML, CellML) should be used instead of scripts (e.g. MATLAB). Authors are strongly encouraged to follow the MIRIAM guidelines (see link list at top right) and deposit their model in a public database such as Biomodels (see link list at top right) or JWS Online (see link list at top right). If computer source code is provided with the paper, it should be deposited in a public repository or included in supplementary information.	NA

G- Dual use research of concern

22. Could your study fall under dual use research restrictions? Please check biosecurity documents (see link list at top right) and list of select agents and toxins (APHIS/CDC) (see link list at top right). According to our biosecurity guidelines, provide a statement only if it could.	NA